From Microplastic Capture to Bio-derived Polymers: Environmental Remediation Strategies for Enduring Petro-based Polymers

by

Tolulope Damilola Lawal

A dissertation submitted in partial fulfillment
of the requirements for the degree of
Doctor of Philosophy
(Materials Science and Engineering)
at the University of Michigan
2026

Doctoral Committee:

Professor Brian J. Love, Chair
Professor Anne McNeil
Professor Mojgan Nejad, Michigan State University
Professor Alan Taub

Tolulope Lawal

lawaltdl@umich.edu

ORCID iD: 0009-0004-4848-657X

© Tolulope Lawal 2026

Acknowledgements

Many stages culminated in my PhD journey, and I am immensely grateful for all of them. From my first exposure to Black PhDs during my time in the PREFACE program at The Ohio State University, to my first Research Experience for Undergraduates (REU) at Johns Hopkins University, which inspired me to continue pursuing research opportunities, I owe so much to these integral moments. When I reached out to Dr. Yael Vodovotz inquiring about research opportunities in her Food Science Lab at Ohio State University, I did not know what to expect or that this experience researching biobased materials would inform much of my subsequent research endeavors afterwards. I am forever grateful for this experience and for my mentor, Dr. Xiaoying Zhao.

When I received my first PhD offer, pursuing a doctoral degree became a dream turned reality, and I am immensely grateful to God and to everyone who believed in me. Special thanks to my P.I., Dr. Brian Love, for being exactly what I needed in an advisor. I would also like to thank my committee for their endless support and advising. I would like to thank lab members from each group for sharing their resources, knowledge, and time; special thanks to Manasseh Agbedam & Sejad Nikafshar (Nejad Lab), Henry Thurber & Malavika Ramkumar (McNeil Lab), and Louise Batta (Taub Lab). In addition, I would like to thank every lab member in the Love Lab that I've had the pleasure of sharing a space with: Julie Rieland, Attri Bezbaruah, Priya Patel, Dylan Payne, Ethan Bryant, Erin Clingerman, Xue Ping, Keon Beigzadeh, Sharon Song, and Brandon Zhang. Lastly, I would like to thank my collaborators, Timothy (Raz) Jugovic and Griffen Josephs.

To my communities both at The Ohio State University (PREFACE, National Society of Black Engineers and Scientists, Christ International Community Church) and at The University of Michigan (Graduate Society of Black Engineers and Scientists, Office of Academic Multicultural Initiatives, Engineering Teaching Consultants, Graduate Engineering Ambassadors, the Department of Materials Science and Engineering, Redeemed Campus Fellowship, and The Redeemed Christian Church of God), thank you for shaping me. To my friends, thank you for the laughs, the beautiful memories, and free therapy. And to my family, this one was for you.

Table of Contents

Acknowledgements iii

List of Tables viii

List of Figures ix

List of Appendices xiv

Abstract xv

Chapter 1 : Problem Statement and Background 1

1.1 Problem Statement 1

1.2 Strategies for Environmental Remediation 3

1.2.1 Microplastic Sequestering Using the Pressure-Sensitive Adhesive, Polyethyhexyl Acrylate (PEHA) 3

1.2.2 Natural Polymers and Lignocelluloses for Future Biopolymer Synthesis 7

1.3 Research Scope and Research Aims 24

1.3.1 Study 1: MP Sequestering Using Polyethyl Hexyl Acrylate Pressure-Sensitive Adhesives 24

1.3.2 Study 2: Exploring Biopolymer Extraction Using Ionic Liquids 25

Chapter 2 : Microplastic Remediation in Laundering Systems Using Pressure-Sensitive Adhesives and the Impact of Surfactants on Capturability 26

2.1 Introduction 26

2.2 Experimental Methods 28

2.2.1 Materials 28

2.2.2 Adhesive Preparation and Coating on a Glass Slide Substrate. 29

2.2.3 Adsorption Shake Tests 30

2.2.4 Image J Analysis of Glass Slides Post MP Capture 30

2.2.5 Probe Tack on Exposed P2EHA Adhesives for Aqueous Work of Adhesion Analysis 32
2.2.6 Computational Methods 34
2.3 Results And Discussions 34
2.3.1 Laundry Additives Interact with Adhesives by Swelling Them 34
2.3.2 MP Capture by Adhesives in the Presence Of Additives as Interferences 36
2.3.3 Adhesive Physical Properties of the Adhesive in the Presence of Additives via Work of Adhesion Measurements 38
Chapter 3 : Differences in MP Binding Between Monopolymer and Multipolymer Mixtures Dispersed in Aqueous Solutions Using an Adhesive-Based Capture Mode 43
3.1 Introduction 43
3.2 Materials and Methods 44
3.2.1 PEHA Preparation and Coating on the HDPE Foam Substrate 45
3.2.2 MP Collection 46
3.2.3 Particle Count Determination 46
3.3 Results and Discussion 49
3.3.1 PEHA Adhesive Has an Affinity for Collecting Smaller Microparticles 49
3.3.2 Different Mechanisms Seem Functional with Different Particles on the Adhesive Foams 51
3.4 Conclusions 54
Chapter 4 : Water Regulates Ionic Liquid Solvation and Can Fine-Tune the Rheological Behavior of Dissolved Cellulose 55
4.1 Introduction 55
4.2 Materials and Methods 56
4.2.1 Cellulose Composition 56
4.2.2 Cellulose Cri (% Crystallinity of Commercial Cotton) 57
4.2.3 Ionic Liquid (IL) Preparation and Cotton Solvation 58
4.2.4 Rheology of Water/IL/Cotton Systems 59

4.2.5 Cellulose Fiber Regeneration and Characterization 60

4.3 Results and Discussion 62

4.3.1 Water Suppresses Cellulose Solubility in [DBUH][-Oac] 62

4.3.2 The Presence of Dispersed Cellulose and Water Contributes to the Measured Solution Viscosity 64

4.3.3 Fiber Characterization from Extruded Precipitates 67

4.4 Conclusions 71

Chapter 5 : Water/[DBUH][Acetate] Mixtures for Controlled Lignin/Cellulose Isolations from Corn Stover 72

5.1 Introduction 72

5.2 Materials and Methods 75

5.2.1 Liquid Hot Water Treatment of Corn Stover 75

5.2.2 Corn Stover Structural Changes 76

5.2.3 Compositional Analysis of LHW-Treated Biomass and Hemicellulose Hydrolysis 77

5.2.4 Ionic Liquid Water Mixtures Preparation 80

5.2.5 Lignin/IL Processing and Initial Lignin Composition 80

5.2.6 X-Ray Diffraction of Cellulose-Rich Portion of the IL Treated Corn Stover 83

5.2.7 Thermal Analysis 83

5.2.8 GPC 83

5.2.9 31P-NMR 84

5.3 Results and Discussion 85

5.3.1 Lignin and Cellulose Remain Comingled After IL Solvation of Cellulose; 85

5.3.2 Cellulose Crystallinity is More Pronounced After IL-Water Treatments 86

5.3.3 With Trace Amounts of Water, Lower Elution Times and Less Lignin Impurities are Observed 89

5.3.4 Analysis of Lignin Hydroxyl Content for 0WIL And 20WIL 92

5.3.5 Lignin Solubility Analysis 94

5.4 Conclusions 96

Chapter 6 : Conclusions and Future Works **97**

6.1 Conclusions: PEHA Sequestering of Microplastics **97**

6.1.1 Challenges 98

6.1.2 Future Direction – Life of Sequestered Microplastics After Collection 99

6.2 Conclusion: Ionic Liquid/Water Mediated Lignocellulose Extraction **100**

6.2.1 Challenges 101

6.2.2 Future Direction: Ionic Liquid Recycling 102

6.2.3 Future Direction: Lignin Characterization for Residual Carbohydrates 102

6.2.4 Future Direction: Exploring Intrinsic IL Modifications by Altering Acid Pka 103

6.3 Closing statement **104**

List of Tables

Table 1-1: Chemical compositions of lignocellulose plant discards. Adapted from Hassan et al. [67] 8

Table 1-2: Industries that use cellulose and their applications 9

Table 1-3: Examples of delignification treatments that improve biomass crystallinity 12

Table 1-4: Delignification Methods and Lignin Properties 17

Table 2-1: Texture analyzer Probe tack parameters..... 33

Table 4-1: Solvation conditions for 5% cellulose dissolved in ionic liquid/water solutions..... 59

Table 4-2: Mechanical testing parameters using TA.XT.plus Texture Analyzer 62

Table 4-3: Zero Shear Viscosity and Power law coefficients for 5% cotton in water/IL slurries at 60°C, coefficients n and K are derived from the power law equation: $\ln\eta = (n-1)(\ln\gamma) + \log K$ [288]. 67

Table 5-1: LHW conditions vs severity Factor..... 76

Table 5-2: Abbreviations for IL/Water treated Lignin samples..... 80

Table 5-3 ^{31}PNMR Parameters for IL-treated lignin..... 85

Table 5-4: ^{31}PNMR ppm ranges for aliphatic, phenolic, and carboxylic acid hydroxyl groups.. 85

Table 5-5: Comprehensive TGA values for lignin treated with Water/IL..... 92

List of Figures

Figure 1-1: Estimates for a. exponential plastic generation projections[9] and b. areas where generated waste ends up..... 1

Figure 1-2: Schematic of good vs poor adsorption of an adhesive to a substrate..... 4

Figure 1-3: PEHA synthesis scheme involving a polyacrylic acid, 2-ethyl hexanol, and a sulfuric acid catalyst 6

Figure 1-4: Cellulose, hemicellulose and lignin structures..... 7

Figure 1-5: XRD patterns for (a) cellulose I and sulfuric acid-treated cellulose I nanocrystals (CNC-I) (58%, 61%, 64%) and XRD patterns for (b) cellulose II and sulfuric acid-treated cellulose II nanocrystals (CNC-II). [94] 10

Figure 1-6: XRD diffractograms of untreated microcrystalline cellulose (MCC) and amorphized celluloses (Acs) obtained from different Ionic Liquid treatment durations. From the diffractograms, the fundamental peak (representative of the (002) lattice plane) consistently shifted with increasing IL treatment. Appearance of (020) (shifted peaks) and (110) lattice planes indicated the transformation of cellulose I to cellulose II. [96]..... 11

Figure 1-7: Schemes for polyol-based synthesis of polyurethanes, epoxies, and phenol formaldehyde. Polyurethanes involve the polyaddition reaction between a polyol and a polyisocyanate. Bisphenol A epoxies are synthesized using bisphenol-A and epichlorohydrin. 15

Figure 1-8: Simplified schematic of a lignin dimer with a β-O-4 linkage..... 16

Figure 1-9: Phenolic lignin unit structures: hydroxyphenyl (H-unit), Guaiacyl (G-unit), and Syringyl (S-Unit) 18

Figure 1-10: Protic Ionic liquid synthesis (acid-base neutralization reaction) using Diazabicyclo [5.4.0]undec-7-ene acetate, [DBUH][Acetate], synthesis as an example..... 20

Figure 1-11: Common superbases and acids used in Ionic Liquids for lignocellulose extractions..... 21

Figure 1-12: Schematic of cellulose dissolution and regeneration mechanism via Ionic liquid hydrogen bond displacements. Cationic substituents interact with partially negative oxygen groups while anionic substituents interact with partially positive hydrogen groups, separating cellulose chains. 22

Figure 1-13: Proposed mechanism for [C_3SO_3HMIM][HSO_4] cleavage of β-O-4 bonds.[193] 23

Figure 2-1: structures of PEHA adhesive, glycerol, citrate anion, and tergitol laundering additives 28

Figure 2-2: Glass slide preparation where the adhesive-coated area is limited to a 24 by 24 area of the 25 by 25 portion of the glass slide. B. Optical microscopy of taped-off adhesive matrix with embedded nylon MPs. Only particles captured by the adhesive layer were considered in % area calculations. 29

Figure 2-3: Image J analysis process of microscope covered slides. A. image is in its unprocessed state. B. Image is set to an 8 bit, monochrome image to eliminate interreferences from color. B. Brightness and contrast adjusted to remove shadows and enhance MP areas. C. A threshold was set where all particle edges and appropriate sizes of interest are fully identified. 31

Figure 2-4: A. Recorded Macro for batch processing of % MP area data. B. % MP coverage on the glass slide 32

Figure 2-5: a. Schematic of probe tack configuration showcasing the texture analyzer, PETE and Nylon probes, surfactant solution, and P2EHA-coated adhesive slide. B. Adhesive-coated glass slide 33

Figure 2-6: detachment Work determination using MATLAB trapz() function which calculates the area within curve using A trapezoidal integration formula..... 34

Figure 2-7: Relative mass gain of PEHA after 3% dilute additive exposure with error bars representing _+/- 1 standard deviation. All the additives show significant mass gain ($p<0.05$) at both shake test times, relative to DI water as a control and are essentially invariant with exposure time comparing 1 and 5 minutes of exposure with the exception of sodium citrate. 35

Figure 2-8: Total percent area of coverage for A) nylon (30 micron) and B) PETE (100-1100 micron) on 3by3 grid on adhesive coated glass slides. % Area coverage was approximated for MP capture in DI Water, glycerol, sodium citrate, and tergitol for 1 and 5 minutes. MPs were collected under flow conditions created by a shaker table and % coverage on the glass slide matrix was used to determine capturing efficiency. Tergitol exposure results in statistically significant ($p<0.05$) MPs coverage at 5 minutes compared to water for nylon and both time points for PETE particles. The other additives were not statistically significant. 37

Figure 2-9: Optical Imagery of MPs bound on a PEHA coatings captured after 1 and 5 minutes in DI water, glycerol, Sodium citrate, and tergitol (top down). Images were taken with a 5x optical lens. 38

Figure 2-10: Experimental $WoA_{(aq)}$ values assessed as a probe tack-measurement for PETE and nylon probes at dry conditions (blue) and in 3% v/v static, dilute solutions of DI Water (green), glycerol (grey), sodium citrate (yellow) and tergitol (purple). There is a cross-sectional

area for the probe, a force at failure and a strain at from failure, and from that, one can resolve work. 39

Figure 2-11: Computational WoA plots vs. concentration for A) Sodium citrate, B) glycerol and C) tergitol, with an exponential decay line of best fit. 41

Figure 3-1: Schematic of the foam collection apparatus. The PEHA-coated foam is manually lowered completely into the reservoir and then raised to isolate the adsorbed particulates on the foam. 46

Figure 3-2: Trainable Weka Segmentation of labeled classifiers distinguishing between HDPE, PET, PP, and foam background 48

Figure 3-3: Probability Maps of a. Multipolymer capture sample b. HDPE, c. PETE, d. PP used to determine particle count (under Analyze particles)..... 49

Figure 3-4: Particle size distributions for **a/b/c.** ground HDPE/ PETE/PP particles (pre-capture), **d/e/f.** HDPE/ PETE/PP monopolymers captured on an adhesive+foam substrate, and **i/j/k.** HDPE/ PETE/ PP multipolymer mixtures captured on an adhesive+foam substrate. Pre-capture distributions were determined from 0.25 grams of polymer. Average particle sizes are reported for each distribution..... 50

Figure 3-5: Capture efficiency of monopolymer and multipolymer dispersions of HDPE, PETE, and PP. Particle count-based capture efficiencies were observed based on the number of captured particles vs the estimated number of particles originally deposited in the reservoir. The deposited. The particle system was determined by estimating particles over a gram of HDPE (3780 ± 290 particles/gram), PETE (10,100 ± 757 particles/gram), and PP (4400 ± 385 particles/gram). Deposited particles were 1.5 g of plastic for monopolymer systems and 0.5 g each for multipolymer systems. 52

Figure 3-6: Particle counts for the upper side of the foam vs the bottom of the foam post capture for a. monopolymer dispersions and b. multipolymer dispersion..... 53

Figure 4-1: XRD of commercial cotton showcasing lattice parameters of cellulose used to calculate crystallinity index 57

Figure 4-2: Fiber testing configuration modified from ASTM Standard D3822-07: a. Example of a cellulose 25.4 mm long fiber used for mechanical testing, b. The Cellulose fiber is taped on a 1 by 3 in paper with 10 mm gage. The paper is hole punched to allow ease of snipping prior to starting the mechanical testing (red dashed line), c. Testing configuration post-mechanical testing. Note that cellulose breaks in the middle. 61

Figure 4-3: Cotton dissolution vs Water content in [DBUH][-OAc] at 80°C at 1, 2, and 4 hours. 10% water content is enough to significantly reduce the solubility of cellulose in [DBUH][-OAc] solutions..... 63

Figure 4-4: Optical micrograph of solutions made from 0-5% DI Water, [DBUH][-OAc] and 5% cotton disolved at 80 °C. The fine strands in b and c are residual undissolved cotton fibers 64

Figure 4-5: Arrhenius plots of 0-5% water/[DBUH][-OAc]/cotton slurries a. 2 hours of solvation and b. 4 hours of solvation, including the activation energies of cotton slurries derived from the slope of the Arrhenius line (Ea/R), where R is the gas constant. 65

Figure 4-6: Viscosity v. Shear rate graphs of **2 and 4 hour exposed** water/cotton/ionic liquid mixtures where rheology is conducted at 60°C. 66

Figure 4-7: Optical and SEM images of reformed fibers cast from slurries made from the following conditions: a/b and c/d: 0%water/IL, dissolved for a/b) 2 hrs and c/d) 4hrs; e/f and g/h: 3%water/IL, dissolved for e/f) 2hr and g/h) 4 hrs; i/j and k/l): 5%water/IL dissolved for i/j) 2 hrs. and k/l) 4hrs. RMS roughness values were calculated Gwyddion open source software. 68

Figure 4-8: Plots of a. Young's modulus and b. Ultimate Tensile Strength and c. Strain at break for syringe-casted fibers precipitated in methanol for 24 hours. 70

Figure 5-1: Schematic of delignification goal: lignin extraction with minimal cellulose disruption 75

Figure 5-2: Scanning Electron Micrographs of corn stover a. before LHW treatment and after 30-minute treatments at b. 130 °C, c. 150 °C, 30 minutes, d. 170 °C, and e. 190 °C 77

Figure 5-3: Cellulose, Lignin, and hemicellulose content as a function of severity factor (treatment condition) for CS 79

Figure 5-4: The a. mass loss of hydrothermally treated corn stover and b. conductivity of the liquid stream as a function of treatment condition..... 80

Figure 5-5: Schematic of lignin and cellulose isolation from IL/Water treatment of CS, and characterization 82

Figure 5-6: Polystyrene standard calibration curve for Gas Permeation Chromatography (GPC) 84

Figure 5-7: Liquid solvation in IL (80 °C for 3 hours) before and after LHW treatment (170 °C for 2 hours)..... 86

Figure 5-8: Examples of XRD spectra Crystallinity determination using two methods: a. Peak Height Method (PHM) and b. Deconvolution Method (DM). 87

Figure 5-9: Cellulose XRD data for LHW-pretreated (black), 20% water/IL-treated (blue), and pure IL-treated (red) corn stover b. crystallinity as a function of water content of IL/Water treated corn stover, where LHW-pretreated corn stover is black, PHM (blue – square) and DM

(red – circle) crystallinities. IL/water-treated samples are solid colored; pure IL-treated samples have open squares and circles. 88

Figure 5-10: Lignin extraction rates for IL-Water mixtures: 0WIL (0% water), 5WIL (5% water), 10WIL (10% water), 20WIL (20% water) 89

Figure 5-11: GPC Curves for IL/Water extracted lignin. Duplicate lignin samples are plotted.. 90

Figure 5-12: a. Degradation curves from 100-800 °C and b. Derivative of degradation curves from 100-800 °C 91

Figure 5-13: Phospourous-31 NMR spectra for 0WIL and 20WIL showcasing specific aliphatic, phenolic, and carboxylic acid regions 93

Figure 5-14: Solubility of IL/Water treated lignin samples in Acetone and DMSO 95

Figure 6-1: Schematic of DBU Acetate hydrogen bonding interactions between the carboxylate anion (conjugate base) and the DBUH+ cation (conjugate acid) 103

Figure 6-2: DBU Carboxylates examples made from acid with varying pKas 104

Appendix Figure A-1: This code inputs the raw data from viscosity vs shear rate data and matches the data to an appropriate cross model curve fit……105

Appendix Figure A-2: A plot fit is created using the MATLAB curve-fitting package using the equation for the cross model “n0/((1+p*x)^(1-n))” 107

Appendix Figure A-3: Predicted values of η_0 (n0), $\eta 0/\tau^*$ (p) where τ^* is the critical shear stress, and the viscous constant (n) based on curve fitted data.vs shear rate. 107

Appendix Figure A-4: Viscosity vs shear rate for a. 2-hr solvation solutions and b. 4-hr solvation solution 108

Appendix Figure B-1: Cellulose XRD data of DBU-Carboxylates treated corn stover where UNCS is non-IL treated CS 111

Appendix Figure B-2: a. Mn, Mw and Polydispersity index of DBU-Carboxylate Lignin samples with b. corresponding PNMR curves with hydroxyl content 112

List of Appendices

Appendix A: Supplemental Instructions for "Water Regulates [DBUH][-OAc] Solvation of Cellulose and can Fine-Tune its Rheological Behavior" 105

A.1 Matlab Code for Cross Model Curve Fitting for Zero Shear Viscosity..... 105

A.2 Viscosity vs Strain Rates 2 and 4 Hours and All Rheology Temperatures..... 108

Appendix B: Preliminary Work on the Impact of Reducing the Acid pKa on Ionic Liquid-Mediated Lignin Extraction..... 109

B.1 Preliminary Work 109

B.2 Materials 109

B.3 Ionic Liquid Synthesis..... 110

B.4 Cellulose XRD..... 110

B.5 Lignin Characterization 110

B.6 Preliminary Results..... 110

B.6.1 Cellulose Structural Changes are Inconclusive but Suggest That DBU Glycolate may Maintain Cellulose Structure 110

B.7 Summary of Preliminary Observations and Future Considerations 113

Abstract

Polymers are essential to our modern world, and they have become a key material for most, if not all, major industries. The consequence of polymers' ubiquity is their accumulation in our environments and the reliance on finite fossil fuels for their production; this means that polymers remain enduring parts of our ecosystem and do not readily degrade but instead break down into smaller microparticles. To reduce the presence of enduring microplastics in our environments, two plastic remediation projects were studied that address both polymer cleanup and the replacement of petro-based polymer reactant products with environmentally benign, biocompatible cellulose and lignin from plants, which are more likely to degrade into natural materials (water, carbon dioxide, and organic matter).

To address plastic cleanup in water, two microplastic (MP) capture studies were conducted using polyethyl hexyl acrylate (PEHA) adhesive. The high tack, low surface energy properties of PEHA make it an excellent candidate for efficient plastic substrate adsorption, even in water. In both studies, a 92k-950k adhesive was spray-coated onto glass and foam substrates and exposed to MP dispersion. These studies were done to understand how an adhesive-based capturing mechanism may be impacted by the capturing environment. In Chapter 2, the capturing environment was a laundering effluent environment, with detergent additives. Results from this study indicate an >90% reduction in MP capturability and adhesive detachment work in the presence of a surfactant effluent (tergitol). For both non-surfactant effluents (glycerol and citrate), theoretical adhesive work reduces with concentrations as low as 0.25 %mol. In Chapter 2, PEHA efficacy in a single polymer vs multiple polymer systems was evaluated. Overall, adhesive-based capturing was enhanced in multipolymer environments, with a x2 increase in capturing rate (by particle count) when multiple polymers were present vs a single polymer dispersion. These studies reveal that the capturing environment highly influences PEHA sequestering of MPs. Capturing efficiencies were measured by particle count and surface area of coverage using optical imagery and Fiji (Image J)

open-source image analysis software. Adhesive work was used as a metric for measuring binding capacity in Chapter 2.

The second study explores petrochemical polymer replacements with lignocellulose biopolymers, cellulose and lignin. This study addresses effective isolation of cellulose and lignin from corn stover for sustainable plastic synthesis. Extraction was conducted using an ionic liquid (IL) solvent, Diazo bicycloundec-7-ene (DBU) acetate ([DBUH][-OAc]. Water was added to the ionic liquid mixtures to regulate biopolymer solvation since water swells hydrophilic cellulose, thus competing with ionic liquids. At 10% water, the ionic liquid solvation of cellulose was almost completely inhibited. For pure cellulose, water/IL mixtures impacted rheological properties of viscous melts (<10% water), and structural properties of the regenerated fibers (from viscous melts) were impacted. The reduction of cellulose solvation was reconciled for more complicated lignocellulose (corn residue) systems, aided targeted lignin extractions, improved cellulose crystallinity due to delignification, and tuned the ratio of aliphatic vs phenolic hydroxyl groups in lignin. Water/ionic liquid-treated samples saw a 4:1 aliphatic: phenolic hydroxyl content ratio, while pure IL-treated samples saw a near 1:1 ratio of aliphatic: phenolic hydroxyl content. Water/IL systems also observed increased molecular weights. X-ray diffraction was used to determine cellulose crystallinity; gas permeation chromatography and Phosphorus-31 NMR were used to determine differences in molecular weight and lignin hydroxy content, features that affect lignin valorization for biopolymer use.

Chapter 1 : Problem Statement and Background

1.1 Problem Statement

Polymers have become a ubiquitous feature of our modern world, with their presence in most, if not all, engineering industries. If plastic production continues at its current rate, roughly 1.2 billion tons of plastic will be produced by 2060 (Figure 1-1a). [1–4] The world's reliance on plastic has led to a consequential amount of plastic debris in aquatic environments, soil, and air. On land, it is estimated that over 90% of plastic worldwide is improperly discarded, accumulates in landfills, or is incinerated, with only about 9% of plastic recycled worldwide (Figure 1-1b). [5] Natural degradation processes may take over 400 years to break down polymers like polyethylene (PE), polyethylene terephthalate (PET), and polypropylene (PP), though different polymers have variable degradation kinetics,[6,7] and synthetic polymers often will not degrade into natural materials on their own, but instead will break down into smaller microplastic (MP) particles. [8]

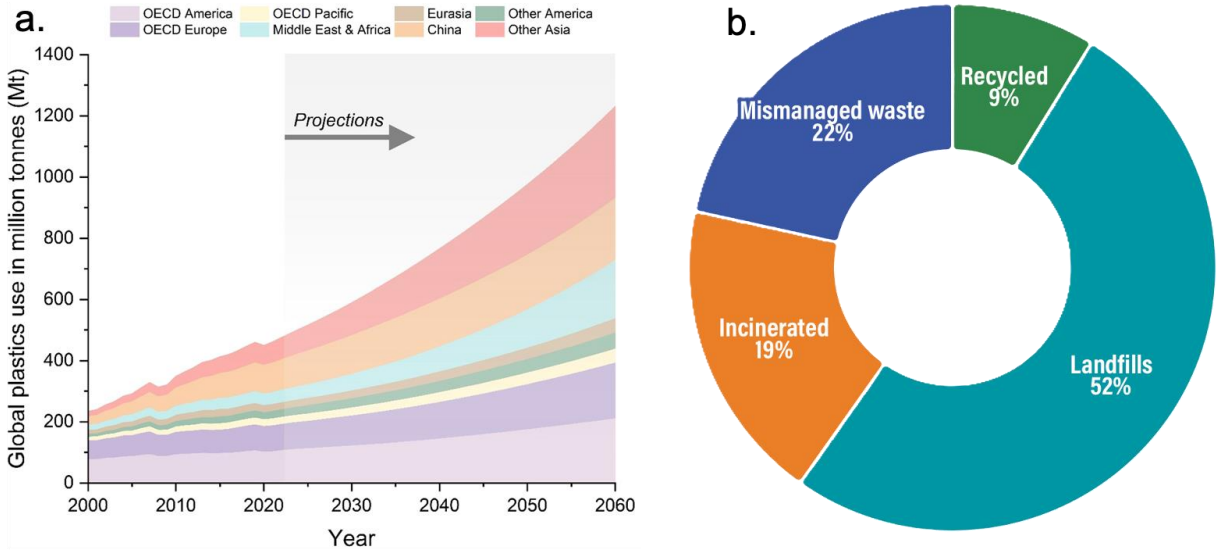


Figure 1-1: Estimates for a. exponential plastic generation projections[9] and b. areas where generated waste ends up.

MPs can be generated from environmental weathering, chemical wear, or physical abrasion.[10] For example, Ultraviolet (UV) exposure from sunlight can break down bulk plastic forms into microplastics through photo-oxidation. In the photo-oxidation process, free radicals are formed from UV exposure, which initiate chain scission in plastic chains. [11] In the automotive industry, polymers in tires release MPs simply from abrasion between tires and roads.[12] Because tires are made with vulcanized rubber, which is heavily crosslinked, they never truly degrade into natural elements.[13] These are only a couple of the countless ways that plastics are broken down into MPs.

Even though many of these consumer plastics start on land, bulk plastics and MPs can end up in aquatic environments through runoff.[14] Research shows that water is one of the primary ways in which MPs are consumed by humans and organisms, with measurable levels of MPs found in blood and tissue, even in fetal tissue. [15–17] Micro and nanoplastics also find themselves taken up through soil, water, and air into the roots and leaves of plants, and from water into aquatic organisms.[18–20] This adsorption of MP particles in most living organisms means that there are multiple pathways for MPs to ultimately find themselves in humans beyond primary exposure. To prevent MP access to humans, they should be collected before finding their way to aquatic environments, or at least before being consumed by humans via drinking water and food. Currently, most industrialized nations regulate and maintain water quality using large industrial-scale purification plants;[21–23] such plants ensure that drinking water is safe for human consumption and that wastewater doesn't present an ecological or human health hazard when emitted into local hydrological systems.

The generation of MPs in the environment is something that can also be addressed during polymer synthesis. Traditionally, the use of petroleum-based chemicals as precursors in polymer synthesis has been widely adopted because their polymer conjugates are lightweight, durable, chemically inert, and the liquid hydrocarbon itself has a perceived ease of access and manufacturability. [24–26] Unfortunately, the chemical inertness of petrochemical polymers makes them a persistent environmental contaminant, which is why bulk plastics degrade into smaller MPs instead of biodegrading into natural elements. [8] Petroleum is also a finite resource, and while plastic production is estimated to only make up 4-6% of the crude oil industry, the depletion of worldwide crude oil for transportation, electricity, and heating has made petroleum usage unfavorable. [27–29]

Lastly, the use of crude oil itself poses several environmental issues, such as marine pollution and greenhouse gas emissions. [30–32]

To address the issue of persistent plastic contamination, bio-based reactant products can be explored for plastic synthesis. For example, in polyurethane (PU) synthesis, castor oil-based reactants are capable of cutting polymer degradation rates in half when compared to traditional crude-oil-based PUs.[33] Natural polymers and their oligomers and monomers can provide environmentally sustainable feedstocks for an increasingly growing class of materials called bioplastics; this bioplastic market is projected to reach 44.8 billion dollars by the year 2030. [34] Natural feedstocks such as seed oils[33], lactic acid[6], sugars and starches[35], amino acids[36], and plant-derived polymers such as cellulose[37] and lignin[38] (from plant materials) can be utilized as bioplastics precursors.

Overall, there is strong evidence for the need for plastic remediation. To address the presence of enduring petroleum-based synthetic polymers in our environment, polymer industries must make advancements both in their cleanup and in their synthesis.

1.2 Strategies for Environmental Remediation

There is undeniable evidence that plastic innovation is needed to address the problems associated with their accumulation in our ecosystems. This work explores two avenues for plastic remediation: MP capture and the extraction of lignocellulose plant materials for eventual bioplastic synthesis.

1.2.1 Microplastic Sequestering Using the Pressure-Sensitive Adhesive, Polyethyhexyl Acrylate (PEHA)

The adhesive-based capturing of MPs has been of interest in the past decade because adhesives serve as effective interfaces for overcoming their random movements in water, which make them evasive to capture during physical MP capturing using surface skimming tools or plastic-gathering robots. [39–45] This renders physical capturing methods ineffective for MP capture on their own. [44,46] Pressure-sensitive adhesives (PSAs) have been studied for MP capture, particularly due to their low glass transition temperatures, Tg, which leads to rapid adsorption and adhesion to irregular MP surfaces. [39]

1.2.1.1 Polymer Adhesion to Pressure-Sensitive Adhesives

Pressure-sensitive adhesives (PSAs) are materials that stick to surfaces by applying light pressure and without any chemical reactions.[47] The pressure required for adhesion is so small that micro- and nanoplastic materials can stick to them with little momentum.[48] Because of this, PSAs have been hailed as a new generation technology for MP sequestering.[39,41] Though MPs adhere readily to PSAs, effective adhesion is needed for efficient MP binding.

Adsorption (or wetting for liquids) describes the interfacial bond between two disparate surfaces and is heavily impacted by the surface energy differences between two materials.[49] Surface energy, γ, is a measure of broken bonds on the surface of a material; in comparison, at the bulk level, there are fewer broken bonds.[50] Surface energy describes a material's potential to interact with another surface to stabilize the energy that is induced due to broken surface bonds. When a low surface energy adhesive interacts with a higher surface energy substrate, the substrate will pull the adhesive via intermolecular interactions to stabilize the high-energy surface.[49] As equilibrium is established to stabilize the substrate surface, higher thermodynamic adsorption is induced, thereby increasing the contact angle between the adhesive and the substrate (Figure 1-2). [51] Polymers typically have lower surface energies (19-50 dynes/cm).[52] This means that, to achieve effective adsorption, the adhesive must have an even lower surface energy than the plastic substrate.

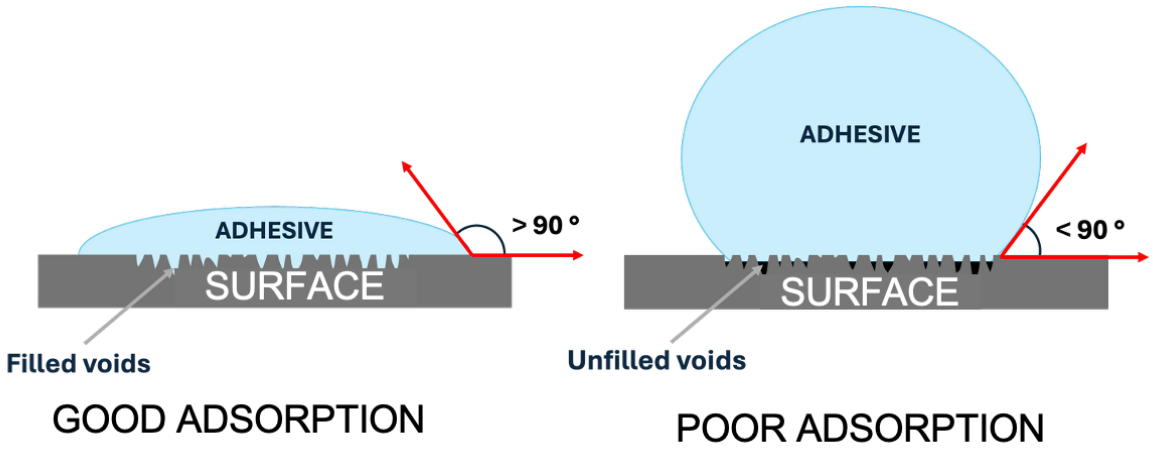


Figure 1-2: Schematic of good vs poor adsorption of an adhesive to a substrate

A few binding mechanisms that have been explored extensively include: mechanical interlocking based on surface topography and roughness, or chemical interactions (covalent and

intermolecular). [53–55] Combinations of these factors may induce improved substrate-adhesive binding. Mechanical interlocking of adhesives by plastic refers to the flow of adhesive into polymer topographical irregularities. Essentially, adhesives are anchored by cracks and pores on the polymer surface. [56] Lastly, chemically crosslinking can be done intentionally to facilitate adherence, while Van der Waals forces and hydrogen bonds may drive intermolecular interactions between polymers and adhesives.[57,58]

1.2.1.2 Polyacrylate Adhesives

Polyacrylate adhesives are promising for MP capture and are a class of vinyl polymers that are made from an acrylate-based monomer that is polymerized via addition polymerization.[59] The base for all polyacrylates is a polyacrylic acid, which makes a polyacrylate monomer by first reacting with an alcohol such as ethyl alcohol or methanol[59]. Once the monomer has been synthesized, it is polymerized using an active initiator that facilitates chain propagation.[60]

The use of polyacrylates in adhesive applications is widespread across many industries because they are highly customizable, cost-effective, and chemically resistant. For example, in the pharmaceutical industry, adhesive hydrogels made from polyacrylate materials can be used for transdermal drug deployment.[61] In the automotive industry, their great impact resistance makes them a vital feature of modern manufacturing; they are used for binding metals, interior/exterior parts, and even electrical components.[62] Lastly, in the packaging industry, they are at the forefront of the pressure-sensitive adhesive market with their use in tapes and protective films to name a few application areas. [63]

Polyethyl hexyl acrylate, P(2-EHA), or PEHA, is a synthetic polyacrylate adhesive that is hailed for its high tack even in water.[40,64] Its low surface energy (~26 dynes/cm) encourages binding to a wide variety of polymers with greater surface energies than the adhesive.[41] Figure 1-3 demonstrates a possible reaction scheme for its synthesis according to Chazovacchi et al. [39]

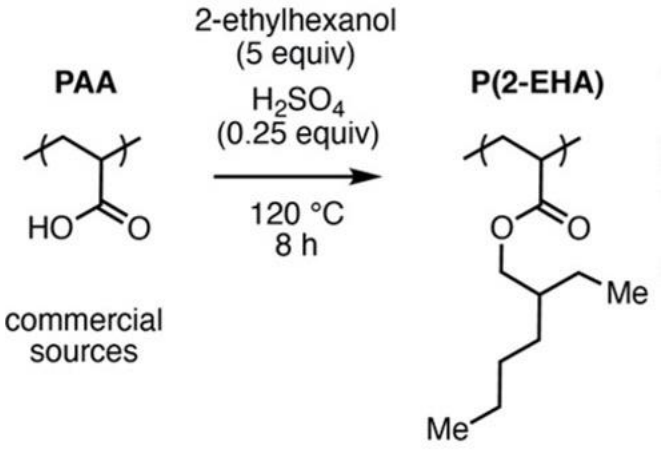


Figure 1-3: PEHA synthesis scheme involving a polyacrylic acid, 2-ethyl hexanol, and a sulfuric acid catalyst

A few factors that may impact effective polymer binding and retention on an adhesive surface include adhesive molecular weight, polymer morphology, polymer-adhesive work of adhesion and surface energy, MP density, the binding environment, and particle momentum.[39–41,63,65,66] The presence of impurities or variabilities in polymeric species may also impact binding behavior.[41] Several of these factors may be at play individually or in combination to reduce or improve MP capturing. For example, Rieland et al.[41] found that a bimodal mixture of 95K and 950K Molecular Weight (MW) PEHA was stable for MP capture, but the presence of fouling agents like debris may reduce adhesion efficacy. This is because fouling agents inhibit binding sites, reducing adsorption efficacy between the adhesive and the polymer. As of 2026, there are very few studies involving adhesive-assisted capturing of MPs in aquatic environments; gaps still exist in understanding what environmental conditions contribute to MP binding onto adhesive surfaces and what MPs may look like in non-idealized systems. For example, Chazovachii et al. [39] and Rieland et al.[41] conducted studies quantifying MP capture using zirconium silicate[39] and glass[41] substrates, though reagent-grade particles were captured, and capturing conditions such as temperature, the presence of other species, and potential MP selectivity based on plastic type have not been studied. The novelty of adhesive-assisted MP capturing means that there are many discoveries to be made regarding MP efficacy for adhesives.

1.2.2 Natural Polymers and Lignocelluloses for Future Biopolymer Synthesis

Polymer remediation may also be accomplished by replacing crude-oil-based polymers with bio-derived alternatives. Lignocelluloses (plant biomasses) are of great importance because they contain the most abundant biopolymers in the world: cellulose, hemicellulose, and lignin (Figure 1-4).[67] Cellulose is the most abundant polysaccharide and the most crystalline portion of the lignocellulose; hemicellulose is an amorphous, short-chain polysaccharide; and lignin is an amorphous, cross-linked component that provides stability to the cell wall.[68–70] Most plants have cellulose, hemicellulose, and lignin in their cell walls, and their abundance means that there is tremendous potential for their extraction and subsequent use in bio-based materials.[71,72]

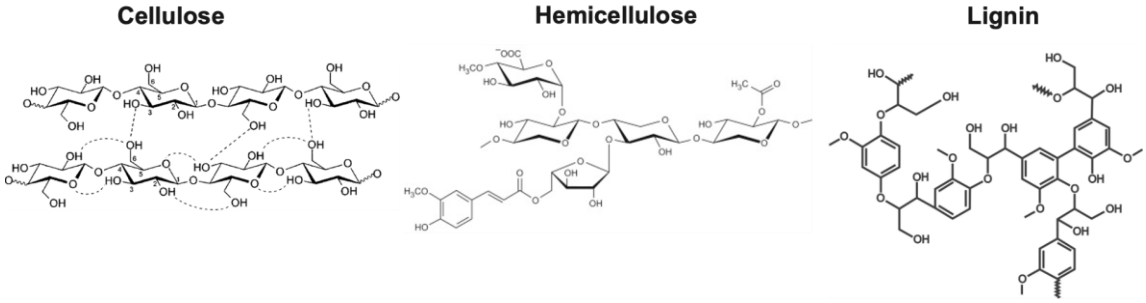


Figure 1-4: Cellulose, hemicellulose and lignin structures

Since different types of biomasses have different concentrations of lignocellulose biopolymers, one can vary the amounts of cellulose and lignin that are isolated by changing the plant type (Table 1-1). Using plant discards is a way to diversify the type of feedstocks that are available without the need for cultivation.[67] It is important to note that farmers still make use of the plant residues as fertilizers and animal feed, though there is an opportunity to increase the value of lignocellulose materials through biopolymer innovations. [73]

Table 1-1: Chemical compositions of lignocellulose plant discards. Adapted from Hassan et al. [67]

Lignocellulose Plant discards	Cellulose (%)	Hemicellulose (%)	Lignin (%)
Corn Stover	43.9	28.9	21.8
Pistachio shell	15.2	38.2	29.4
Spent Coffee grounds	33.1	30.0	24.5
Hemp stalk	52.0	25.0	17.0
Almond shell	27.0	30.0	36.0
Coconut coir	44.2	22.1	32.8
Sugarcane peel	41.1	26.4	24.3
Bamboo leaves	34.14	25.55	35.03

1.2.2.1 Cellulose Structure, Properties, and Applications

Many industries utilize cellulose in their materials due to its abundance, versatility, and its ability to be functionalized (Table 1-2). Cellulose can be used as a precursor material for aerogels, films, and high-performance carbon fibers. [74–77] Cellulose is also used as fiber reinforcements in structural materials, as fillers in cosmetic products, and can be burned for biofuel. Lastly, the polysaccharide is widely used in textile fibers such as rayon and viscose amongst many other applications. [78,79] Of all lignocellulosic biomasses, cotton plant fibers are considered to have the purest form of cellulose (>90% cellulose), and while cotton is a renewable, natural resource, its environmental impacts force us to interrogate the magnitude of its sustainability. [80,81] For example, cotton cultivation requires the use of large amounts of water, and has a non-negligible carbon footprint, which puts a strain on the environment. [82] Finding cellulose alternatives, perhaps from plant discards that do not require cultivation, will be beneficial in evading the problems associated with cotton cultivation.

Table 1-2: Industries that use cellulose and their applications

Industry	Cellulose type	Application
[83]Textiles	Cellulose acetate	Rayon, clothing material; artificial silk
[84]Biomedical	Bacterial cellulose	Advanced wound dressing
[85]Food	Carboxymethyl cellulose	Binder and stabilizer in ice-cream sauces, and gluten free products
[86]Food	Micro-fibrillated Cellulose	Food packaging films
[87]Cosmetics	Microcrystalline cellulose	Thickeners and stabilizers in creams
[88]Pharmaceutical	Cellulose acetate	Inactive ingredient for medicinal coatings and drug release agents
[89]Energy	Native Cellulose (specifically cellulose II)	Biofuel
[1]Construction	Nanocellulose	Binders in particle boards
[90]Stationary	Native cellulose	Paper and packaging materials
[91]Aerospace/Automotive	Native cellulose	Carbon fibers for structural components

Before being used as high-value fibers, cellulose-rich materials must first undergo processing either to extract high-purity cellulose or to break down its highly crystalline structure for ease of subsequent modification.[67] Often, cellulose processing can lead to the disruption of hydrogen bonds between cellulose chains, allowing them to be molded into any desired form; this is true for rayon, a silky cellulose-based material.[79] Rayon is first made by dissolving cellulose into caustic soda to disrupt its native crystal structure.[78] After dissolving and being taken through a series of aging processes, a cellulose solution is formed, shaped, and then taken through an acidic bath to reintroduce hydrogen bonds.[78] Once intermolecular hydrogen bonds are reintroduced between cellulose chains, phase transformations occur in cellulose to a more thermodynamically stable, monoclinic structure known as cellulose II. [92]

The differences between the two cellulose types lie primarily in their hydrogen-bond arrangements, which ultimately determine their characteristic crystal planes and, consequently, their X-ray diffraction patterns. [93] Cellulose I has a doublet that appears at values between 14.5 °-16.5 °, a principal peak that appears between 22°-23°, and a smaller peak between 34°-40° corresponding to the $(1\bar{1}0)$, (100), (200), and (400) crystal planes, respectively (Figure 1-5a).[68,92] Alternatively, regenerated cellulose (cellulose II) has characteristic peaks that occur at 12 °- 13°, and the principal peak from cellulose I splits into two distinct peaks that appear between 20 ° - 23 ° [68,92]. These peaks correspond to the $(1\bar{1}0)$ (110), (200) crystal planes, respectively (Figure 1-5b). [94]

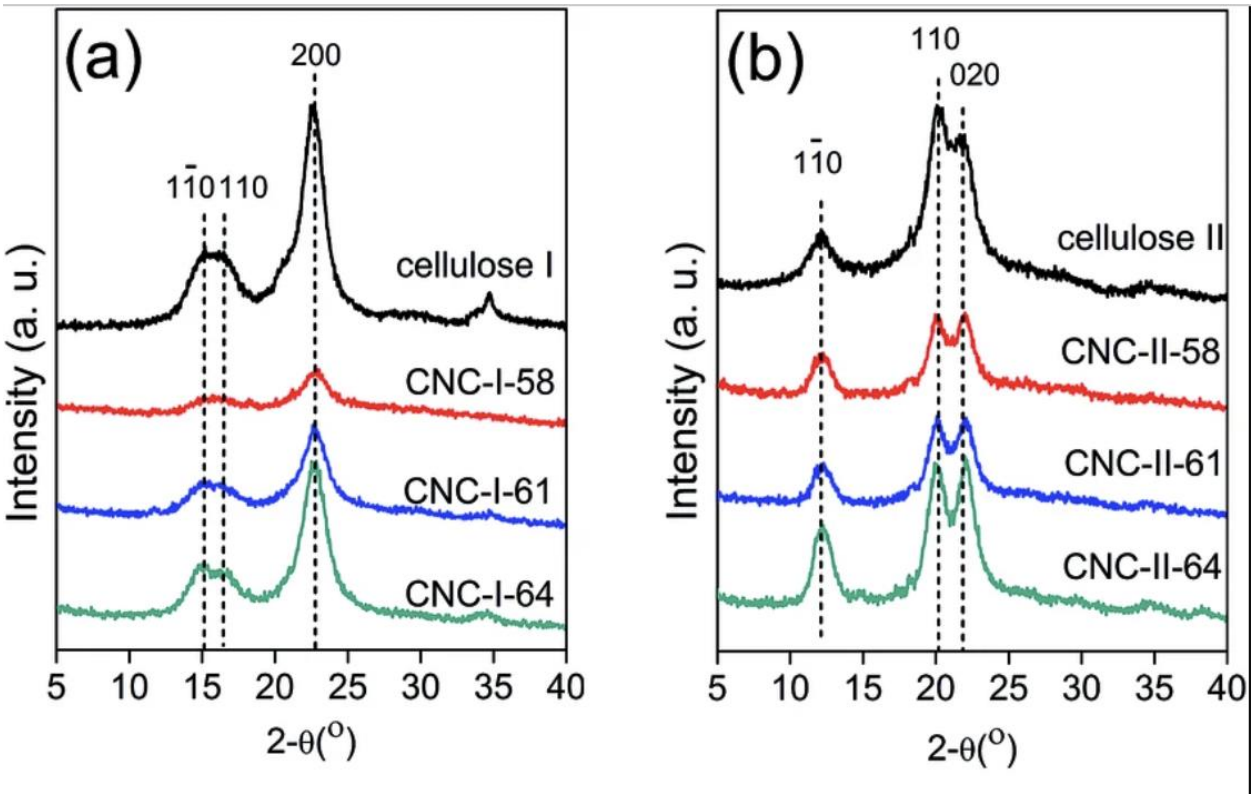


Figure 1-5: XRD patterns for (a) cellulose I and sulfuric acid-treated cellulose I nanocrystals (CNC-I) (58%, 61%, 64%) and XRD patterns for (b) cellulose II and sulfuric acid-treated cellulose II nanocrystals (CNC-II). [94]

In lignocellulose biomasses, harsh processing may also result in an amorphous cellulose XRD spectrum; distinct peaks are muddled due to a broad, diffuse amorphous halo that overlaps with characteristic cellulose peaks (Figure 1-6). [95] Alternatively, mild treatments that do not disrupt the

cellulose structure may improve cellulose crystallinity by removing amorphous lignin and hemicellulose components that may muddle cellulose crystallinity (Table 1-3).

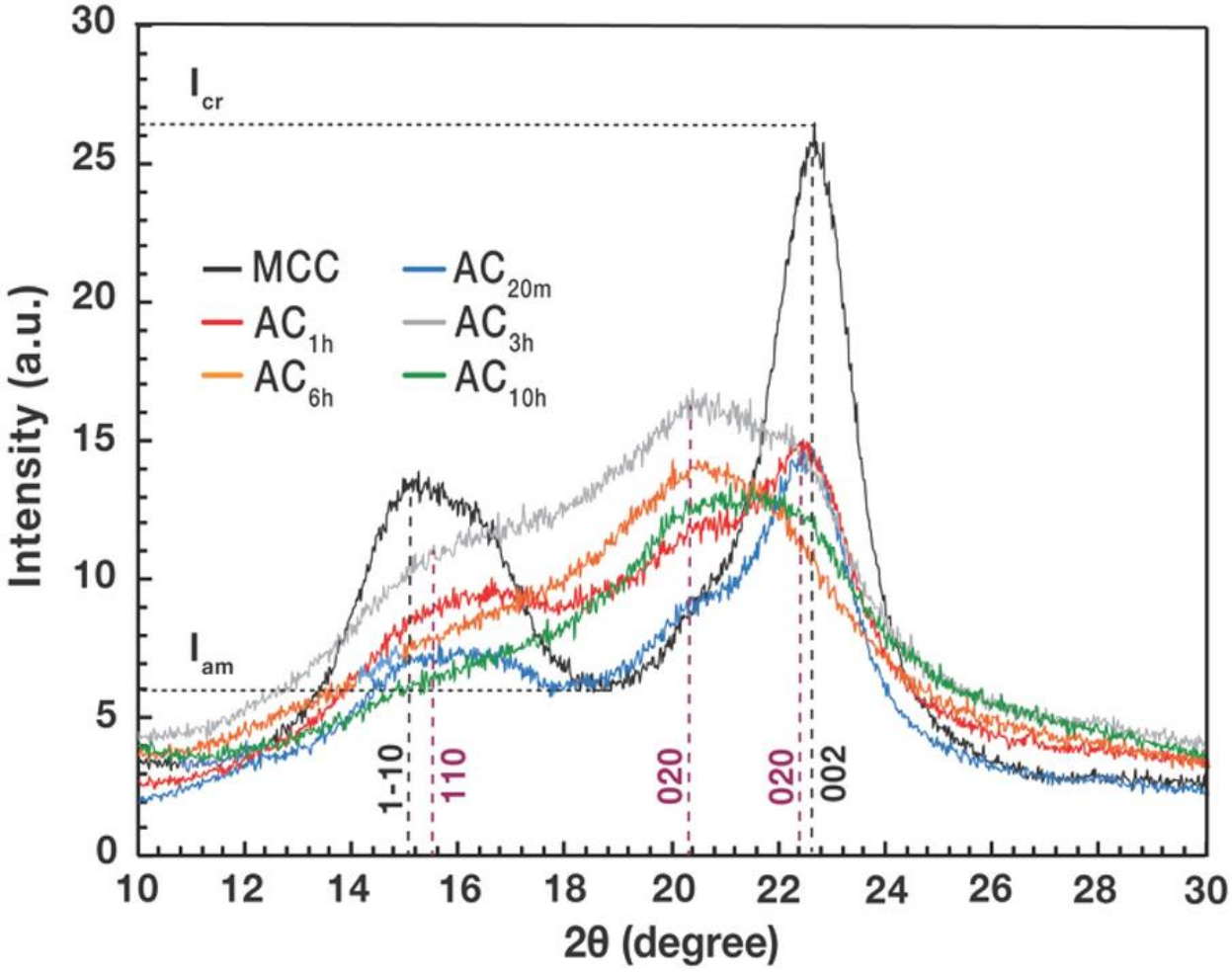


Figure 1-6: XRD diffractograms of untreated microcrystalline cellulose (MCC) and amorphized celluloses (Acs) obtained from different Ionic Liquid treatment durations. From the diffractograms, the fundamental peak (representative of the (002) lattice plane) consistently shifted with increasing IL treatment. Appearance of (020) (shifted peaks) and (110) lattice planes indicated the transformation of cellulose I to cellulose II. [96]

Table 1-3: Examples of delignification treatments that improve biomass crystallinity

Treatment	Biomass	%Crystallinity of untreated biomass	%Crystallinity of mildly treated biomass
[97]Lacasse Enzyme Treatment	Wheat Straw	26	28.6
[98]5% Sodium Hydroxide	Corn Stover	21.6	26.5
[99]Acid-Alkali Treatment (2% NaOH)	Palm Biomass	25.9	62.9
[100]Microwave-assisted [TEA][HSO_4] Ionic liquid	Corn Stover	45	57.2

1.2.2.2 Hemicellulose, Structure, Properties, and Applications

Hemicelluloses are bound to cellulose via strong hydrogen bonds and to lignin via covalent bonds, acting as a structural bridge between the two components.[101] The most popular methods for hemicellulose extraction are alkaline treatments, like sodium hydroxide (NaOH) extraction, and Liquid Hot Water (LHW) treatments.[102,103] In alkaline treatments, ester and ether bonds are broken between lignin and hemicellulose, dissolving the hemicellulose from the cell wall. The hemicellulose is primarily solubilized and extracted, but not depolymerized. In hydrothermal LHW pre-treatments, which occur in a contained vessel at high temperatures (130 -240°C), hemicellulose is rapidly depolymerized into oligomers (xylooligosaccharides), sugars (xylose - the most abundant, mannose, galactose, glucose, arabinose, and uronic acids), organic acids, and furfural.[104] In LHW reactions, the acetyl groups in the hemicellulose backbone are cleaved via highly reactive hydronium ions (H_3O^+) that are formed at elevated temperatures.[105]

Hemicelluloses are a class of polysaccharides that are often overshadowed by lignin and cellulose counterparts due to low utilization. [101] However, in recent years, hemicelluloses have been used as renewable feedstocks for biobased chemicals, biomaterials, and fuels.[101,106,107] For example,

hemicelluloses can be hydrolyzed into sugars to create commercial sweeteners such as xylitol. The sugars that are made from hydrolyzed hemicellulose can also be used to produce alcohol by fermentation and sorbitol by reduction, which is used in cosmetics and food applications. [106] In addition, xylooligosaccharides are widely used in the pharmaceutical field as prebiotic carbohydrates [108] and have been hailed for their reduction of cholesterol levels, antioxidant properties, and gastrointestinal benefits.[109] Lastly, highly reactive hydroxyl groups make biopolymer synthesis from hemicelluloses possible, though their biopolymers are highly hydrophilic and lack strength due to hemicelluloses' short chain, non-crystalline structure.[110] Through hydrolysis, hemicelluloses can be separated into the liquid stream, thereby leaving the biomass cellulose and lignin-rich.

1.2.2.3 Lignin Structure, Properties, and Applications

Lignin is nature's most abundant aromatic polymer and is found in the plant cell wall, serving as a type of glue that holds the cell wall together. [111] Lignin is mostly bonded to hemicellulose via secondary bonds and covalent, complex lignin-carbohydrate networks. [112] Because of the abundance of aromatic and aliphatic hydroxyl (-OH) groups in lignin, it has gained traction as a reactant material for polymers such as polyurethanes and epoxies that are synthesized with hydroxyl-based reactants [108–112113–117](Figure 1-7). [100–104] To address the reality that petroleum-based raw materials still dominate the polymer synthesis space, the replacement of petroleum-based, hydroxyl-rich reactants with abundantly available lignin is a way to make the market greener.[24]

Polyurethanes are a versatile class of materials that have both thermoset and thermoplastic conjugates.[118–120] They are hailed for their simplicity of production, durability, chemical resistance, and market versatility. [121] They also come in many forms and can be used as coatings, foams (mattresses, shoes, insulation materials), and cast plastic materials. [121–123] In PU synthesis, polyols are reacted with diisocyanate, and the resulting polymer contains a polyurethane bond (Figure 1-7)[124]. Due to this simple reaction scheme, many types of PU materials may be synthesized, though polyether and polycarbonate polyols, most of which are petro-based, dominate the polyol world. [125] To offset petrochemical use, Gondaliya et al. [109] and Acquah et al. [113] have reported the

integration of ligin in PU synthesis for flexible foams. Both studies report improved mechanical strength, thermal stability, and biodegradability, and found that aliphatic hydroxyl-rich lignin tends to be more suitable due to low steric hindrance with isocyanates and the presence of stable aromatic structures in lignin. [126]

Epoxy is another class of material that benefits from lignin's structural stability. They are common thermosetting materials that are used for a wide variety of applications, like protective coatings, bonding resins in the marine and automotive industry, or encapsulation resins for electronics.[127] Epoxy is used in applications that require durable, heat-resistant, and waterproof polymers.n[128,129] Bisphenol-A-based epoxy is one of the more common epoxies and is made by reacting bisphenol-a with epichlorohydrin in the presence of a sodium hydroxide catalyst. [113,130] Biobased epoxy can be synthesized by lignin replacements of bisphenol-A. For example, Nikafshar et al. [113] has shown that low MW phenolic-OH-rich lignin is ideal for almost-complete bisphenol A replacement due to their similar aromatic structures. The resulting polymer had comparable thermomechanical performance to traditional epoxy.

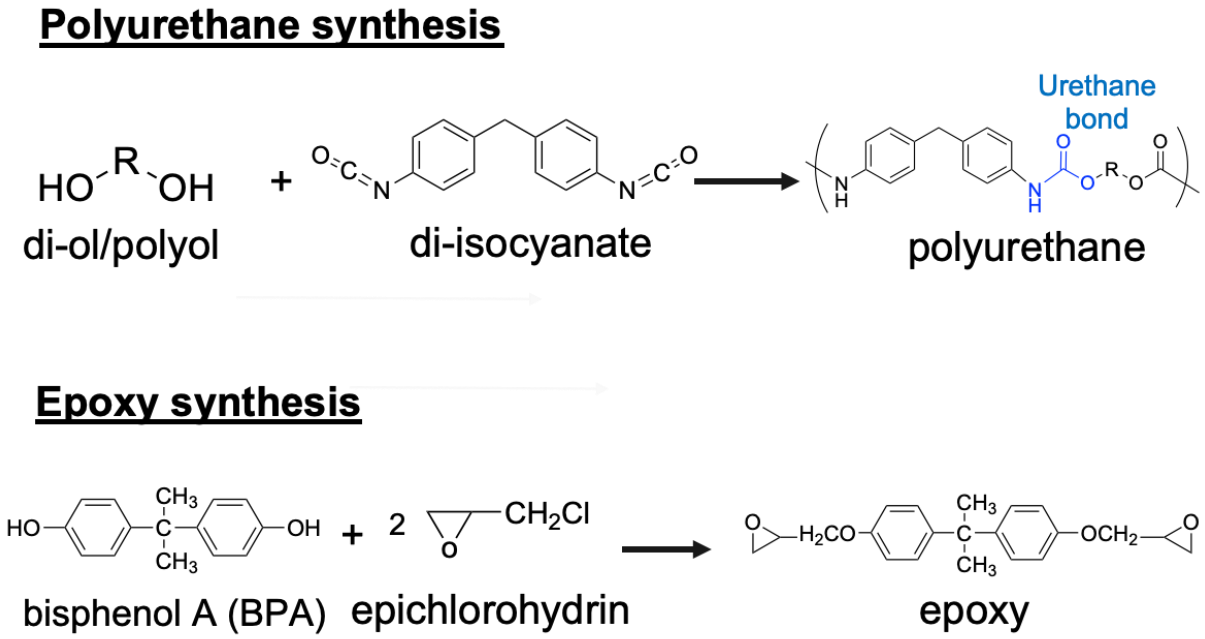


Figure 1-7: Schemes for polyol-based synthesis of polyurethanes, epoxies, and phenol formaldehyde. Polyurethanes involve the polyaddition reaction between a polyol and a polyisocyanate. Bisphenol A epoxies are synthesized using bisphenol-A and epichlorohydrin.

Lignin has also been explored as a precursor for carbon fiber materials due to its high carbon content (~60%).[131] Carbon fibers are typically petroleum-derived, with polyacrylonitrile (PAN) leading the carbon fiber industry, accounting for 90% of global carbon fiber production. [132] PAN-based carbon fibers are made by first polymerizing acrylonitrile, then forming it into thin filaments. The thin filaments are then stabilized in an oxygen-rich environment (200°C to 350°C) to induce the formation of a more thermally stable bonding pattern. Afterwards, the oxygenated fiber is carbonized at 1,000-3,000° C to remove non-carbon components and to form tightly bonded carbon crystals. [133,134] PAN carbon fibers are hailed for their low weight, high strength, high thermal resistance, and cost effectiveness, and lignin precursors are capable of reducing costs while meeting performance requirements for filtration systems, automotive applications, and as graphite electrode reinforcements, according to the U.S Department of Energy.[135] Carbon fibers can be produced via melt spinning, [136] wet spinning, [137] and electrospinning, [138] though lignin's heterogeneity and highly branched structure present a challenge for carbon fiber development

because more linear structures are preferred.[139] To mitigate this issue, modifications via fractionation and chemical treatments, and blending with PAN materials have been explored. [140]

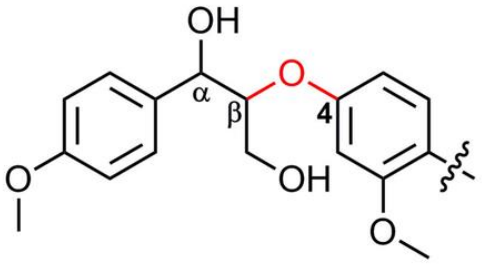


Figure 1-8: Simplified schematic of a lignin dimer with a β-O-4 linkage

In the paper industry, lignin is an abundant natural byproduct[141]. During Kraft processing, lignin is separated from wood fibers, yielding two main biomass streams: cellulose fiber and a waste, lignin-rich stream, called "black liquor." [142] Before the 1980s, most extracted black liquor was burned at paper-making mills to recover steam and energy for mill use.[141,143] On the other hand, the incorporation of lignin as a bio-based feedstock for polymers has become much more pervasive in the 21st century. [143,144] Lignin β -O-4 linkages account for 40-60% of bonds in the lignin structure[145] and these β -O-4 linkages (Figure 1-8) can be cleaved to extract lignin and increase hydroxyl content. The resulting lignin from β -O-4 cleavage is rich in phenolic hydroxyl groups and has a lower MW. Lower MW fractions of lignin are preferred because the fragmented chains correspond to higher hydroxyl exposure. [146–148] To specifically isolate the low-MW and homogeneous fractions of lignin, post-extraction membrane separation, pH-based separations, and solvent-based isolation methods have been studied. [149–151]

Table 1-4: Delignification Methods and Lignin Properties

Delignification Method	Biomass	Treatment conditions	Lignin Properties	Hydroxyl Content (mmol/g)
[152]Organosolv	Hardwood (birch) Softwood (spruce)	182 °C; "50-60% ethanol content" ; 60-100 min	High purity; Spruce MW 603-1657 Da; Birch MW 587-1100 Da; Extensive β- cleavage	Birch: <4 ; Spruce: <4; Phenolic-rich
[153]Kraft	Eucalyptus Wood	170 °C; 50-90 min	Mn = 2370-2440 Da; Mw = 3490-4340 Da; Extensive β-O-4 cleavage	<2.20 aliphatic; <2.05 phenolic
[154]Ionic Liquid 1-butylimidazolium hydrogen sulfate [HC4im][HSO4]	Miscanthus giganteus	182 °C; 80% IL: 20% H2O; 1-24 hours	Lignin-Carbohydrate complexes under 5 hours; Thorough β-O-4 cleavage	1 h: <5, Low phenolic; 12 h: <11, High phenolic
[155]Microwave Assisted Ionic Liquid [Emim][OAc]	Hardwood lignin (poplar)	110-170 °C; 1-16 hours	Conservative β-O-4 cleavage; Mn = 1310-2200 Da; Mw = 2890-4090 Da	150 °C, 1 hr: Phenolic OH = 4.81; 170, 1 hr °C: Phenolic OH = 3.66

The concentration of homogeneous, hydroxyl-dense, low-MW lignin can be altered by the processing conditions. [146–148] For example, Organosolv lignin is derived from a milder extraction process involving a hot organic solvent (ethanol, methanol, butanol), and is sometimes paired with

low-concentration acids (acetic acid, sulfuric acid, hydrochloric acid) in a sealed pressure vessel to precipitate lignin. [156] Organosolv lignin is a higher-purity lignin, which makes its valorization much easier, though it is still characterized by its high heterogeneity[156–159]. Ionic liquids are also useful for delignification[146,160] . Table 1-4 compares popular delignification pathways, the types of biomasses involved, and their effect on lignin properties.

Hydroxyl groups in lignin can either be aliphatic, showing up on carbon-carbon chains, or phenolic, showing up on one of lignin's aromatic monomer groups: syringyl (sinapyl alcohol), guaiacyl (coniferyl alcohol), and p-hydroxyphenyl (p-coumaryl alcohol), or a carboxylic acid. [113,122,161,162] The presence of aliphatic (primary and secondary) and phenolic (aromatic) hydroxyl groups determines the valorization pathways for lignin. [162] For example, lignin with a high content of primary aliphatic hydroxyl groups is most reactive for polyurethanes, while lignin with high phenolic concentrations is most effective for epoxies and phenolic resins.

Oftentimes, the plant type determines what aromatic lignin monomers are available for extraction. [163–165] While plants may have some level of phenolic syringly, guaiacyl, and hydroxyphenol units (Figure 1-9), the plant type determines which hydroxyl groups dominate. For example, hardwood biomasses have a high syringyl to guaiacyl ratio, softwoods have high guaiacyl content, and hydroxyphenols show up in trace amounts in both plant types.[166] In comparison, grassy or herbaceous plants like corn stover have all 3 aromatic lignin types. [167]

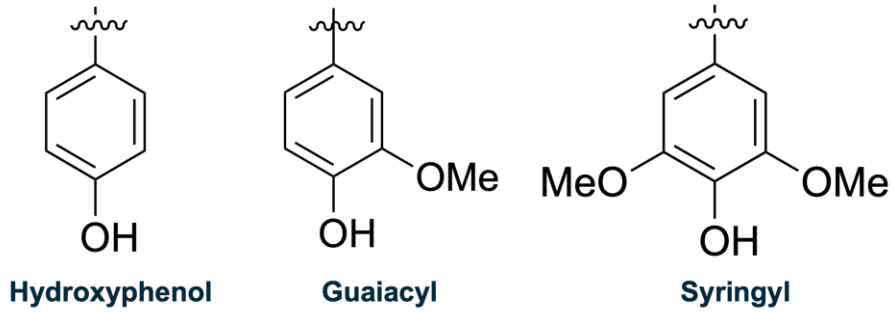


Figure 1-9: Phenolic lignin unit structures: hydroxyphenyl (H-unit), Guaiacyl (G-unit), and Syringyl (S-Unit)

Structurally, the two methoxy groups on syringyl cause it to be less densely packed than guaiacyl, which has only one methoxy group, and hydroxyphenol, which has no methoxy groups. [168] Due to

low packing density, syringyl groups tend to be easier to extract and may be more susceptible to mild extractions. [169] Due to a lower condensed structure, syringyl groups can be useful for thermoplastic materials that require flow for melt processing. [170] Overall, processing can either change the ratio of aliphatic vs phenolic groups and/or alter the ratio of phenolic monomers conveyed into the lignin stream. [171]

1.2.2.4 Ionic Liquids and Liquid Hot Water Treatments for Efficient Biomass Fractionation

Lignocellulose components are extremely commingled in the cell wall, which makes their individual isolation difficult, though the effective use of these bioproducts relies on their efficient separation. [172–174] Ionic liquids (ILs) have been explored as lower temperature separation media for their ability to efficiently isolate lignin and cellulose-rich components through delignification. [172,173,175] ILs are composed of organic and inorganic cations and anions that are stable at room temperature and have melting points that typically do not exceed 100 °C. [176] Most importantly, given the rich organic chemistry that can be used to form these ionic structures, their properties, such as melt temperature and solvent extraction potential, can be tuned by altering the organic chemical makeup of the cationic and anionic constituents.[177,178]

Protic ionic liquids are liquid salts formed by the deprotonation of an acid by a superbase. They are often formed from the acid-base neutralization of organic superbases (Bronsted bases, or proton acceptors) with constituent acids (Bronsted acids, proton donors). (Figure 1-10). The products from the reaction include both the organic IL salt and usually water or some other small molecule. Superbases are organic compounds that have a high affinity for proton capture, which makes them ideal for secondary hydrogen bond displacements. [179] During the acid-base reaction, the superbase readily deprotonates the acid constituent, leaving a reactive anion. [180–182] The mechanism for bond breaking in Superbase-Carboxylate ionic liquids has not been explored extensively, but it is generally accepted that ionic liquids made with carboxylic acids are very efficient at lignin extraction due to their dual H-bond and β-O-4 linkage breakage characteristics. It is also known that for protic ionic liquids, both the anion and the cation participate in bond breaking. [183–185]

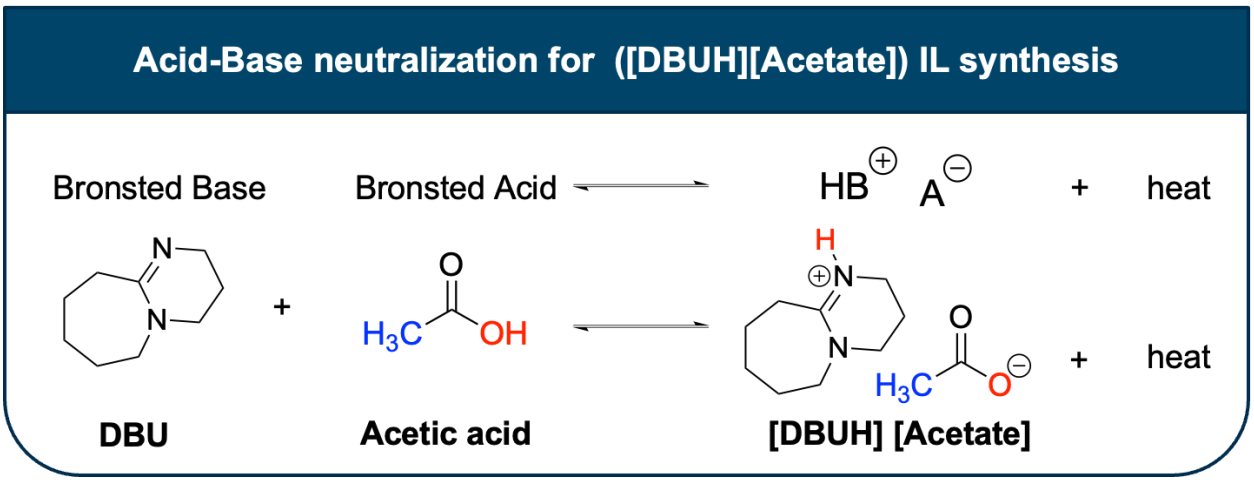


Figure 1-10: Protic Ionic liquid synthesis (acid-base neutralization reaction) using Diazabicyclo [5.4.0]undec-7-ene acetate, [DBUH][Acetate], synthesis as an example.

Delignification occurs through the interruption of the secondary and covalent bonds between and within cellulose, hemicellulose, and lignin, and the breaking of β-O-4 linkages in lignin. Other inorganic molten salts might function to swell the biopolymer for delignification, but their melt temperatures are so high that the organics decompose before the inorganic salts actually melt. [186–188]

Figure 1-11 shows a few types of the many acids and superbases that can be used to make ILs that facilitate lignocellulose extraction. Some of these superbases include Diazabicyclo [5.4.0]undec-7-ene (DBU), imidazole-based superbases like ethyl-3-methylimidazole (EMIm), 1-butyl-3-methylimidazole (BMIm), 1-alkyl-3-methylimidazole (Mim), and pyridine. [189–191] Bronsted acids can be any array of proton donors, like acid halides, sulfuric acid, and carboxylic acids. [192–194] Technically, any acid should work, but reducing potential side reactions of the remaining organic molecule will aid in the stability of the formed product. The possibilities of ILs that can be made by modifying the acid and base substituents are extensive, and some are more widely available based on the cost and accessibility of acquiring the starting constituents.

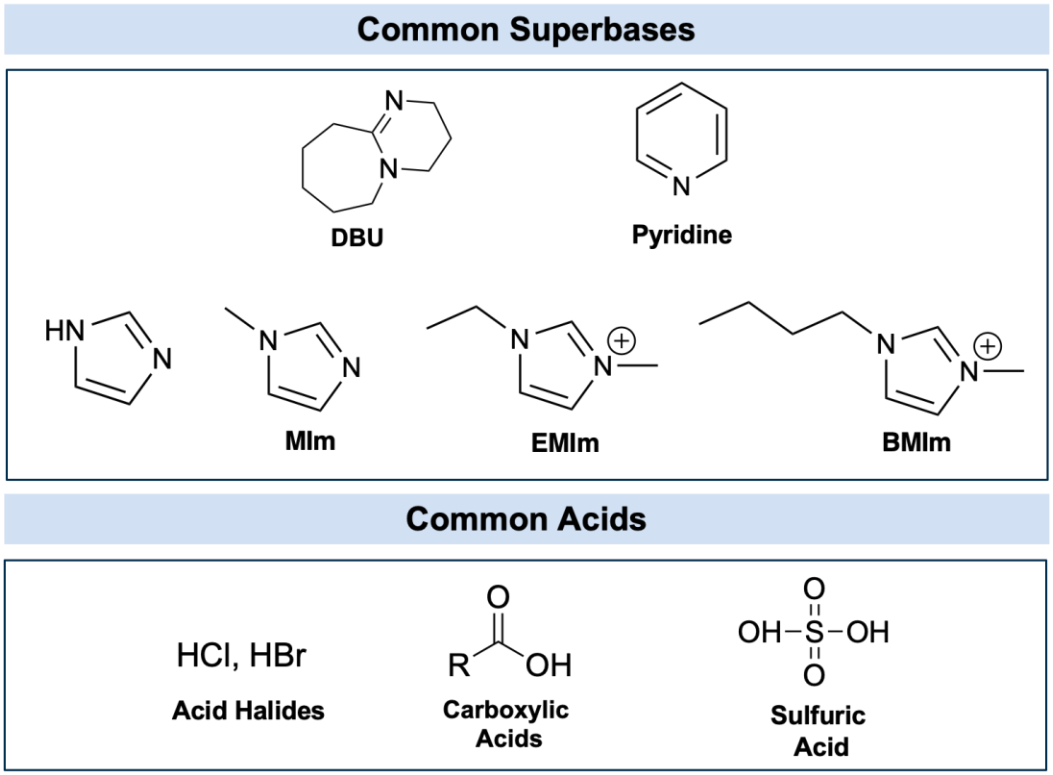


Figure 1-11: Common superbases and acids used in Ionic Liquids for lignocellulose extractions

The easier the IL can diffuse into the lignocellulosic structure and swell the components, the more effective the IL can be, so working in the melt and reducing the viscosity of the IL will facilitate reaction, but too high a temperature can contribute to side reactions that can degrade both the lignocellulose and the IL.[195]

Cellulose is considerably tractable to acetic acid-based ILs when exposed to the molten liquid at modest temperatures (60- 120 °C).[81,196,197] Cellulose chains are held primarily by hydrogen bonds, so they are susceptible to IL hydrogen bond displacements (Figure 1-12). [198] After hydrogen bond displacements using molten ILs, viscous IL/cellulose solutions are produced that vary in viscosity depending on the biomass loading in solution. These solutions can then be shaped to a desired form. [199,200]

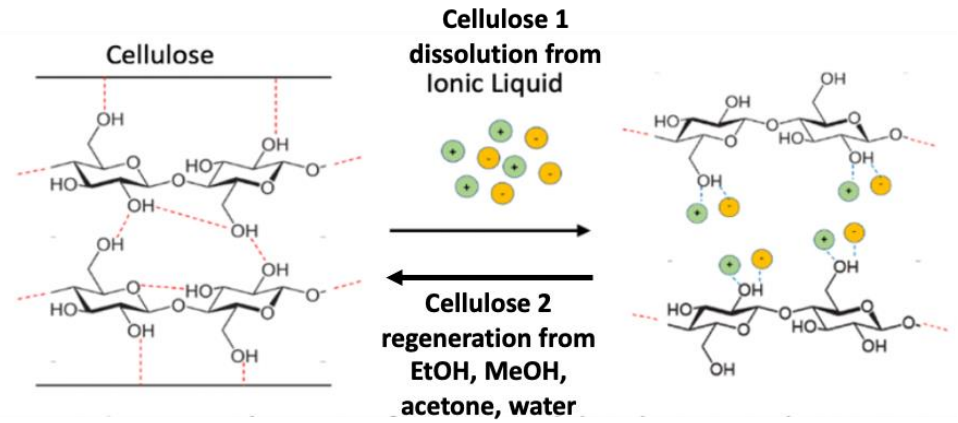


Figure 1-12: Schematic of cellulose dissolution and regeneration mechanism via Ionic liquid hydrogen bond displacements. Cationic substituents interact with partially negative oxygen groups while anionic substituents interact with partially positive hydrogen groups, separating cellulose chains.

After dissolution in IL and shaping, dissolved fibers of cellulose and other lignocellulose residues can be coagulated via regeneration. During regeneration, IL ions hydrogen-bonded to cellulose chains are displaced by an anti-solvent, or mixtures of anti-solvents, such as water, acetone, ethanol, or methanol.[194] These polar solvents resupply hydrogen bonds to the cellulose structure, resulting in their precipitation in aqueous or polar solvent/IL mixtures. The precipitation results in the more thermodynamically stable, monoclinic cellulose II structure [77]. A study from Kirchberg et al.[201] found that the coagulation medium of choice has a major effect on the quality of precipitates. After soaking a 4%/IL solution for 2 hours, this study revealed that ethanol and methanol yield fibers with the most structural integrity. [201]

Ionic liquids delignify lignocellulosic structures by cleaving interconnected β-O-4 aryl ether bonds found in lignin. [183,202] Depending on the processing time, those β-O-4 cleavages result in depolymerization and lower molecular weight oligomers. The extent of β-O-4 linkage bond breaking can be impacted by a variety of factors, including temperature, the IL viscosity, the acid and base strength, and the extent of dissociation between the acid and superbase.[203]

For example, mechanistic insights into imidazolium hydrogen sulfate [C_3SO_3HMIM][HSO_4] IL show that strong acid Ionic liquids are efficient at β-O-4 cleavage. Both the imidazolium ion and the deprotonated sulfate anion participate in β -O-4 breakage via a proposed 5-step process: 1. Protonation-dehydration, 2. β-H elimination, 3. Protonation, 4. Hydroxylation, 5. Then 5. β-O-4

bond cleavage (Figure 1-13). [193] Not much is known about the β-O-4 linkage breakage mechanism for carboxylic acid-based ILs, but studies have shown them to be effective for lignin extractions due to dual hydrogen-bonding and β-O-4 cleavage capacities. [204] Overall, efficient delignification will be essential for effective biopolymer extractions from lignocelluloses and subsequent biopolymer synthesis.

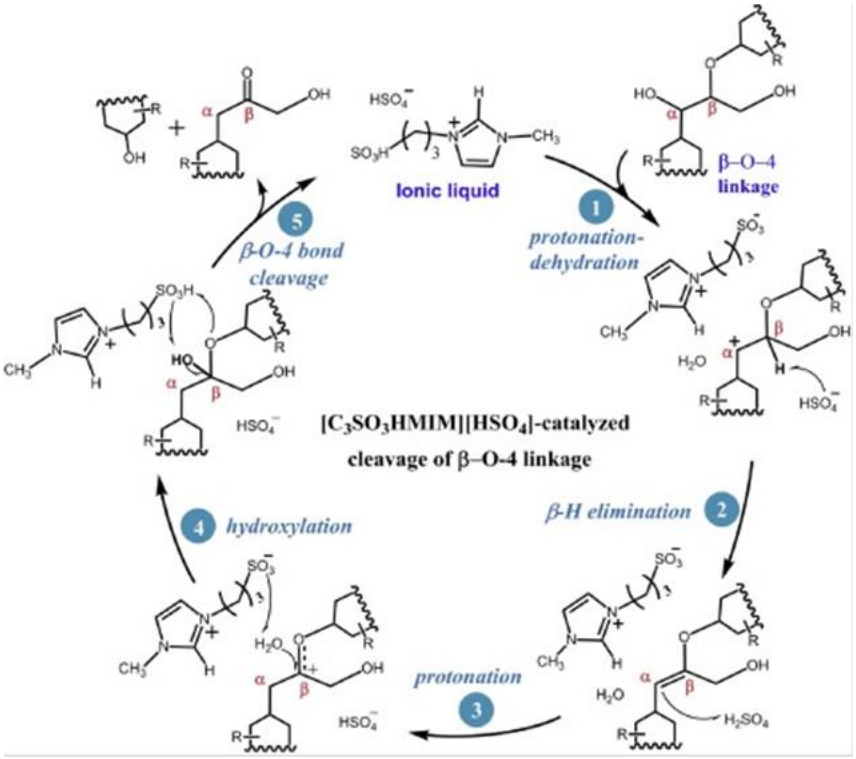


Figure 1-13: Proposed mechanism for [C_3SO_3HMIM][HSO_4] cleavage of β-O-4 bonds.[193]

1.3 Research Scope and Research Aims

This dissertation explores two avenues for plastic remediation: MP capture, which represents discards left to degrade in the environment, and the extraction of lignocellulose components, to reduce the demand on petroleum by providing biological materials for polymer synthesis

It is important to note that plastic remediation is an ongoing feat that requires both technological solutions and policy updates to fully manage their afterlife, but my goal was to do a deeper study into two distinct areas: one in which I investigate how capturing environment impacts PEHA-assisted isolations of MPs, and another in which I make use of ionic liquid/water technology to improve the efficacy of lignocellulose extractions of cellulose and lignin for potential use in bioplastic materials.

1.3.1 Study 1: MP Sequestering Using Polyethyl Hexyl Acrylate Pressure-Sensitive Adhesives

In Chapters 2 and 3, a bimodal mixture of 92k and 950k Molecular Weight (MW) PEHA was prepared and used for Microplastics (MP) capture, and both chapters assess how the capture environment impacts effective adhesive-assisted MP capturing. The polyethyl hexyl acrylate (PEHA) adhesive is a high-tack pressure-sensitive adhesive that can attach to low surface energy substrates, even in water, making it an ideal candidate for MP capture in aquatic environments. In Chapter 2, MP collection was conducted at an MP generation source, a simulated laundering environment. MPs were captured onto PEHA-coated glass slides in a dilute detergent additive to assess how MP capturing was affected in laundering systems. Gravimetric analysis, probe tack, and functional assessments of MP-capturing efficiencies were conducted to understand which factors affect MP-capturing in laundering environments. Chapter 3 assesses short-term (1-minute) PEHA exposures to two types of dispersions: monopolymer (single polymer dispersions) and multipolymer (mixed polymer) dispersions of HDPE, PETE, and PP. A Keyence optical microscope was used to capture images of foam substrates post-MP capture, and capture efficiency and particle size distributions were gathered using the FIJI Trainable Weka Segmentation plugin which is capable of distinguishing between polymers on the basis of color and texture. Chapter 2 shows that, in the presence of amphiphilic detergents, MP capturability is drastically hindered.

Chapter 3 shows that multipolymer dispersions facilitate more efficient capturing due to the presence of multiple bonding mechanisms.

Research Aims

1. MP remediation in laundering systems using pressure-sensitive adhesives and the impact of surfactants on capturability
2. The effect of single-polymer and multipolymer dispersions on pressure-sensitive adhesive sequestering of MPs

1.3.2 Study 2: Exploring Biopolymer Extraction Using Ionic Liquids

Chapters 4 and 5 explore cellulose and lignin processing using diazobicycloundec-7-ene (DBU) acetate ([DBUH][Acetate]), an ionic liquid that is made from a 1:1 molar ratio of diazobicycloundec-7-ene (DBU) and acetic acid. In both chapters, water was added to the ionic liquid to regulate cellulose solvation (Chapter 4) and lignin extraction from corn stover (CS) (Chapter 5). In Chapter 4, solvation efficiencies were analyzed as functions of time and water content, viscosity assessments were done using a TA Instrument ARES—2 rheometer, and regenerated fiber properties were assessed by optical imagery and tensile testing. In Chapter 5, extraction efficiencies of lignin were conducted, and thermal and structural properties of lignin were assessed using Thermogravimetric Assessment (TGA), Gas Permeation Chromatography (GPC), and Phosporous-31 NMR (^{31}P-NMR). Both studies show that water can be used to tailor solvation capacities for cellulose and lignin and may impact their thermal and structural properties. With water, cellulose solvation reduces after only 5% water in the ionic liquid, and undissolved fibers remain in solution, which impacts the rheological properties of cellulose/IL slurries and increases regenerated fiber roughness. In Chapter 5, the reduction in cellulose solvation in Chapter 4 was remediated for targeted lignin isolations. Both studies show that water can be used as a low-cost solvent for regulating IL processing.

Research Aims

1. Using water to regulate ionic liquid solvation and fine-tune the rheological behavior of dissolved cellulose
2. Effect of water on ionic liquid-mediated lignin extraction from corn stover

Chapter 2 : Microplastic Remediation in Laundering Systems Using Pressure-Sensitive Adhesives and the Impact of Surfactants on Capturability

2.1 Introduction

Laundering of synthetic fabrics is a common entry point for textile-derived Microplastics (MPs) into wastewater systems.[206–208] Researchers estimate that 14 million tons of microfibers from textiles are released into the world's oceans yearly, accounting for roughly 35% of the world's MP pollution; laundering MPs make up about 93.7% of all textile MPs. [209,210] MPs are an enduring environmental contaminant with conservative estimates of their lifetimes measured in centuries.[6] Fortunately, existing water treatments have shown high efficacy (>95%) in removing MPs from water, but they remain co-located with sludge. [21,207,211] The small size and heterogeneous composition of MPs make purification a significant challenge, hindering recycling and remediation efforts. In addition, continued environmental breakdown of MPs has led to 'nanoplastics', which can escape existing filtration technologies.[6,212,213] Of particular concern, there is growing evidence of long-term impacts on human health, with measurable levels of MPs found in blood and tissue, including fetal tissue. [16,17816,19016,20916,214] Thus, the development of isolation schemes that purify water is needed to help solve the growing proliferation of MPs in aquatic environments.

Contributions: This chapter is a subset of work that is published in Environmental Pollution. I did experimental work, the analysis, and made inferences tied to the modeling work that was also included. Details on modeling work can be seen in Timothy Jugovic's thesis titled: Advances in the Modeling of Synthesis, Design, and Properties of Polymers[205].

Lawal, T. D.; Jugovic, T.; Josephs, G.; Zimmerman, P. M.; Love, B. J. Surfactants Can Compete with Microplastics for Surfaces Using Adhesives as Substrates for Microplastic Sequestration. Environ. Pollut. Barking Essex 1987 **2025**, 364 (Pt 2), 125372. https://doi.org/10.1016/j.envpol.2024.125372.

Studies have shown that the filtration technologies used by these wastewater treatment plants (WWTP) have high, sometimes as much as >99.9%, separation efficacy for MPs. [208,215,216] However, these separated MPs are commingled, both with many types of plastics but also biosolids from marine environments. [19,217,218] As such, targeted site applications (such as at the washing machine effluent into the wastewater drain) where collections of MPs exist in relatively high quantities and with lower secondary contaminant concentration are an area of intensive academic and industrial research.[94,95]

In recent years, several filters have been proposed to reduce MP emission in laundry effluents at the individual consumer level. These technologies can largely be described as either porous bags or solid filters, which can contain MPs inside, while being permeable to water, or as pronged balls designed to entangle MP fibers in their geometric structure during the wash cycles. [221] Alternatives, such as in-line filtration and adhesive technologies, have yet to be comprehensively integrated into new laundry machines at the commercial level. [219–221] For in-line filtration, the required regular maintenance and the continued issue of commingling of MPs mean that the remediation of such household level waste remains cost-ineffective.

To consider MP collection in real dispersions, pressure-sensitive adhesives (PSAs) have demonstrated reasonably efficient extraction and purification of MPs from aqueous media. [39,41] Previous efforts have shown that, under pure water conditions, capturing efficiencies of >90% can be realized using poly-2-ethyl-hexyl acrylate (PEHA) PSA. [39] Proposing an adhesive as a binder for MPs in laundry machines is challenging because capturing efficiencies can also be impacted by the chemicals in detergents. Previous research has already shown that impurities such as salts and clays have reduced capturing efficiencies in aqueous systems. [41]

A few ingredients found in commercially available laundry detergents that could interfere include glycerol (solvent), sodium citrate (pH adjustment and softener), and tergitol (a non-ionic, amphiphilic surfactant) among hundreds of others. The detergents and softeners clean the soiled clothing that can contain oils, sweat, blood and fecal material that may desorb from clothing. These

additives could also adsorb onto adhesives which may impact the affinity of polyacrylates to bind with MPs. [222–224]

In this study, a combined modeling and experimental effort probed disparate interactions among a polyacrylate adhesive, MPs, and detergent additives (glycerol, sodium citrate, and tergitol) (Figure 2-1). Insights into the binding potential of poly-2-ethyl-hexyl acrylate adhesive (PEHA) in the presence of laundry additive interferences were gleaned. Each additive of interest will be observed individually to understand what limitations they may have on PSA efficacy during MP capture. Adhesive effectiveness in dilute additive systems will be probed via MP counting from imaging and aqueous Work of adhesion (WoA(aq)) calculations.

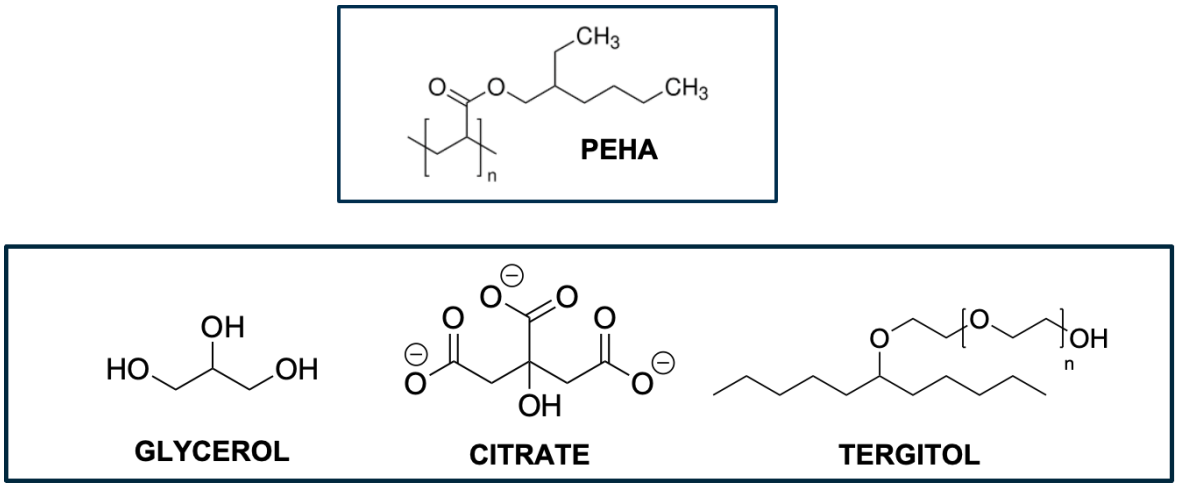


Figure 2-1: structures of PEHA adhesive, glycerol, citrate anion, and tergitol laundering additives

2.2 Experimental Methods

2.2.1 Materials

92k molecular weight (MW)poly-2-ethylhexyl acrylate (PEHA) adhesive dissolved in toluene was purchased from Millipore Sigma, and rotary evaporated to remove the toluene solvent. 950k PEHA was synthesized from a procedure from Chazovachii et al.[39] using 2-ethylhexanol and sulfuric acid (H_2SO_4) from Millipore Sigma, and polyacrylic acid (1033 kg mol^{-1}) from Scientific Polymer Products. Tetrahydrofuran (THF) solvent and glycerol, trisodium citrate, and tergitol 15-S-9 detergent additives were acquired from Thermo Fisher Scientific. These detergent additives were

purchased to consider a broad array of additives that may possibly impact adhesion to a polyacrylate adhesive. Borosilicate glass substrates (25 by 75 by 1 mm) for MPs capture were acquired from Thermo Fisher Scientific. nylon-6 powder MP (30-µm) was purchased from Goodfellow Cambridge Ltd. and Polyethylene terephthalate (PETE) particles were formed from soda bottles via grinding in a Vitamix® blender; 10 g plastic were blended in 10 g water for 2 min, filtered in a 100-µm sieve, then dried to produce generally larger and more polydisperse particles about 100–1100 µm in size.

2.2.2 Adhesive Preparation and Coating on a Glass Slide Substrate.

A 2% w/v adhesive solution was prepared with a bimodal mixture of 0.1g 92k and 0.1g 950k PEHA, dissolved in 10 mL THF. We found experimentally that this combination of resins was functionally more stable when deposited on a substrate and dispersed in water and migrated less during water exposure, while still capturing MPs. [41] Each resin mixture was shaken vigorously, then heated to 60 °C for 10 min to promote spraying ability from an AGPTEK Mini Airbrush (Amazon) onto a 25 × 25 mm area of labelled borosilicate slides (taped off using masking tape). To lessen MP accumulation along the edges, 2 mm of each edge of the square section was taped off (Figure 2-2). The resin was loaded into the airbrush cartridge, and air was forced through the brush, coating the substrate with a thin mist. Each slide was spray-coated with adhesive until a coating mass of ~30 mg (after drying for 24 h to evaporate THF) was achieved. The exact mass of each coated glass slide + adhesive was measured before immersion in aqueous additive solutions with MP particles.

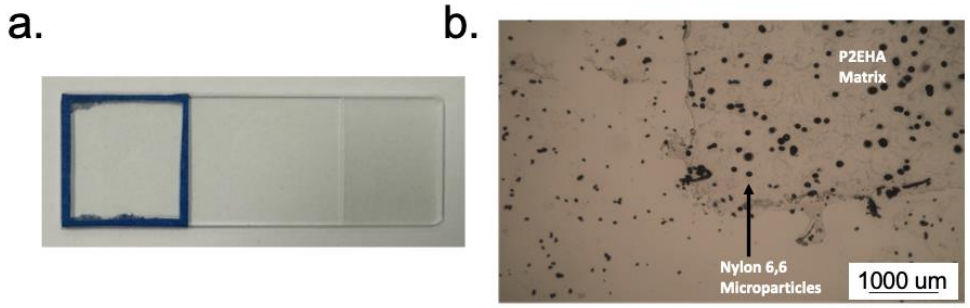


Figure 2-2: Glass slide preparation where the adhesive-coated area is limited to a 24 by 24 area of the 25 by 25 portion of the glass slide. B. Optical microscopy of taped-off adhesive matrix with embedded nylon MPs. Only particles captured by the adhesive layer were considered in % area calculations.

2.2.3 Adsorption Shake Tests

MP adsorption tests were done to gauge how additive exposure affects adhesive capture of MPs in simulated laundering conditions. 3% w/w additive/DI water stock solutions for glycerol, sodium citrate, and tergitol were first prepared. In real-world laundering, these additives are usually present in low concentrations of about 1 tbs/gallon (or 0.3–0.4% v/v) due to the large dilutions during laundering. [225] We used higher additive fractions, 3% (w/w), to trigger competition with the adhesive surfaces. At such high concentrations, any interference can be better seen. Glycerol solution was prepared by adding 11.9 mL glycerol to a 500 mL volumetric flask, then filling with DI Water to the 500 mL line. Sodium Citrate solution was prepared by adding 3 g sodium citrate to a 500 mL volumetric flask, then filling to the 500 mL line. Lastly, tergitol solution was prepared by adding 14.9 mL tergitol to a 500 mL volumetric flask, then filling to the 500 mL line. The adhesive- coated slides prepared previously were then placed into 0.5% w/v nylon in 30 mL additive dispersions, which amounted to about 15 mg MPs in 30 mL additive solution.

MP binding on the coated glass slides was conducted at both 1- and 5-min exposure intervals in the MP/additive/DI water suspensions. Capturing was limited to short exposures because, unlike previous polyacrylate MP capture studies that were conducted in DI water, [39,41] the stability of resins can be affected by the resin swelling caused by laundry effluents. After 1- and 5-min exposures to the 3% additive solutions on the shaker table, samples were gently rinsed to remove non-bonding MPs and set aside to dry. Potential swelling of the adhesive by the additives was also measured by tracking mass differences of the adhesive-coated glass slide before and after additive exposure. No effort was made to perform combinational experiments combining additives or sequentially exposing additives in different sequences, although that could also influence binding. Samples for each exposure condition were collected in triplicate.

2.2.4 Image J Analysis of Glass Slides Post MP Capture

Total calculations were determined by conducting analysis on a 3by3 grid of the adhesive-sprayed portion of the glass slide (Figure 2-3A). Microscope images were collected with a Nikon Brightfield Upright Optical Microscope, and surface area coverage (%SAC) of MPs was calculated

using ImageJ software (Figure 2-3B-E) following a modified numeric counting procedure from Rieland et al. [41] Modifications made were in the batch processing method, highlighted later in this section (Figure 2-4).

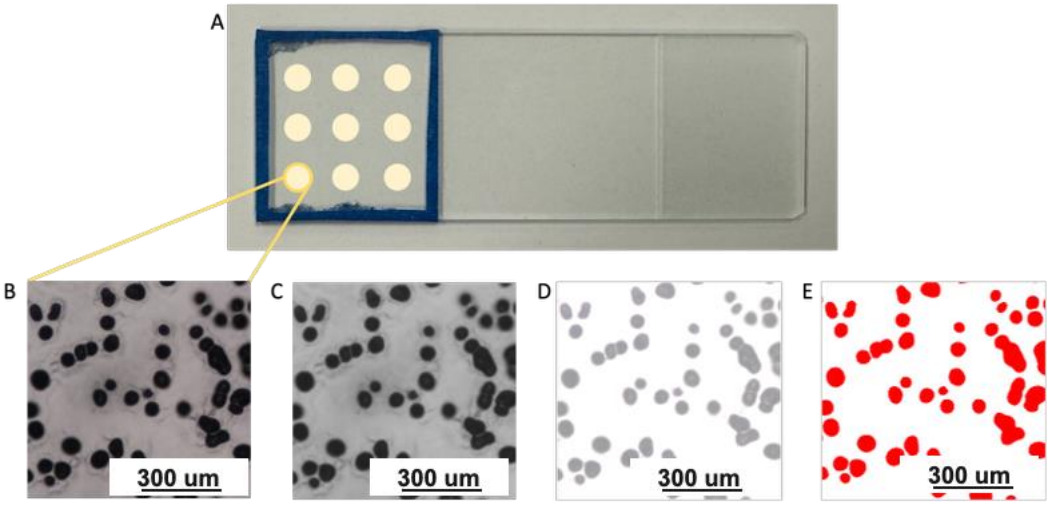


Figure 2-3: Image J analysis process of microscope covered slides. A. image is in its unprocessed state. B. Image is set to an 8 bit, monochrome image to eliminate interreferences from color. B. Brightness and contrast adjusted to remove shadows and enhance MP areas. C. A threshold was set where all particle edges and appropriate sizes of interest are fully identified.

These samples were batch processed for quicker data collection. The batch processing procedure can be seen below:

Batch Processing Method

i. The sample was first set to an 8-bit image. (Figure 2-3B)

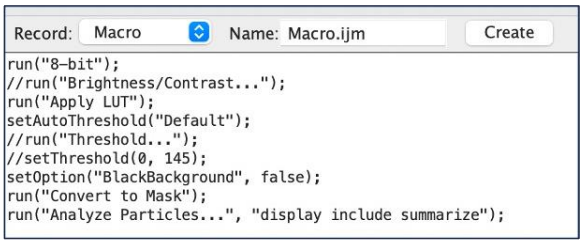
ii. Brightness was increased to isolate MP particles and rid the image of shadows. (Figure 2-3C)

iii. Contrast was increased to an optimal level where MP particles were enhanced, but where shadows remained absent. (Figure 2-3D)

iv. The threshold was set to identify the particle size of interest and determine the total area of coverage. Figure 2-3E)

v. The total % area coverage was measured using the "Analyze Particles" function and would be used to determine capture efficiency for adhesive-captured MPs in each environment of study (DI water, dilute sodium citrate, dilute glycerol, dilute tergitol) (Figure 2-4).

A.



B.

Slice	Count	Total Area	Average Size	%Area	Mean
N-W-1m-ST-004-1.png	589	247349	419.947	13.896	254.573

Figure 2-4: A. Recorded Macro for batch processing of % MP area data. B. % MP coverage on the glass slide

After the macro is set, separate MP-covered slides were analyzed simply by processing the image using the recorded and saved macro. The total % surface area of coverage (%SAC) was calculated using Equation 1.

$$\%SAC = ((\sum A_{\text{particles and clusters}}) / (9 * A_{\text{image area}})) \times 100 \qquad \text{Equation 1}$$

2.2.5 Probe Tack on Exposed P2EHA Adhesives for Aqueous Work of Adhesion Analysis

Aqueous probe tack tests were conducted to measure the aqueous work of adhesion, WoA(aq), of the PEHA adhesive in the presence of 3% w/w additive solutions. Using a TA Technologies Texture Analyzer, 0.5 mL of 10% bimodal 92 K/950K adhesive solution in THF was deposited onto a 25-by-25 mm section of a glass slide and allowed to dry overnight. Nylon and PETE probes with 0.5 mm diameter contact were affixed to the texture analyzer, and force (N) vs displacement (mm) was measured after probe contact with adhesive-coated glass slides submerged in separate 3% solutions of DI water, and solutions of citrate, glycerol, and tergitol. Figure 2-5 gives a schematic of the probe tack configuration as well as the thickness of the adhesive on the glass slide. The probe tack parameters used in the Texture analyzer can be seen in Table 2-1.

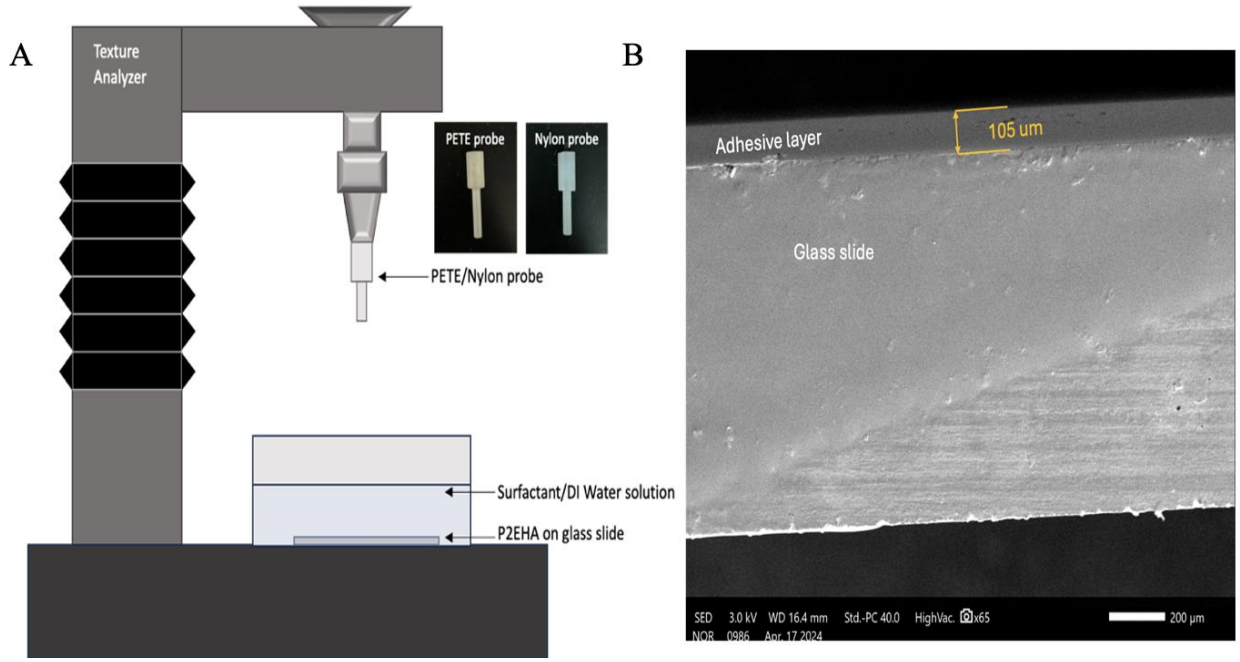


Figure 2-5: a. Schematic of probe tack configuration showcasing the texture analyzer, PETE and Nylon probes, surfactant solution, and P2EHA-coated adhesive slide. B. Adhesive-coated glass slide

Table 2-1: Texture analyzer Probe tack parameters

Parameter	**Value**	**Units**
Test Mode	Compression	
Test Speed	0.01	mm/sec
Post Test Speed	10.00	mm/sec
Force	0.078	N
Trigger Force	0.049	N
Stop Plot at	Trigger Return	

Detachment work (mJ) was determined by calculating the area within the Force v. Displacement curve using a trapz() function in MATLAB. (Figure 2-6).

A.

```
clc
clear

tbl = readtable("P2EHA-Tergitol-PETE10.csv");
Distance = tbl{:,2}; % Distance in mm
Force = tbl{:,1} % Force in N
m = plot(Distance, Force); % plot of Force vs distance (adhesive displacement)

Force(Force>0)=0; % Force values below 0 (region of significance)
Force(Distance<-2)=[]; % Force of Distance values below above -2 (region of
significance)
Distance(Distance<-2)=[]; % Distance values below above -2 (region of
significance)
Area = area (Distance, Force); % Highlights area under the curve
Work= (trapz(Distance, Force)) % Calculates and outputs adhesive energy (ml)
xlabel( 'Distance (mm)', 'Interpreter', 'none', 'FontSize',20 );
ylabel( 'Force (N)', 'Interpreter', 'none', 'FontSize',20 );
```

B.

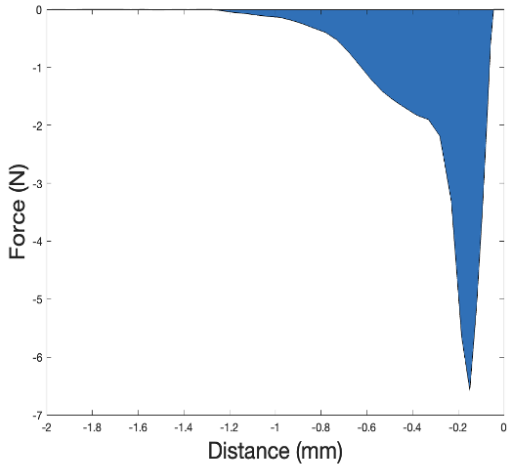


Figure 2-6: detachment Work determination using MATLAB trapz() function which calculates the area within curve using A trapezoidal integration formula.

2.2.6 Computational Methods

Computational work was conducted by Timothy Jugovic, PhD. All work related to the computational methodology can be viewed in his thesis titled: Advances in the Modeling of Synthesis, Design, and Properties of Polymers. [205]

2.3 Results And Discussions

2.3.1 Laundry Additives Interact with Adhesives by Swelling Them

Gravimetric assessments for detergent additive-exposed PEHA were measured to gauge whether additive molecules were embedded into the PEHA matrix (Figure 2-7). After rinsing and drying, all aqueous additive solution exposures resulted in gravimetric increases in PEHA resin mass,

while exposing adhesives to pure DI water gave virtually no absorption. Sodium citrate showed the most absorption, which may be explained by the higher solubility of ionizable molecules in water, [226] but all the additives swelled against the acrylate resin.

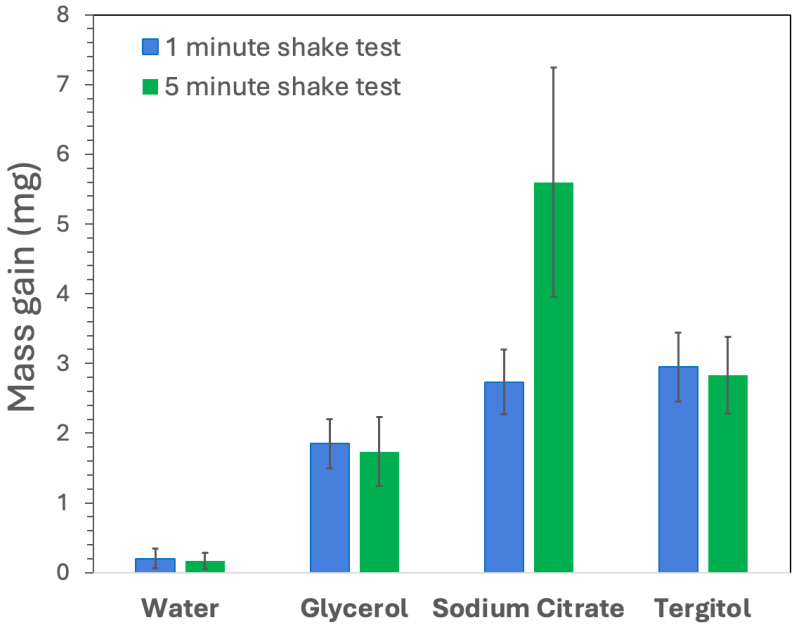


Figure 2-7: Relative mass gain of PEHA after 3% dilute additive exposure with error bars representing _+/- 1 standard deviation. All the additives show significant mass gain ($p<0.05$) at both shake test times, relative to DI water as a control and are essentially invariant with exposure time comparing 1 and 5 minutes of exposure with the exception of sodium citrate.

Functionally, swelling may affect the resin tackiness due to its affinity for other MP particles. Other studies have shown a decrease in Tg and surface tension, and increases in tackiness, for resins exposed to both ionic and non-ionic surfactants. [227,228]

Atomistic simulations of polymer/additive interactions can be found in Chapter 5 of Timothy Jugovic's thesis titled "Advances in the Modeling of Synthesis, Design and Properties of Polymers". From this work, 2-EHA, which is largely non-polar, has minimal interactions with the strongly polar pure water. The interactions between citrate, glycerol, and 2-EHA suggest pockets of additives interacting on the 2-EHA matrix. This compares to tergitol, where the contaminants more comprehensively coat the surfaces of the 2-EHA. Modeling from Jugovic's work supports the experimental swelling and suggests that all additives bind to the adhesives both through absorption (citrate and glycerol), and adsorption (tergitol), blocking other surface sites for MP

binding. They are also in line with previous studies that suggest fouling behavior of tergitol with PEHA. From modeling results, an additional concern is that if the resin affinity for a surfactant is stronger than that for MPs, the surfactant might act as a blocking agent, preventing MP wettability by the acrylate adhesive. [144]

2.3.2 MP Capture by Adhesives in the Presence Of Additives as Interferences

MP binding tests give a more holistic picture of how PEHA/additive interactions impact nylon and PETE binding to the adhesive surface (Figure 2-8). Approximations for binding efficiencies were conducted by calculating the %SAC (Equation 1). PETE particles are much larger than nylon, yet a similar capturing phenomenon was seen for both MPs, where binding is observed in water, glycerol, and sodium citrate, but is dramatically reduced in tergitol. As an amphiphilic surfactant, tergitol's hydrophobic tail interacts with hydrophobic PEHA and coats the PEHA surface, reducing binding efficiency. Erosion of the PEHA matrix is also observed with tergitol exposure, as thinning and crazing of the PEHA matrix causes globular areas where no adhesive is present (Figure 2-9H).

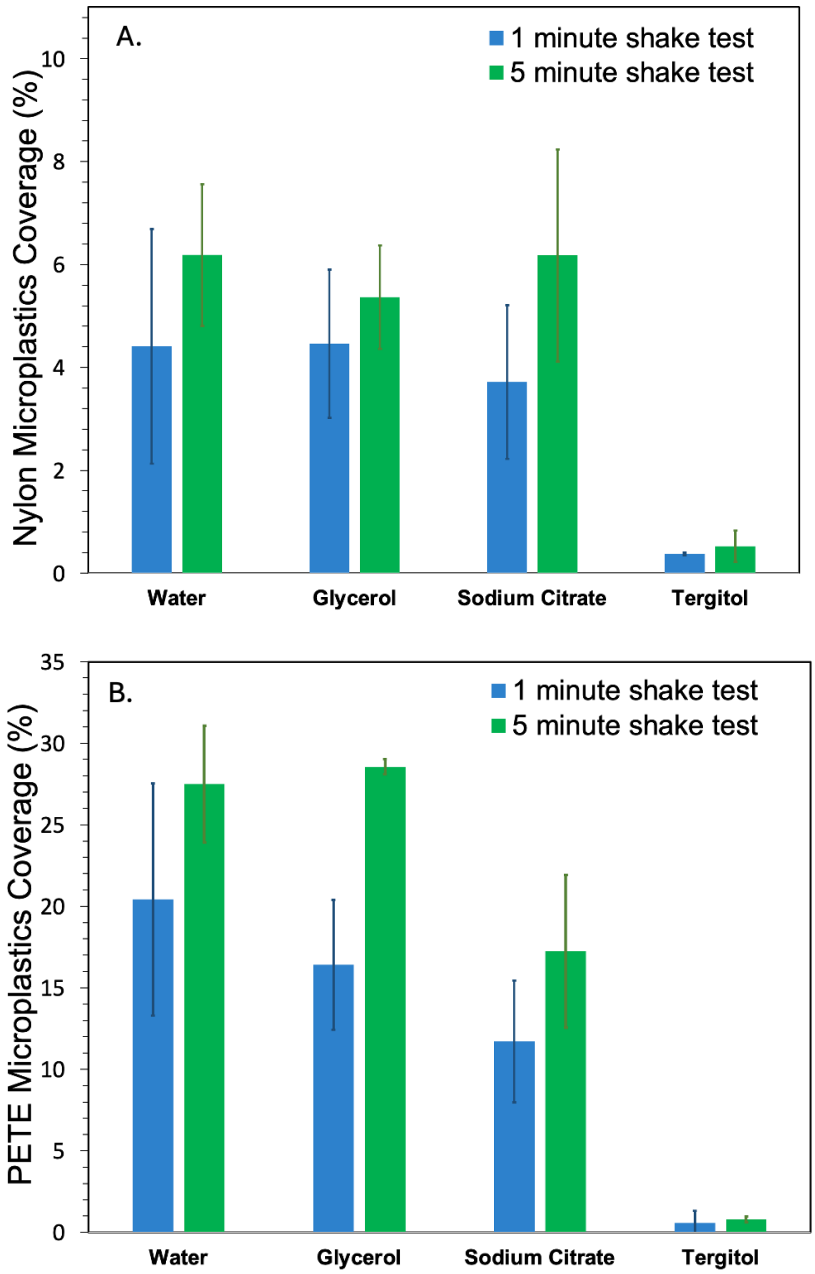


Figure 2-8: Total percent area of coverage for A) nylon (30 micron) and B) PETE (100-1100 micron) on 3by3 grid on adhesive coated glass slides. % Area coverage was approximated for MP capture in DI Water, glycerol, sodium citrate, and tergitol for 1 and 5 minutes. MPs were collected under flow conditions created by a shaker table and % coverage on the glass slide matrix was used to determine capturing efficiency. Tergitol exposure results in statistically significant ($p<0.05$) MPs coverage at 5 minutes compared to water for nylon and both time points for PETE particles. The other additives were not statistically significant.

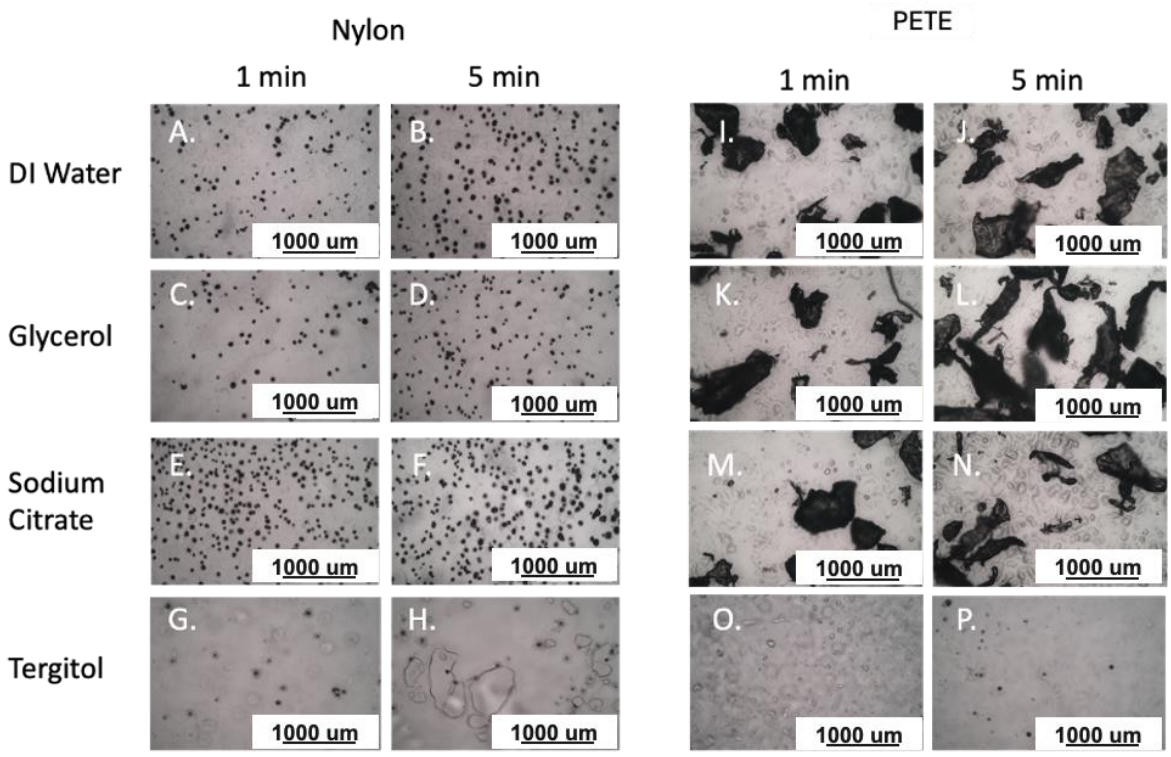


Figure 2-9: Optical Imagery of MPs bound on a PEHA coatings captured after 1 and 5 minutes in DI water, glycerol, Sodium citrate, and tergitol (top down). Images were taken with a 5x optical lens.

2.3.3 Adhesive Physical Properties of the Adhesive in the Presence of Additives via Work of Adhesion Measurements

Probe testing in static aqueous solutions (3% w/w in DI water), DI water, and air was conducted to compare adhesive strength between additives and nylon or PETE probe surfaces (Figure 2-10). Experimental results show that the WoA(aq) for submerged PEHA in the aqueous solutions were lower than that in air by a factor of about 2. Similar adhesive response was observed using the nylon probe; higher WoA(aq) was observed in air relative to those submerged in DI water, citrate, and glycerol solutions. When the Nylon probe was exposed to the tergitol solution, there was a 30-fold reduction of the WoA(aq) when compared to experiments done in air. The probe tack results in tergitol are consistent with MP capture tests that show reductions in nylon/PEHA interactions in tergitol.

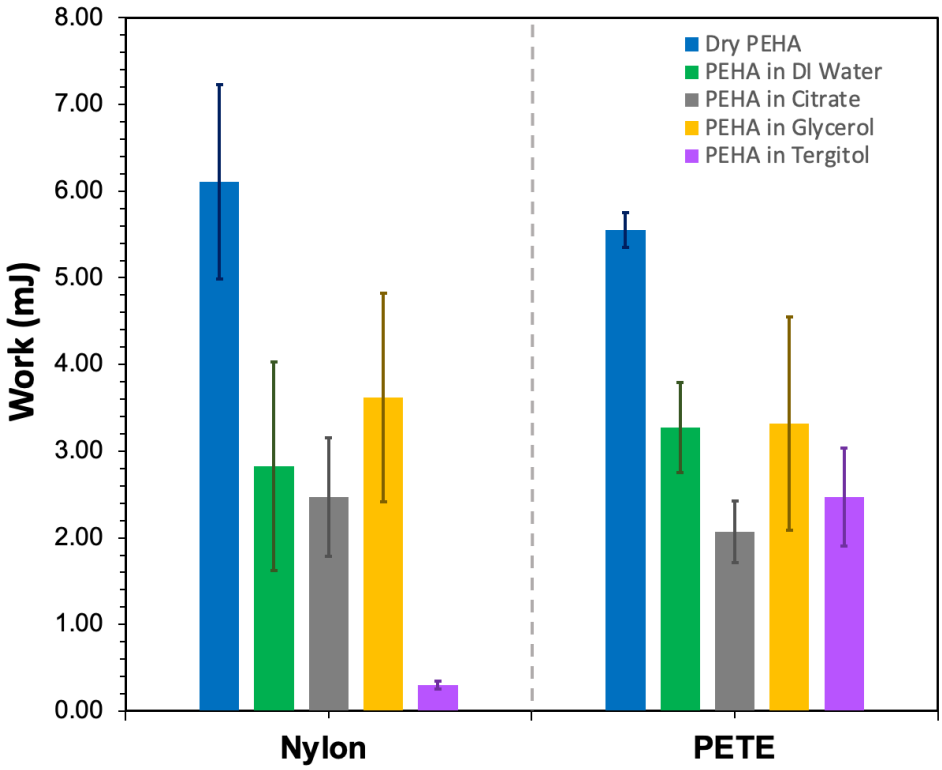


Figure 2-10: Experimental $WoA_{(aq)}$ values assessed as a probe tack-measurement for PETE and nylon probes at dry conditions (blue) and in 3% v/v static, dilute solutions of DI Water (green), glycerol (grey), sodium citrate (yellow) and tergitol (purple). There is a cross-sectional area for the probe, a force at failure and a strain at from failure, and from that, one can resolve work.

Most WoA values for PETE are comparable to those observed for nylon. WoA reductions of 38, 61, 39, and 54% were seen for DI Water, sodium citrate, glycerol, and tergitol, respectively when compared with dry adhesion in air, indicating reduced attachment force when submerged in the aqueous environments. PETE results for tergitol suggest, though, that adhesive interference is not as notable as nylon interferences and that adhesion properties in tergitol are comparable to citrate, glycerol, and DI water. While PETE/tergitol results do not align with MP capture tests (Figure 2-7, Figure 2-8), which show low PETE capture in tergitol, PETE fragments are plate-like and bigger than the nylon particles. We anticipate that particle size is a factor inhibiting binding to additive-loaded adhesives. In addition, during MP capture tests, longer exposure times in tergitol (1 and 5 min), and high adhesive erosion from shaking turbulence cause large increases in PEHA-tergitol interactions, reducing capture efficiency for PETE. Regardless, MP capture data shows that tergitol inhibits binding to both nylon and PEHA.

WoA vs Concentration curves were generated using the CHARMM general force field (cgenff) to model interactions between individual molecules (Figure 2-11) more details are found in work by Jugovic et al. [205]). Through WoA vs Concentration curves, limitations of higher concentration aqueous dispersions and solutions were observed. Because higher concentrations increased molecular interactions between additives and polymers, WoA values, and thus adhesive behavior, are impacted. Computational data shows that each of the tested contaminants with nylon and PETE demonstrates an exponential decay for WoA with concentration. As suspected, high concentrations of each of the contaminants have significant and negative impacts on the WoA for both PETE and nylon, especially for tergitol. Glycerol and sodium citrate have a sharper initial reduction in WoA, but tergitol is strongly inhibitory of adhesion; even at 0.1 mol%, both nylon and PETE should theoretically no longer adhere to PEHA. The relationship between concentration and adherence is further proven by negative WoA results, which are synonymous with unstable adherence conditions. [230] Both sodium citrate and glycerol have very rapid decaying curves, indicating that the maximum impact on WoA occurs at ∼0.5 mol%. Interestingly, tergitol has yet to reach its maximum impact, even at 2.5 mol%, which indicates strong inhibition.

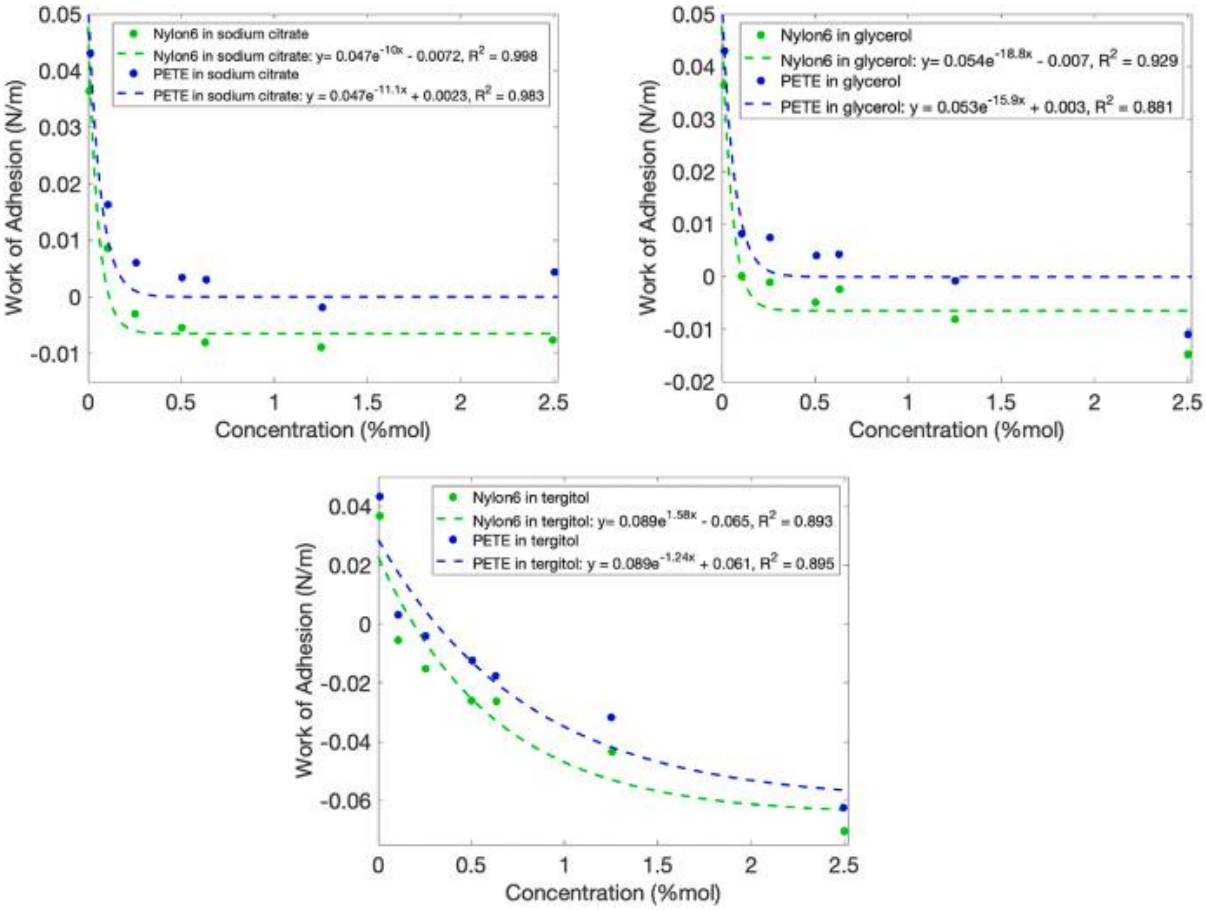


Figure 2-11: Computational WoA plots vs. concentration for A) Sodium citrate, B) glycerol and C) tergitol, with an exponential decay line of best fit.

Experimental trends suggest that tergitol is an inhibitory additive to MP adherence to the PEHA surface adhesive. Nonetheless, experimental capturing results will not directly correlate with real laundering conditions. For one, experimental WoA measurements were done under non-turbulent, static conditions. Turbulent shear has an erosive effect on the adhesive, complicating our quantification of particulate binding by visual monitoring. In addition, while MP capture tests used modest shearing conditions, those tests were short, much shorter than a typical laundry cycle (30 min–1 h). Nonetheless, the predicted and measured in situ effect indicates that PEHA captures MPs in laundry effluents, though likely with minimal efficiency in the presence of detergent additives.

There remain a number of open questions such as how one might adapt new generations of washing machines or retrofits to existing machines to accommodate the capacity to collect MPs over time. If the resins could be tuned for maximum adsorption for the most commonly shedding MPs in laundry, that would be a great start. If the adhesive substrate offers promise for collecting and isolating MPs from the washer, details to address the robustness and functionality will need to be considered. Some of these details include extending the stable functional time of the resin, increasing its resistance to erosion and abrasion in the turbulent flow of the washing, rinse, and spin cycles, and maintaining the adhesive quality of the resin in the presence of dirt, soaps and detergents, surfactants and fabric softeners. Overall, a more durable and functional adhesive system capable of capturing over multiple wash cycles will be necessary for real-world deployment.

1. Conclusion

This work shows the experimental MP capture by an adhesive in the presence of three common additives in soaps and detergents: glycerol, sodium citrate, and tergitol (3% w/w in DI water). The adhesive evaluated was a common polyethyl hexyl acrylate (PEHA) resin. Experiments show that all additives interfered with adhesive-mediated binding for MP capture, due primarily to molecular blocking of the adhesive resin and swelling. These surface interactions were reinforced by modeling efforts that showed that there was a driving force for additives to block adhesives from the MP particles. Significant reductions in binding are observed for tergitol-exposed adhesives, which are caused by surface coating from interactions between tergitol's hydrophobic tail and the mostly hydrophobic PEHA. In addition, large decreases in experimental Work of Adhesions (94.9% for nylon and 54.5% for PETE) for tergitol-exposed samples support low binding efficiencies (<1% SAC for both nylon and PETE MPs onto PEHA). Using slides, optical measurements, and rapid sampling to assess microplastic adsorption grants insight into binding characteristics for MPs in additive-exposed systems, but further optimization is required either by modeling or by further experimentation to learn more about implementation in real-world laundry applications.

Chapter 3 : Differences in MP Binding Between Monopolymer and Multipolymer Mixtures Dispersed in Aqueous Solutions Using an Adhesive-Based Capture Mode

3.1 Introduction

The world's reliance on plastic has led to a consequential loading of plastic debris in aquatic environments. It is estimated that, each year, 52 million tonnes of plastic enter aquatic environments worldwide and that over 80% of these plastics leach into these marine environments from land, in a myriad of sizes, shapes, and configurations. [231,232] Smaller particles are more easily distributable and end up being consumed by fish, bivalves, and other higher-order species. [233–236] According to the National Oceanic and Atmospheric Administration (NOAA), MPs are plastics that are under 5 mm in length and can be classified into two groups: primary and secondary MPs. [237,238] Primary MPs are plastic particles like microbeads, fibers, and plastic pellets that were intentionally made to be small, and can be found in, but not limited to, personal care, cosmetic, and biological products. Secondary MPs are plastics that degrade from larger sources such as plastic water bottles, tires, textiles, etc. These secondary MPs can break down by way of physical and chemical weathering, environmental weathering like solar UV radiation scission, mechanical stress, and microbial degradation, among others. [237–240]

While some synthetic micro-polymers are biodegradable and do not pose as great a risk to human health, many synthetic MP materials are resistant to biodegradation. [33,241,242] Many of the MP fragments in our environments come from consumer goods that are made from, but are not limited to, low- and high-density polyethylene (LDPE and HDPE), polyethylene terephthalate (PETE), polypropylene (PP), polyurethane (PU), Nylon, polyesters, acrylics, and polytetrafluoroethylene (PTFE). [243,244] They can be inadvertent discards from ships, residues from paints and coatings from ships and buoys, and can be conveyed in the liquid runoff from rivers and streams. [245,246]

Contributions: This paper is submitted to Environmental Sciences: Advances. The experimental work and analysis were done by me and a summer student, Dylan Payne, a Biomedical Engineering Student.

Several types of sequestration technologies have been developed to facilitate MP collection. A popular method is surface skimming. One sort of surface skimming technology is the use of barriers, meshes, or even robotic cleaners to physically gather, then uptake plastics from water into the cleaning apparatus. [44,45,247] Unfortunately, these surface skimming methods are most useful for larger plastic debris and do not account for much smaller MPs. To account for smaller-scale particles, MP capturing enhancements such as capillary skimming via hydrophilic entrapment or chemical aggregation have been explored for more controlled MPs removal. [44,248] Another notable enhancement for MP capturing is acrylate-based pressure-sensitive adhesives (PSAs). Research has shown that polyethyl hexyl acrylate (PEHA) is an effective adhesive for MP collection due to its retention of effective adhesion characteristics under water. [39–41,249]

While adhesive-based sequestering and other MP collection technologies can address MP capture on aquatic surfaces, the stratification of MPs based on density poses a notable threat to effective MP collection. For example, higher density MPs like PETE (ρ = 1.3 g/cm^3) may sink below the water's surface, making collection more arduous. Alternatively, regardless of density, multiparticle dispersions have been proven to have high particle agglomeration due to compatible surface chemistry, surface energies, and electrostatic forces, which help to facilitate particle capturing. While many studies exist that highlight MP sequestering of homogeneous and heterogeneous plastic dispersions, there are currently no studies that explore acrylate adhesive-based capturing for both classes of MP dispersions, even though PEHA efficacy for MP capture has been documented.

This paper explores how single-polymer (monopolymer) and different polymer (multipolymer) systems may limit or improve MP capture via PSAs, and seeks to deduce whether there are tradeoffs in MP capturing when several types of polymer debris with variable densities are present in an aqueous environment. Overall, this paper aims to understand how variations in polymer chemistry, polymer/adhesive interactive strengths, and density contribute to HDPE, PETE, and PP binding characteristics on an acrylate substrate.

3.2 Materials and Methods

The PEHA adhesive used was prepared from a bimodal mixture of 92k and 950k molecular weight (MW) PEHA. The 92k adhesive was purchased in toluene from Millipore Sigma; the toluene was

removed from the adhesive via rotary evaporation. The 950k PEHA was prepared via a procedure from Chazovachii et al. [39] Sulfuric acid, 2-ethylhexanol, and tetrahydrofuran (THF) used in the 950k PEHA synthesis were all purchased from Millipore Sigma. HDPE, PETE, and PP MPs were prepared from consumer goods by grinding in a Vitamix Blender (50 w/v in DI Water), yielding coarse MPs that had a significant size distribution, but might also be a good example of degraded plastic encountered. Green consumer goods were gathered for PETE, white consumer goods were gathered for PE, and red consumer goods were gathered for PP, allowing one to more easily distinguish particles during MP collection. Commercial polyethylene foam (2-inch diameter tube) was purchased from a local hardware store, sprayed with dilute PEHA in THF, and used for MP collection.

3.2.1 PEHA Preparation and Coating on the HDPE Foam Substrate

A 2% solution of adhesive was prepared in THF with a bimodal combination of 92k and 950k PEHA (500 mg 92k and 500 mg 950k in 50 mL THF). A benchtop vortex mixer was used to effectively dissolve the materials in the THF. According to Rieland et al.,[41] this bimodal combination was ideal because of its larger stability in water, particularly for MP collections. Previously, when resins were immersed in water, they tended to absorb water and soften, which caused them to have some dimensional stability issues if immersed for long times (hours). [249] To remedy this, schemes were developed to consider the short-term immersion of adhesive-coated blocks and foams that could mimic ropes being dropped into lakes and then being quickly drawn up after some immersion in an MP environment. To coat the substrates with adhesive, solutions were prepared and warmed to 60 °C before spraying on the polyethylene foam substrates using an airbrush.

Before spraying, the PE foam substrates were first cut into 4-inch samples, and roughly 0.5 mm of material was removed with a razor from the surface of the foam pieces to expose their porous features. 12 foam pieces were prepared, 3 for each capture type (HDPE, PETE, PP, and a multipolymer capture). Each sample was weighed to obtain the initial weight of the foam substrate without any adhesive. The warmed adhesive mixture was sprayed using an airbrush onto the foam substrates until 50 mg of adhesive was applied evenly to each foam piece. Each sample was allowed to dry for 1 hour before the final adhesive measurement was taken. All adhesive-sprayed foam substrates were set aside for MP collection

3.2.2 MP Collection

In preparation for MP collection, a 5.7 L reservoir (13.63 in L x 8.13 in W x 4.88 in H) was filled with 3 L of DI Water. For homopolymer MP collections, 1.5 g of MP (HDPE, PETE, PP) was measured and mixed into the water. For the heteropolymer collection, 0.5 g of each polymer type (HDPE, PETE, PP) was added instead. A stir bar was placed at the bottom of each reservoir to aid in mixing. The reservoir was then placed below the MP capturing apparatus for MP collection (Figure 3-1).

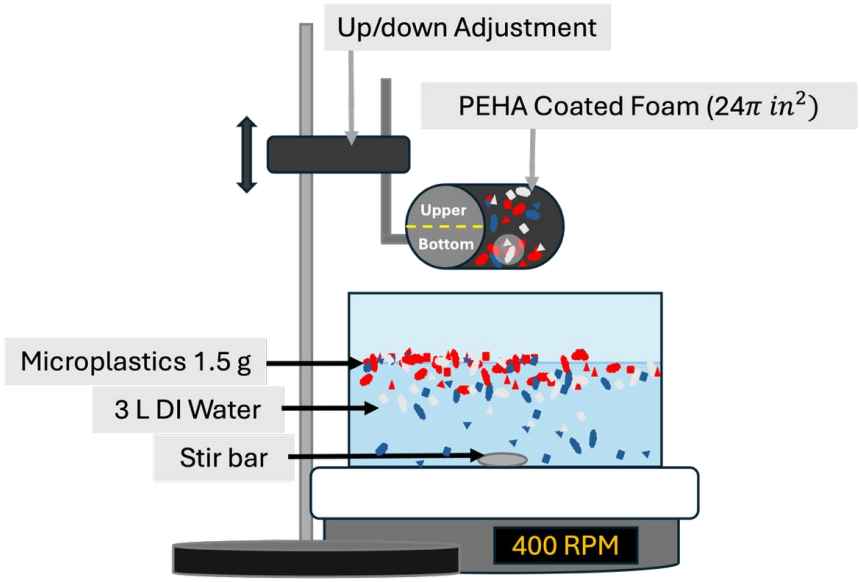


Figure 3-1: Schematic of the foam collection apparatus. The PEHA-coated foam is manually lowered completely into the reservoir and then raised to isolate the adsorbed particulates on the foam.

The adhesive-coated foam substrate was manually lowered into the Water/MP dispersions while stirring at 400 RPM. Each adhesive-coated foam sample was submerged for 1 minute to allow for particle adsorption. After separate incubation, each foam substrate was raised manually along a ring stand from the reservoir. The foam was then carefully set in a weighing boat without dislodging weakly adsorbed particles from the foam. The captured MPs and foam were then dried overnight in a vacuum oven at 60 °C and ultimately reweighed.

3.2.3 Particle Count Determination

After MP collection, the cylindrical foams were imaged using a Keyence Microscope. These foams were divided into 4 sections for ease of analysis, since the samples being analyzed were larger than

the field of view of the Keyence microscope, and to analyze differences between capture on the top and bottom halves of the foam. The top and bottom halves were marked; the top half is the portion of the foam that sits closer to the surface of the water, and the bottom half is the portion of the foam that sits closer to the bottom of the reservoir during MP collection (Fig 1). Thus, when the foam is submerged, the bottom half is wetted first and remains in the water longer and encounters buoyant particles on the surface before those on the top of the foam, potentially reducing what's available to adsorb.

To image the full foam section, 12 images were stitched using the Keyence analyzer image stitching tool. The images were analyzed using the Trainable Weka Segmentation plugin in Fiji (ImageJ). [250,251]

The following steps in Fiji (ImageJ) were taken for MP particle discrimination (Figure 3-2)

1. Set Scale (Under Analyze)
2. Crop image (Under Image)
3. Go to Trainable Weka segmentation (plugins, segmentation, Trainable Weka Segmentation)
4. Create classes for HDPE, PET, PP, foam background, and stage)
5. Highlight the specific classifiers and assign them to the appropriate class label
6. Click on "Train classifier" to train the system to train the software to distinguish between plastic types
7. Click on "Get probability" to generate grey-scale images for specific plastic types (Figure 3-2)



Figure 3-2: Trainable Weka Segmentation of labeled classifiers distinguishing between HDPE, PET, PP, and foam background

The probability maps in Fiji (ImageJ) were then used to get the total particle counts for each MP type (Figure 3-3). For each distinct probability image, particle count was determined by the following procedures:

1. Turn image to 8-bit image (under "Image")
2. Set threshold to only include MP areas of interest (under "Image")
3. Click on "Apply Threshold"
4. Particle count analysis: (Analyze, Analyze Particles), excluding particles under 2 pixels to avoid artifacts that may not be actual particles and to not over-represent small particles

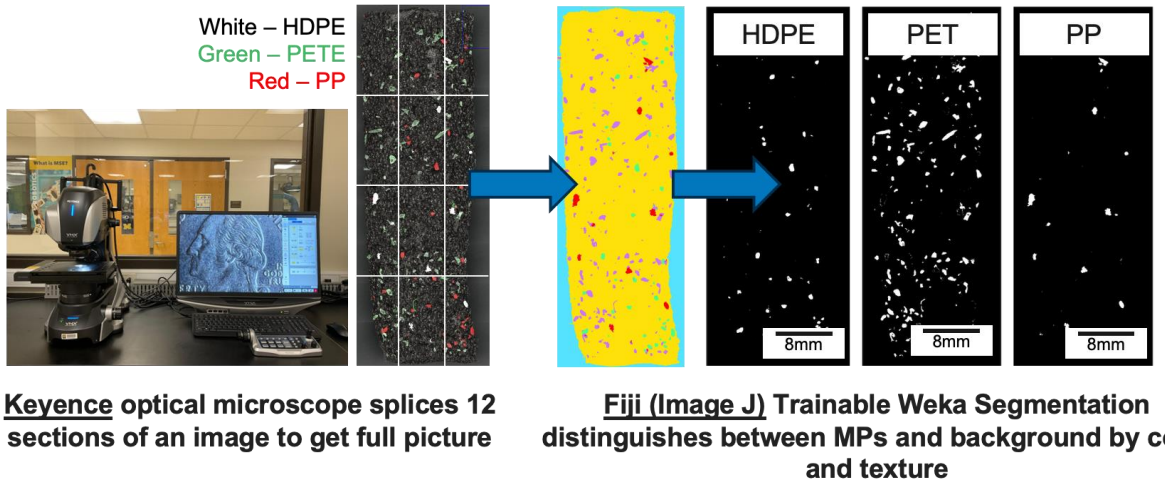


Figure 3-3: Probability Maps of a. Multipolymer capture sample b. HDPE, c. PETE, d. PP used to determine particle count (under Analyze particles)

Both particle count and size (area) were collected to find particle size distributions of MPs before and after collection. The capture efficiency was determined by particle count:

$$\frac{\#\ \text{particleson foam after MP capture}}{\#\ \text{ofMP deposited in resovoir}} \qquad \text{Equation 1}$$

For each polymer (HDPE, PETE, and PP), particles per gram were extrapolated by weighing 0.25 grams of MP and counting, under the Keyence microscope, how many particles there were in the 0.25 grams; this was repeated 10 times for statistical significance. The average particles per gram were determined to be 3780 ± 290, 10,100 ± 757, and 4400 ± 385 particles/gram for HDPE, PETE, and PP, respectively.

3.3 Results and Discussion

3.3.1 PEHA Adhesive Has an Affinity for Collecting Smaller Microparticles

Particle size distributions of captured MPs were first plotted to observe if there were preferences in size ranges captured by the PEHA for each MP type (Figure 3-4). Observed particle size distributions, before adhesive capture, show that the most abundant ground particle sizes were <0.05 mm² (D < ~250 µm) for ground particles (Figure 3-4a,d,g). For distributions of MPs bound from the monopolymer systems, the most abundant particle sizes for adhesive-captured particles were smaller <0.17 mm² (D <460 µm). For distributions of MPs bound from multipolymer systems, particles with areas < 0.05 mm² are common, while capture for particles >0.05 mm² is limited. According to previous studies, particles 20-100 µm were most abundant in aquatic environments and account for roughly 90% of particles found on aquatic surfaces. [252–254] The

distribution of bound particles suggests that PEHA is effective in binding MPs for the size of typical marine MPs. Larger particles might have more inertia with the motion of the solution, which seems to affect their capacity for binding.

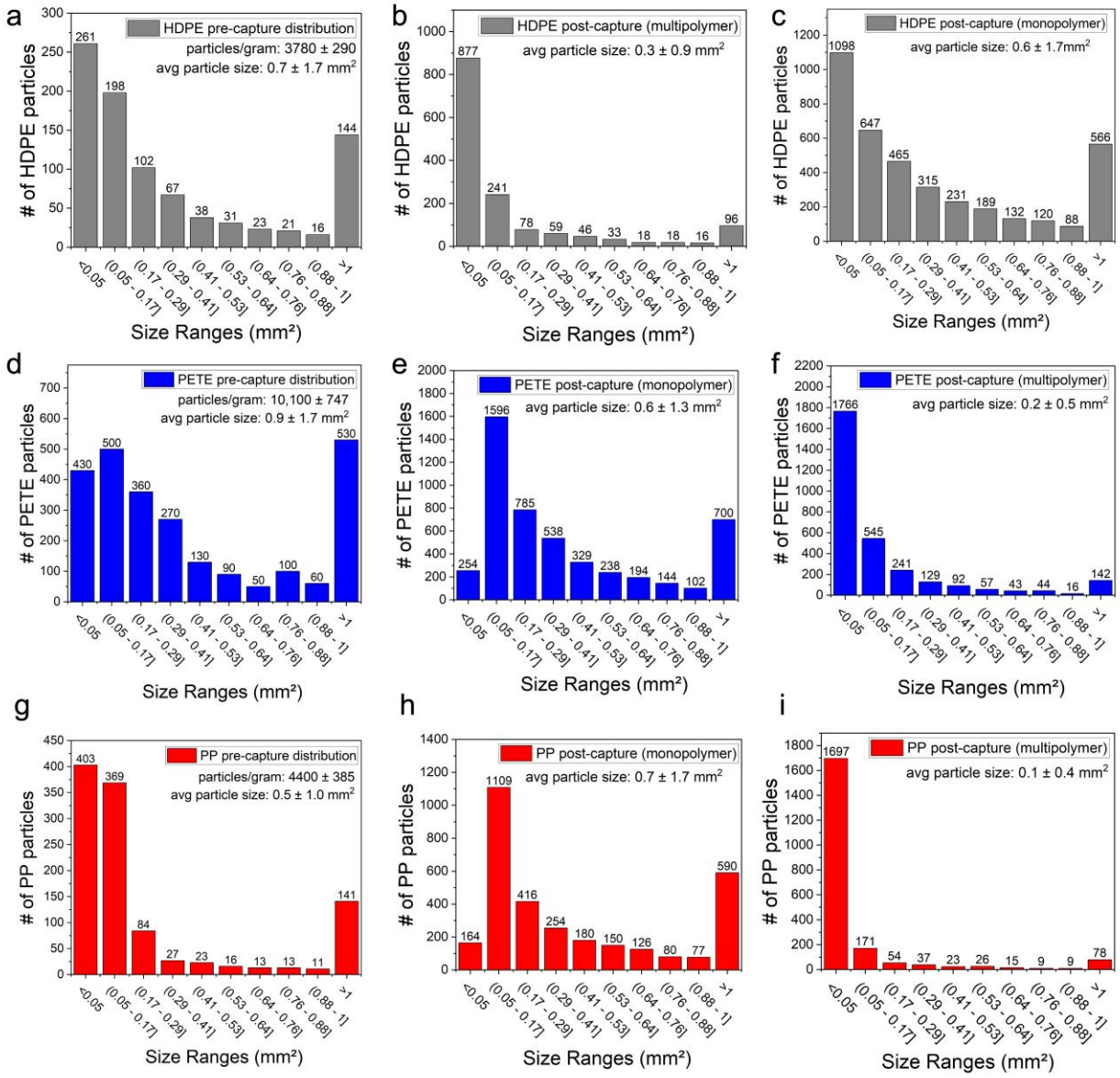


Figure 3-4: Particle size distributions for **a/b/c.** ground HDPE/ PETE/PP particles (pre-capture), **d/e/f.** HDPE/ PETE/PP monopolymers captured on an adhesive+foam substrate, and **i/j/k.** HDPE/ PETE/ PP multipolymer mixtures captured on an adhesive+foam substrate. Pre-capture distributions were determined from 0.25 grams of polymer. Average particle sizes are reported for each distribution

Single polymer dispersions have broader particle size distributions than multipolymer systems, with most bound particles having particle areas < 0.05 mm². Smaller particles are favored as they have higher surface area to volume ratios, which increases their wetting on lower energy substrates. It also might be easier to shield small, bound particles on foams than on flat surfaces. Also, short-range Van der Waals forces likely dominate for smaller particles, resulting in stronger adhesive-particle interactions [255–257].

3.3.2 Different Mechanisms Seem Functional with Different Particles on the Adhesive Foams

First, it was notable that when only one polymer type was dispersed in solution, capture efficiencies of < 30% **(based on particle count)** were measured from what was originally added to the solution, but the multipolymer dispersion saw notably higher capture efficiency (46%). This observation was based on particle count (Figure 3-5a).

Studies have shown that heterogeneous particle mixtures often enhance particle clustering due to asymmetric, yet symbiotic, polymer-polymer interactions that are absent in symmetric, homoparticulate monopolymer systems; [25,29,32,33] this behavior is referred to as heteroaggregation. In monopolymer dispersions, it is postulated that binding is limited to binding mechanisms present for one polymer type. Alternatively, multipolymer systems have greater particle binding efficiencies due to multiple available binding mechanisms. Polymer aggregation on adhesives is complex, and while exact binding mechanisms were not explored in this study, aggregation is regulated by the surface energies of the components being dispersed, polar and secondary bonding interactions, hydrophobic/hydrophilic interactions, surface roughness, and potential morphological and size differences that add to the total surface energy.[259]

Surprisingly, despite high PETE density (ρ = 1.3 g/cm^3), PETE capture in multipolymer systems is still observed (Figure 3-5b), is comparable to HDPE capture, and can be explained by surface energy differences between PETE and PEHA. For good wetting and effective binding, the surface energy of the adhesive must be lower than that of the bound plastic. [262,263] The reported surface energy of 2-ethyl hexyl acrylate (2-EHA) is 26-28 mJ/m² meaning its surface energy is lower than that of PETE (42-36 mJ/m²) but comparable to PP (29-32 mJ/m²) and HDPE (31-34 mJ/m²). [264–267] The large surface energy difference between PETE and PEHA enhances binding even though

PETE's higher particle density disperses particles more into the solution and away from the surface.

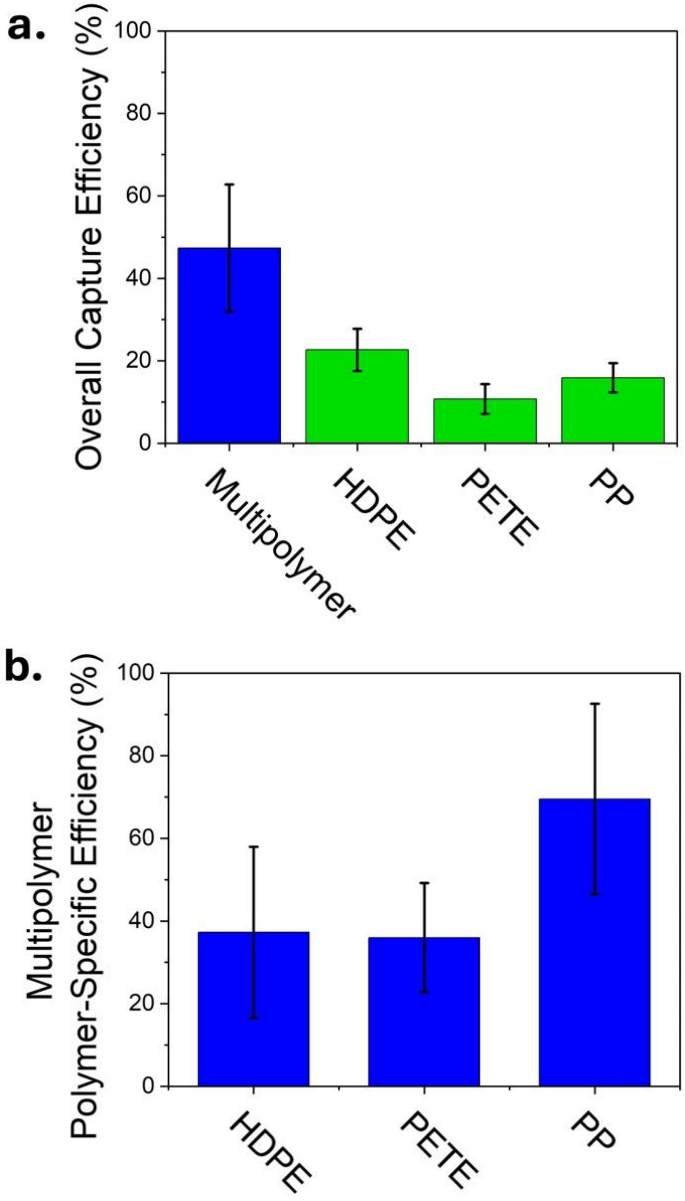


Figure 3-5: Capture efficiency of monopolymer and multipolymer dispersions of HDPE, PETE, and PP. Particle count-based capture efficiencies were observed based on the number of captured particles vs the estimated number of particles originally deposited in the reservoir. The deposited. The particle system was determined by estimating particles over a gram of HDPE (3780 ± 290 particles/gram), PETE (10,100 ± 757 particles/gram), and PP (4400 ± 385 particles/gram). Deposited particles were 1.5 g of plastic for monopolymer systems and 0.5 g each for multipolymer systems.

Lastly, PP binding is enhanced in multipolymer systems (Figure 3-5b). Because the capturing apparatus biased the bottom of the foam surface, the particles remained adhered to the initial contact surface (bottom surface), which is seen particularly by PP. Since PP is a lower-density polymer (ρ = 0.90–0.91 g/cm^3), it sits on the surface of the water [268]. When the foam surface contacts the water, most of the PP particles attach to the bottom surface first, leaving a few particles near the top surface.

Particle counts for the foam upper side and the foam bottom (portion that touches the water first) were assessed to determine if there are any biases in capturing. Regardless of the contact zone on the foam substrate (bottom side or upper side), effective particle uptake is observed across all MP types (Figure 3-6). This means that for both multipolymer and monopolymer systems, particle adherence to PEHA was not compromised even after the substrate was removed from the water, and particles were effectively bound to the PEHA regardless of dispersion characteristics. The adherence observed demonstrates that the PEHA is an effective adhesive for the removal of plastic particles dispersed in turbulent water. Density also does not seem to impact capturing capacity since PETE MP uptake is still observed on both sides of the foam substrate.

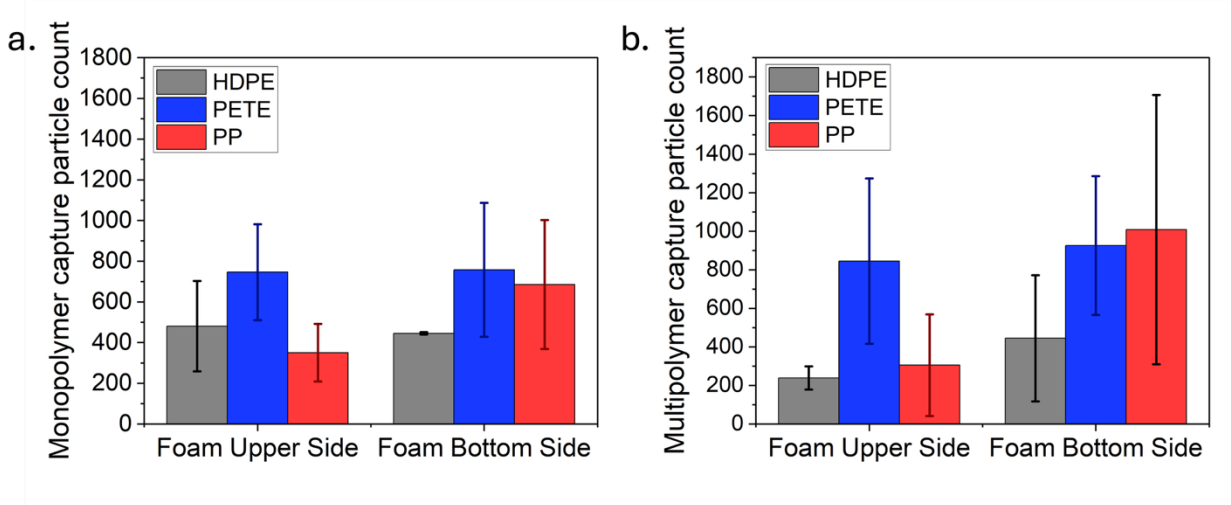


Figure 3-6: Particle counts for the upper side of the foam vs the bottom of the foam post capture for a. monopolymer dispersions and b. multipolymer dispersion

3.4 Conclusions

We leveraged PEHA adhesive to compare the competitive binding between different common MP particle types competing for an adhesive surface in aqueous dispersions. We demonstrated effective MP binding in short-term exposures (1 minute) in both monopolymer and multipolymer dispersions of HDPE, PP, and PETE when adhesives were coated onto foam substrates, which were submerged and then removed from the dispersions. Because of the capturing method, MP capture was biased toward the bottom of the foam, but the binding was sufficient to prevent particles from desorbing when the foams were removed from the solution. No more than 30% capture rates by mass were observed for monopolymer evaluations. However, when multipolymer systems containing all three polymer types were evaluated, the collection rate roughly doubled. The difference in capturing efficiencies is likely due to the presence of multiple binding characteristics for heterogeneous mixtures of plastics on PEHA that may not be available when there is only one polymer type in the dispersion. PEHA is also capable of capturing higher-density polymers (PETE: $\rho = 1.3$ g/cm^3) and small particles (< 0.17 mm^2). The stability of the resin in solution remains a limiting constraint requiring short-term exposure, but we have demonstrated a rapidly deployed and retrieved substrate-based binding scheme that shows efficiency advantages when capturing more than one particle type.

Chapter 4 : Water Regulates Ionic Liquid Solvation and Can Fine-Tune the Rheological Behavior of Dissolved Cellulose

4.1 Introduction

Ionic liquids (ILs) are solvents that are liquid under ambient conditions and are composed of ions. [269] Ionic liquids with anions that are strong hydrogen bond acceptors are generally great solvents for dissolving cellulose-rich materials like the cotton plant, which has chains that interact primarily via Van der Waals and strong hydrogen bond interactions.[190,270,271] Previous studies have identified imidazolium acetate ILs as great cellulose solvents Upon interacting with an imidazolium superbase, the acetic acid is readily deprotonated, meaning that the remaining acetate anion (a hydrogen bond acceptor) can disrupt the hydrogen bonds between cellulose chains, creating new hydrogen bonds with cellulose hydroxyl groups. This results in viscous solutions and dispersions. [190,271,272] Imidazolium-based ILs with acetic acid moieties, such as 1-ethyl-3methyl imidazolium acetate [Emim][-OAc], 1-butyl-3methyl imidazolium acetate [Bmim][-OAc], and 1-octyl-3methyl imidazolium acetate [Omim][-OAc] have shown excellent cellulose solvation. [198,273] After solvation by IL exposure, IL/cellulose solutions and dispersions can be shaped into any desired form, and cellulose can subsequently be resolidified by exposing them to polar solvents like ethanol, methanol, acetone, or water. [274] These polar solvents reintroduce hydrogen bonds into cellulose, reprecipitating the biomass. Since imidazolium is relatively expensive and its ILs require multi-step processing, it makes their immediate use unattractive. Diazabicyclo [5.4.0]undecene acetate ([DBUH][-OAc]) is an ionic liquid that has shown strong lignocellulose solubility and can be made from a simple 1-pot synthesis of 1:1 molar ratio of acetic acid and diazabicyclo [5.4.0]undec-7-ene (DBU). DBU-based ILs are also relatively inexpensive in comparison to their

Contributions: This chapter is a subset of work that is published in Results in Engineering. All the experimental work was conducted and analyzed by me, though MATLAB codes were developed by my colleague, Julie Rieland.

Lawal, T. D.; Rieland, J. M.; Love, B. J. Water Regulates Ionic Liquid Solvation and Can Fine-Tune the Rheological Behavior of Dissolved Cellulose. Results Eng. **2025**, 28, 107550. https://doi.org/10.1016/j.rineng.2025.107550

imidazolium counterparts and are capable of readily deprotonating acetic acid, making them an appealing superbase substitute for cellulose dissolution. [275,276] Although cellulose solubility for ILs is modulated by changing the deprotonated acid moiety, extrinsic factors such as water, an antisolvent, may impact solvation. The -OH groups in cellulose make it a hydrophilic biopolymer; because it strongly interacts with water, its solvation may be impacted by the presence of water. [277,278] Like acetate ILs, water forms strong hydrogen bonds, and can thus compete with ILs' hydrogen bonding abilities. [279,280] Previous research has also shown that at low concentrations, the presence of water in ILs may be even advantageous, lowering processing viscosities and facilitating polymer hydrolysis. [277,278] Alternatively, past studies have also explored how dilute IL mixtures have localized areas of aggregated water, which may reduce the solvation capacity of the IL. [281,282]

While the dissolution behavior of water/imidazolium acetate mixtures is well characterized, there are few studies on [DBUH][-OAc]. To our knowledge, there are few studies – or none – that explore how water impacts [DBUH][-OAc] solvation of cellulose and analyze the subsequent properties of the cellulose/solvent solution and regenerate. Here, we wanted to further probe the phase space tied to water/IL processing of cellulose by assessing water's effects on dissolution capacity, features of the extract, and the mechanical properties of extruded regenerated cellulose fibers. We hypothesized that the solubility [DBUH][-OAc] for crops like cotton (>90% cellulose) would be fine-tuned in the presence of water, thus allowing the modulation of both the rheology and reprecipitated forms.

4.2 Materials and Methods

Commercial cotton, the cellulose source of choice, was purchased from U.S. Cotton LLC, dried to constant weight, and used as received. Ionic liquid chemicals, 1,8-diazabicyclo [5.4.0]-undec-7-ene (DBU) (98.0+%) and glacial acetic acid (99.5%), were purchased from Thermo Fisher Scientific and used as received.

4.2.1 Cellulose Composition

The cellulose composition of our commercial cotton was determined via a procedure from Ramadevi et al.[283] using sodium chlorite. Two grams of cotton were measured and cut into 1 mm sections in preparation for cellulose compositional analysis. The measured cotton was then mixed

with 20 mL of 17.5% NaOH, mixing vigorously for 30 minutes. After the 30-minute incubation period, 35 mL of DI water was poured into the cellulose/NaOH mixture and mixed rigorously for 1 hour. The cotton was then washed via vacuum filtration with 100 mL 8.3% NaOH, 200 mL DI Water, 15% acetic acid, and 200 mL DI water respectively. The resulting solids were dried to constant weight. Cellulose content was determined via equation B3.

$$\frac{\text{Weight}_{\text{cotton}_{\text{initial}}} - \text{Weight}_{\text{cotton}_{\text{final}}}}{\text{Weight}_{\text{cotton}_{\text{initial}}}} \times 100 \qquad \text{Equation 4-1}$$

4.2.2 Cellulose Cri (% Crystallinity of Commercial Cotton)

The crystallinity index (CrI) for the cotton was determined to be 61.4% (Figure 4-1), which makes it tractable to dissolution given its semicrystalline nature. [284] The cellulose crystallinity (CrI) of commercial cotton was determined via X-Ray diffraction (XRD) using a Rigaku SmartLab XRD. Data were collected covering 2θ values of 5-60° with a ramp speed of 10°/min, a CuKa X-ray source (λ = 0.154 nm), and a step size of 0.02°.

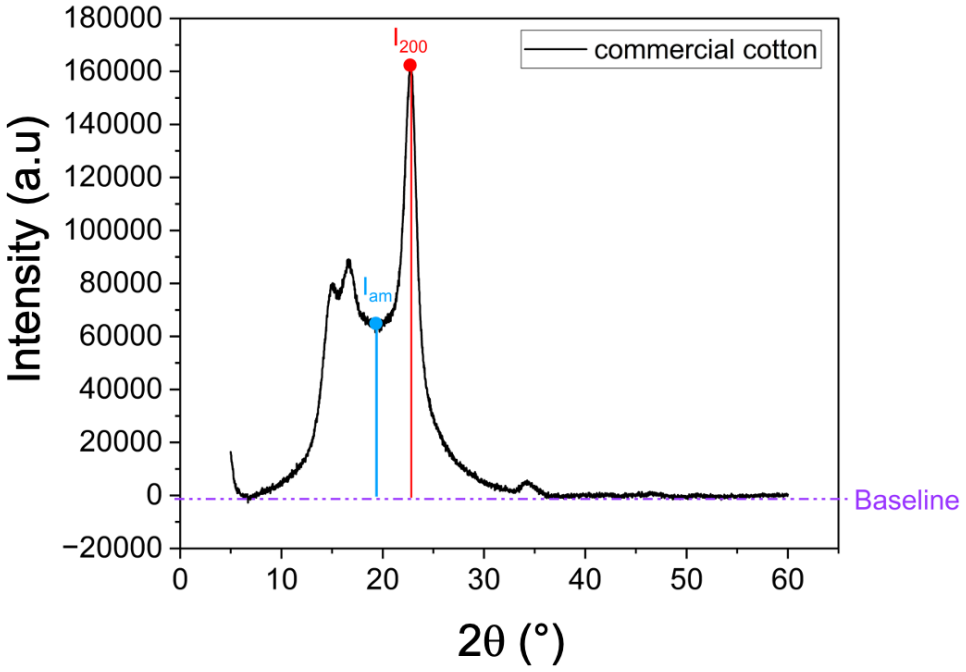


Figure 4-1: XRD of commercial cotton showcasing lattice parameters of cellulose used to calculate crystallinity index

The following equation was used to find %CrI [68]:

$$\%\mathrm{CrI} = \frac{I_{200} - I_{am}}{I_{200}} \times 100 \qquad \text{Equation 4-2}$$

Where I_{200} is the maximum peak that shows up at a characteristic 2θ value of about 22.8° while I_{am} is the amorphous peak (shown in Figure 4-1).

I_{am} and I_{200} values were found using the peak finder tool on Origin8Pro (first correcting the baseline.

4.2.3 Ionic Liquid (IL) Preparation and Cotton Solvation

1,8-diazabicyclo[5.4.0]-undec-7-en-8-ium Acetate ([DBUH][-OAc]) was formed via a prior ice bath reaction protocol. [285] A one-pot synthesis was performed using a 1-to-1 molar ratio of DBU (99.8+%) and acetic acid (99.5-100.5%). Equimolar amounts of acid and base were used to prevent the accumulation of excess water during the reaction per Achinivu et. al. [286] The solution was magnetically stirred in an ice bath until viscous and left to fully react for 3 hours, then stored in a desiccator for 24 hours. No further purification steps were performed prior to use, but [DBUH][-OAc] is prone to crystallize during this latent period, so it was warmed before use for 3 hours at 80 °C to create a more fluid form. After removing the IL from the heat, it remained liquid and uncrystallized. Knowing that ionic liquid is hygroscopic, we used the ionic liquid immediately after melting to prevent ionic liquid hydration

To assess how water influences the IL's affinity for cotton dissolution, 20 mL aliquots of 0-20% DI water in [DBUH][-OAc] were prepared and shaken with a vortex mixture to create homogeneous mixtures prior to cotton dissolution.

The cotton was oven-dried to constant weight, then 5% w/v of cotton was placed in the ~ 20 mL solutions of 0-20% DI Water/IL mixtures. Cellulose solubility was assessed by exposing the mixtures to an oil bath at 80 ºC between 2 and 4 hours. Samples were made in duplicates and set aside for rheology. Abbreviated sample names can be found in Table 4-1.

Table 4-1: Solvation conditions for 5% cellulose dissolved in ionic liquid/water solutions

Sample Name	Treatment Time (Hours)	Water content in Ionic Liquid
2hr0%	2	0
2hr3%	2	3
2hr5%	2	5
2hr7%	2	7
2hr10%	2	10
2hr20%	2	20
4hr0%	4	0
4hr3%	4	3
4hr5%	4	5
4hr7%	4	7
4hr10%	4	10
4hr20%	4	20

4.2.4 Rheology of Water/IL/Cotton Systems

Viscosity vs Shear Rate of the IL/water systems was measured on a TA Instruments ARES—2 rheometer with an oven attachment and parallel plates with a 0.5 mm gap. Constant stress sweeps were carried out in oscillatory shear mode at temperatures of 60, 70, 80, and 90°C for each IL/water/cotton system at shear rates ranging from 1-100 s^{-1}.

Zero shear viscosity, η_0, was extracted directly from the viscosity vs shear rate curve at regions of low shear rate and a plateau. For viscosity vs shear curves without a clear plateau, a MATLAB[287] code following the Cross model for viscous polymers was used (Equation 4-3). MATLAB codes can be found in Appendix A. [288]

Cross model equation:

$$\eta = \frac{\eta_0}{1+(\frac{\eta_0 \gamma}{\tau^*})^{1-n}} \qquad \text{Equation 4-3}$$

Where η_0 is the zero-shear viscosity (Pa·s), τ^* is the critical shear stress, γ is the shear rate, and n is a constant.

The activation energy for viscous flow, E_a, was extracted from the viscous Arrhenius relationship in slope-intercept form (Equation 4-4):

$$\ln \eta_0 = \ln A + \frac{E_a}{RT} \quad \text{Equation 4-4}$$

Where η_0 is zero-shear viscosity, E_a is the Arrhenius Activation energy of viscous flow, R is the gas constant, and A is the pre-exponential factor. [289]

The power law (linear) region of the viscosity vs shear rate curve can be represented by the rearranged power law equation in Equation 4-5 (rearranged into slope-intercept form: y = mx+b):

$$\ln \eta = (n-1)(\ln \dot{\gamma}) + \log K \quad \text{Equation 4-5}$$

where h is viscosity, K is the consistency index which determines relative shear strength, n is the behavior exponent which determines deviation from Newtonian behavior, and $\dot{\gamma}$ is the shear rate. Power law coefficients, n and K, were extracted from the slope of the linear portion of the ln(η) vs ln($\dot{\gamma}$) curve of each water/IL/cotton mixture at 60 °C. [290] Power law behavior gives greater insight into shear-thinning behavior. Cotton Solvation measurements

To gauge solubility, 20 mL of DMSO (99.7%) (Thermo-Fischer Scientific) was mixed into the dissolved cotton/IL and sonicated for 2 hours to release ionic liquid from the cotton before filtration. The sonicated solution or dispersion was then passed through a vacuum filter after which the remaining solids were soaked for 1 hour in 10 ml of ethanol to remove residual IL. The cellulose was then passed through a vacuum filter again and then dried to constant weight at 80°C. The fractional dissolution of the cotton was calculated using the mass of undissolved residue and the initial mass to resolve the percentage dissolved.

4.2.5 Cellulose Fiber Regeneration and Characterization

After a 2- and 4-hour solvation of cotton in [DBUH][-OAc] and water, we formed modest fibers from the dissolved solutions and dispersions (heated to 80 °C) by depositing 15 mL of cellulose solution using a spatula into a 60 mL syringe without a needle. The syringe, with the cotton slurry,

was then heated for 30 minutes at 80 °C to facilitate better flow. Fibers were then extruded by hand into 150 mL of methanol (99.7%) (Thermo-Fischer Scientific). Fibers were extruded to approximately 20 cm long. The extruded fibers were left to coagulate in the methanol bath for 24-hours to liberate IL. After 24 hours, the methanol bath was replaced with 150 mL DI water and the regenerated cellulose was sonicated for an additional hour in DI water. The fibers were then transferred to aluminum foil and dried at room temperature to constant weight.

Tensile testing of dried regenerated cotton was then done on extruded fiber samples (300-500 µm in diameter) with a TA Technologies Texture Analyzer using the ASTM standard: D3822. [291] Young's Modulus, strain at break, and Ultimate Tensile Strength (UTS) were measured from generated Stress-Strain curves to understand how water content in the cotton/IL mixture influences fiber mechanical properties. Fibers were tested using a TA.XT.plus Texture Analyzer. ASTM Standard D3822-07 was used with minimal modifications to the fiber testing configuration (Figure 4-2). [291] 10 samples were collected per regenerated fiber type (2hr0%, 2hr3%, 2hr5%, 4hr0%, 4hr3%, 4hr5%).

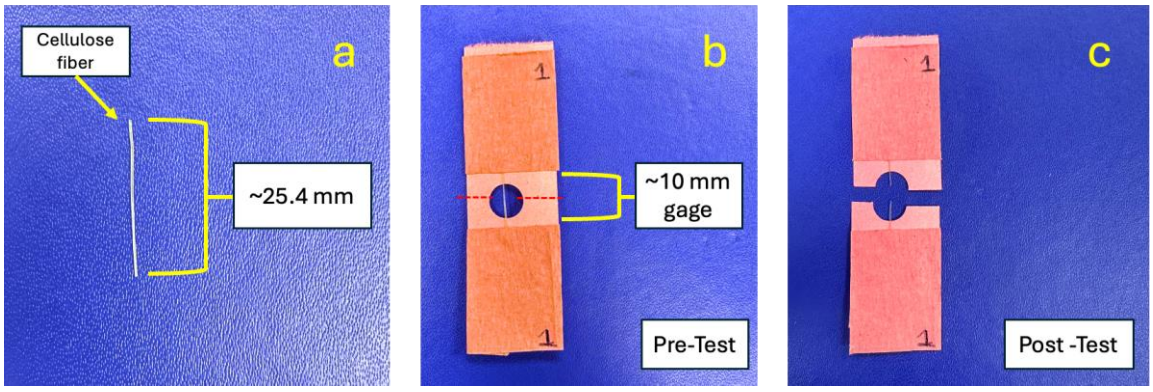


Figure 4-2: Fiber testing configuration modified from ASTM Standard D3822-07: a. Example of a cellulose 25.4 mm long fiber used for mechanical testing, b. The Cellulose fiber is taped on a 1 by 3 in paper with 10 mm gage. The paper is hole punched to allow ease of snipping prior to starting the mechanical testing (red dashed line), c. Testing configuration post-mechanical testing. Note that cellulose breaks in the middle.

The following testing parameters in Table 4-2 were used for mechanical testing of the regenerated cotton fibers on the TA.XT.plus Texture Analyzer.

Table 4-2: Mechanical testing parameters using TA.XT.plus Texture Analyzer

Test parameter	Value	Units
Test Mode	Tension	
Pre-Test Speed	0.02	mm/sec
Test Speed	0.02	mm/sec
Target Mode	Distance	
Distance	20.000	mm
Trigger Type	Auto (Force)	
Trigger Force	0.002	N
Break Mode	Rate	
Break Sensitivity	0.098	N
Break Detect	Return	20
Stop plot at	Target Position	

Optical Microscopy and Scanning Electron Microscopy (SEM) were used to visualize topographical differences between regenerated fibers. Root Mean Square (RMS) values for roughness were measured in nanometers on Gwyddion open-source software using the statistical quantities feature and SEM images. [175] Nine 20x20 mm^2 boxes were used to determine the average RMS value across the SEM image.

4.3 Results and Discussion

4.3.1 Water Suppresses Cellulose Solubility in [DBUH][-OAc]

Cellulose dissolution was measured as a function of time and water concentration (0-20%). As expected, cotton solubility decreased as water content increased, and increased as a function of time (Figure 4-3). Lastly, for all time conditions (1,2, and 4 hours), cellulose solvation reduced dramatically between 5% and 7% water in IL (Figure 4-3). Trends suggest that water is an important factor to consider in solvation capacity, so to more effectively deduce the impact of water on solvation, measuring initial water content in the IL via a Karl Fischer titration, or similar protocol, would be informative. In this case, the cellulose was still tractable to solvation in neat, undried, [DBUH][-OAc] at 2 and 4 hours, so the intrinsic water did not impact the neat solvation

characteristics. Alternatively, additions of extrinsic water content (0-20%) very clearly impact solvation.

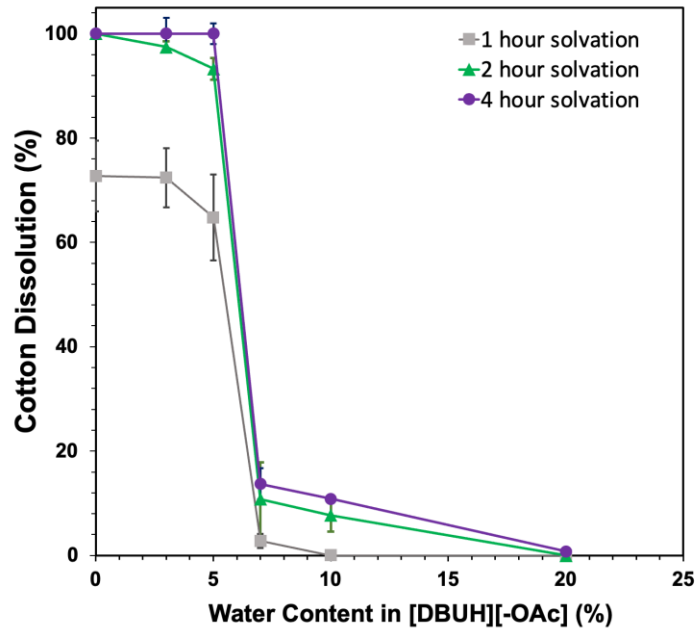


Figure 4-3: Cotton dissolution vs Water content in [DBUH][-OAc] at 80°C at 1, 2, and 4 hours. 10% water content is enough to significantly reduce the solubility of cellulose in [DBUH][-OAc] solutions.

The dramatic reduction in solubility can be rationalized by H-bond competition. Other studies that investigated water/IL mixtures saw local aggregations of water and H-Bond shielding with increases in water concentration. [293,294] For [DBUH][-OAc], such H-bond screening can be assumed to occur between 5-7% water with near complete shielding at 7% water. At 7%, water/IL competition for hydrogen bonding increases considerably thereby impeding ionic liquid affinity for cellulose solvation. From optical images of dissolved slurries, the 2hr3% and 2hr5% samples have thin, residual fibers of insolubilized cotton (<500 μm) floating in the cotton solution (Figure 4-4). These insolubilized threads can be attributed to regions of minimal ionic-liquid/cellulose interaction caused by the H-Bond shielding from water 140.

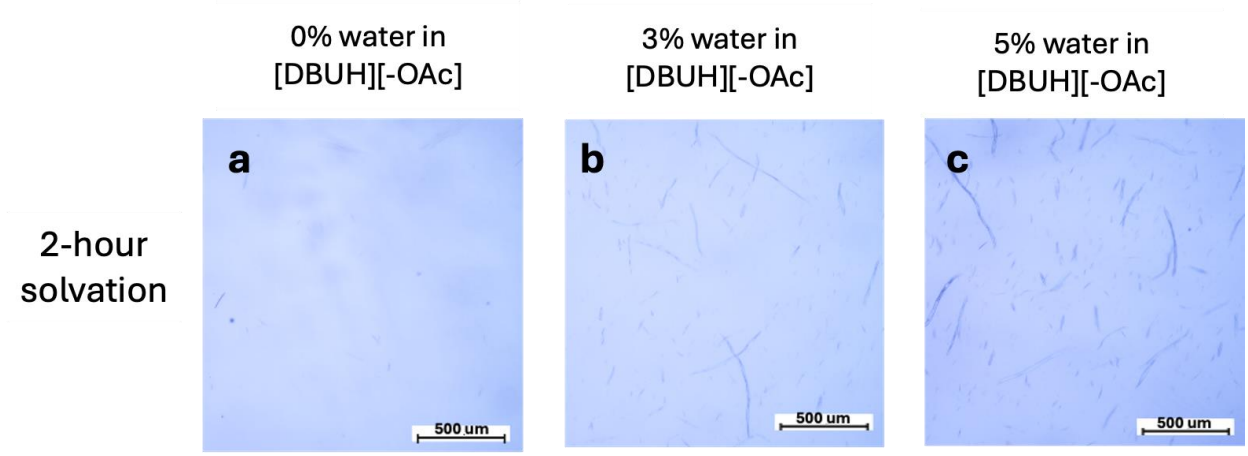


Figure 4-4: Optical micrograph of solutions made from 0-5% DI Water, [DBUH][-OAc] and 5% cotton disolved at 80 °C. The fine strands in b and c are residual undissolved cotton fibers

4.3.2 The Presence of Dispersed Cellulose and Water Contributes to the Measured Solution Viscosity

The rheological properties of cellulose slurries vary with the presence of both water and undissolved fibrils. Arrhenius plots for viscous flow grant insight into viscous energetics of cellulose slurries made at the lower water concentrations (0, 3, 5%) in [DBUH][-OAc] (Figure 4-5). For 2hr0%, 2hr3%, and 2hr5% samples, Arrhenius plots show similar activation energies of 779, 806, and 819 J respectively, and slight increases in viscosity with water (Figure 4-5). We expect this is due to the presence of undissolved fibers. The 4hr0% and 4hr3% solutions have notably higher activation energies (951 and 911 J, respectively) than the 2hr samples. They also have comparable viscosities. In contrast, the 4hr5% sample has both a lower viscosity and activation energy (811 J) (Figure 4-5). These results suggest that, under less dissolved conditions, the presence of residual fibers increases viscosity but may not impact energy of viscous flow. Meaning that, despite the undissolved fibers, the presence of water may lubricate the systems to allow for low-energy flow. On the other hand, at the higher rates of dissolution observed after longer time, higher viscous flow energies are seen because more cotton is allowed to be conveyed into the solution despite the elevated concentration of water. In fact, adding water with longer dissolution time permits higher cellulose extraction while achieving lower viscosities and less viscous flow.

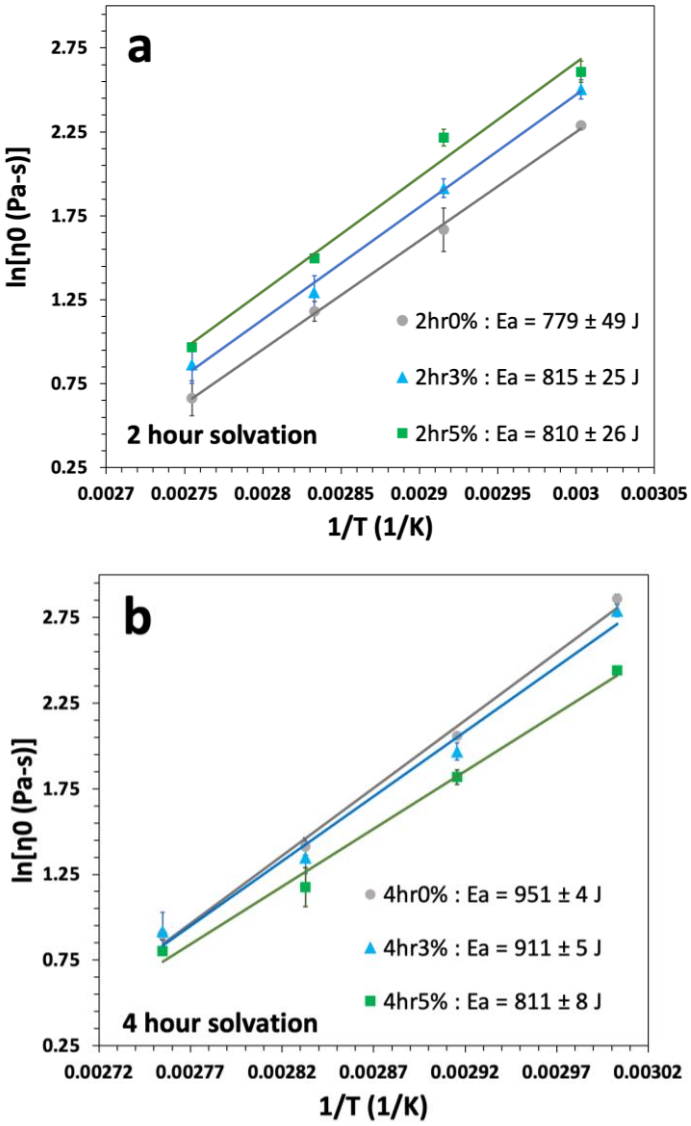


Figure 4-5: Arrhenius plots of 0-5% water/[DBUH][-OAc]/cotton slurries a. 2 hours of solvation and b. 4 hours of solvation, including the activation energies of cotton slurries derived from the slope of the Arrhenius line (Ea/R), where R is the gas constant.

At 60°C, Viscosity vs Shear rate curves reveal that higher solvation times coupled with lower water content resulted in higher viscosities (Figure 4-6). The 4hr0% and 4hr3% slurries saw the highest viscosities with values of 17.4 and 16.3 Pas-s respectively (Table 1). Higher viscosities can be attributed to more cellulose being conveyed into the solution at the higher exposure time. A change in viscous trends is also observed for 2 vs 4-hour dissolution conditions. Where η_0 trended 0%<3%<5% (17.4 ± 0.65, 16.3 ± 0.37, 11.5 ± 0.56 Pa-s) for 2-hour exposures, the 4-hour exposure saw viscous trends of 5%<3%<0% (11.5 ± 0.56, 16.3 ± 0.37, 17.4 ± 0.65 Pa-s). From

this data, it can be assumed that, at the lower exposure duration, the presence of fibers in 3% and 5% water/IL/cellulose slurries has a more notable contribution to viscous trends (Figure 4-6). On the other hand, longer exposure contributes to homogeneous mixtures and, with water, generous reductions in viscosity.

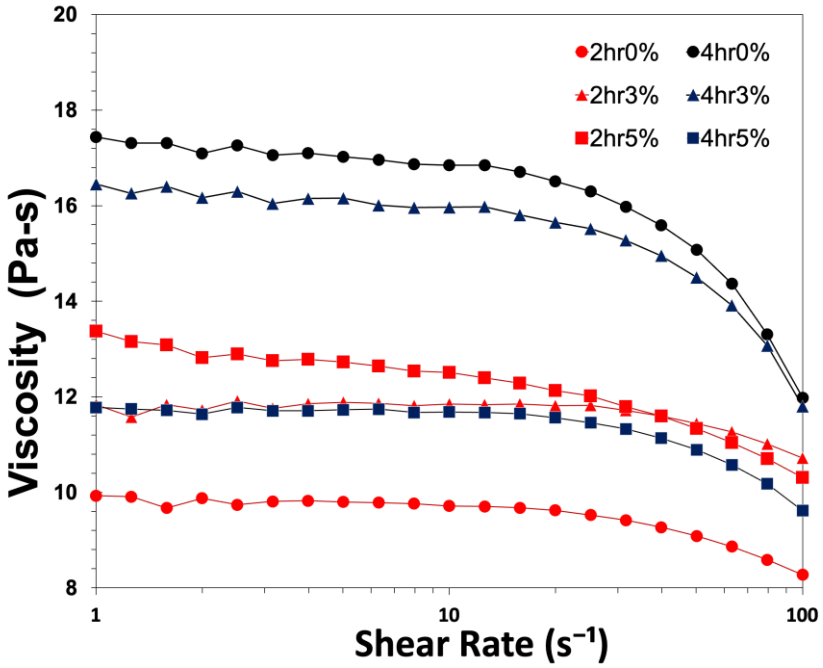


Figure 4-6: Viscosity v. Shear rate graphs of **2 and 4 hour exposed** water/cotton/ionic liquid mixtures where rheology is conducted at 60°C.

Dissolution conditions also impact shear-thinning behavior. Power Law coefficients extracted from the linear power law, shear thinning region show that 2-hour exposed slurries have near Newtonian behavior with behavior exponents close to 1 (Table 4-2) with values of 0.88 ± 0.1, 0.92 ± 0.12, and 0.88 ± 0.09 respectively for 2hr0%, 2hr3%, and 2hr5% slurries. The 4hr0% and 4hr3% samples show shear thinning behavior with values <1 of 0.73 ± 0.05 and 0.77 ± 0.03, respectively while, for the 4hr5% slurry, 5% water content is enough water to cause a Newtonian response similar to the 2-hour exposure slurries; the behavior exponent for the 4hr5% sample is 0.86 ±0.14.

Table 4-3: Zero Shear Viscosity and Power law coefficients for 5% cotton in water/IL slurries at 60°C, coefficients n and K are derived from the power law equation: $\ln \eta = (n-1)(\ln \dot{\gamma}) + \log K$ [288].

Sample	Zero Shear Viscosity (Pa-s)	n (dimensionless)	K (Pa·s^n)
2hr0%	17.4 ± 0.65	0.88 ± 0.1	3.21 ± 0.09
2hr3%	16.3 ± 0.37	0.92 ± 0.12	3.32 ± 0.03
2hr5%	11.5 ± 0.56	0.88 ± 0.09	3.55 ± 0.05
4hr0%	9.8 ± 0.57	0.73 ± 0.05	5.12 ± 0.12
4hr3%	11.4 ± 0.43	0.77 ± 0.03	4.69 ± 0.12
4hr5%	13.2 ± 0.45	0.86 ±0.14	3.63 ±0.11

4.3.3 Fiber Characterization from Extruded Precipitates

Optical microscopy and SEM images show that the casted 2hr5% fibers have an irregular surface due to undissolved cotton particulates (Figure 4-7i and Figure 4-7j). Roughness values were also highest for the 2hr5% fibers and lowest for 4hr0% casted fibers which had RMS values of 198.9 ± 44.2 and 71.6 ± 17.5 nm respectively. RMS values for other fibers were comparable to each other values of 91.0 ± 17.9, 105.6 ± 11.7, 95.1 ± 23.8, and 99.6 ± 18.5 nm for 2hr0%, 2hr3%, 4hr3%, and 4hr 5% respectively. These results confirm the expected observation that the high content of undissolved fiber in slurries would result in a rough fiber surface, and the higher dissolution time result in more homogeneous fibers.

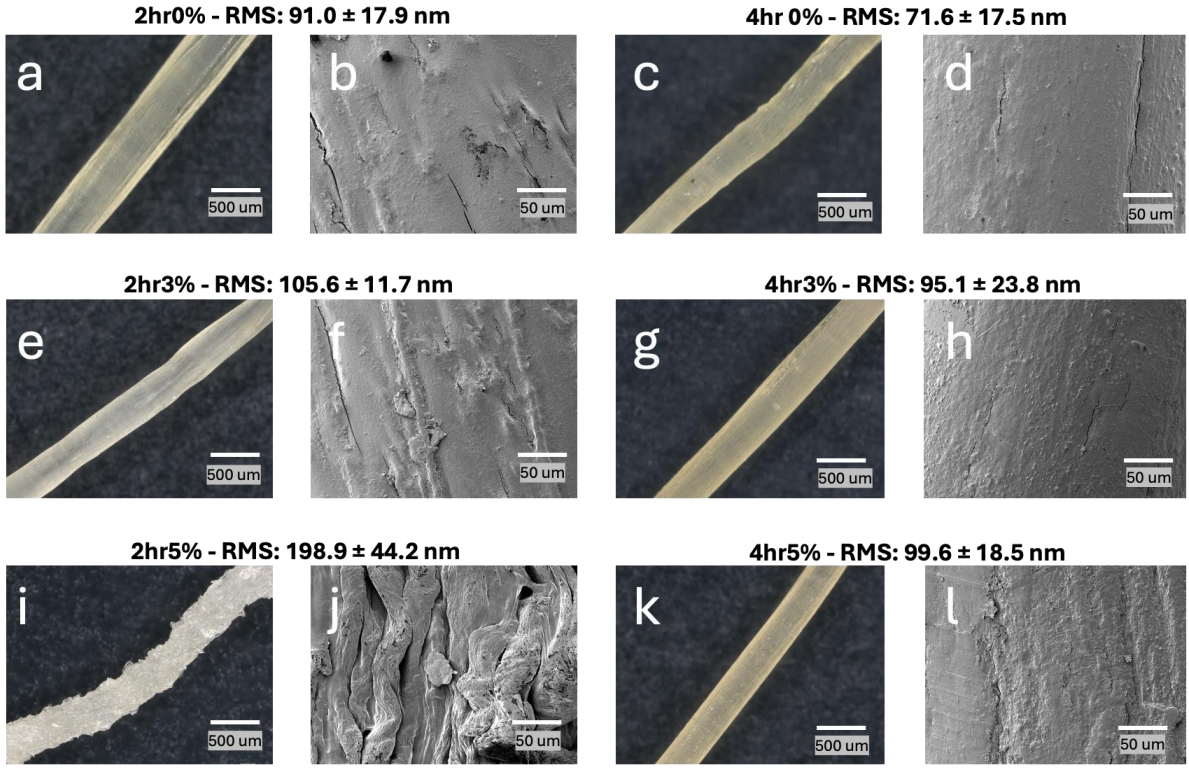


Figure 4-7: Optical and SEM images of reformed fibers cast from slurries made from the following conditions: a/b and c/d: 0%water/IL, dissolved for a/b) 2 hrs and c/d) 4hrs; e/f and g/h: 3%water/IL, dissolved for e/f) 2hr and g/h) 4 hrs; i/j and k/l): 5%water/IL dissolved for i/j) 2 hrs. and k/l) 4hrs. RMS roughness values were calculated Gwyddion open source software.

After regeneration, high aspect ratio fibers were dried and characterized by optical microscopy and mechanical analysis (Figure 4-8). Mechanical assessments of the fibers yielded modulus values on the order of 1-6 GPa and tensile strength values of 60-160 MPa (Figure 4-8), which is comparable to values from other regenerated cellulose and All Cellulose Composites (ACCs) found in literature. [76,77,295] Mechanical properties for extruded fibers did not match typical trends in literature, which suggests that higher particulate ratios and higher viscosities seen for 2hr5% samples would produce cast fibers with higher mechanical strengths and moduli, [76,295] but this can likely be attributed to the presence of stress concentration regions. Trends do not show a strong correlation between fiber mechanical properties, water content, and dissolution time, but that does not mean that additions of water do not impact mechanical behavior. Higher quality fiber extrusions would be needed to confirm trends in the mechanical response of fibers.

In addition, despite higher slurry activation energies and viscosities (Figure 4-6), cotton fibers derived from 4-hour solvation are invariant in mechanical response between regenerated fibers even though water and dissolution time impacted reduced viscous flow, E_a and viscosity, and shear thinning behavior. Longer dissolution times (4-hour) may make slurries more controllable, but the additional energy expenditure and the increase in rheological activation energy are not advantageous.

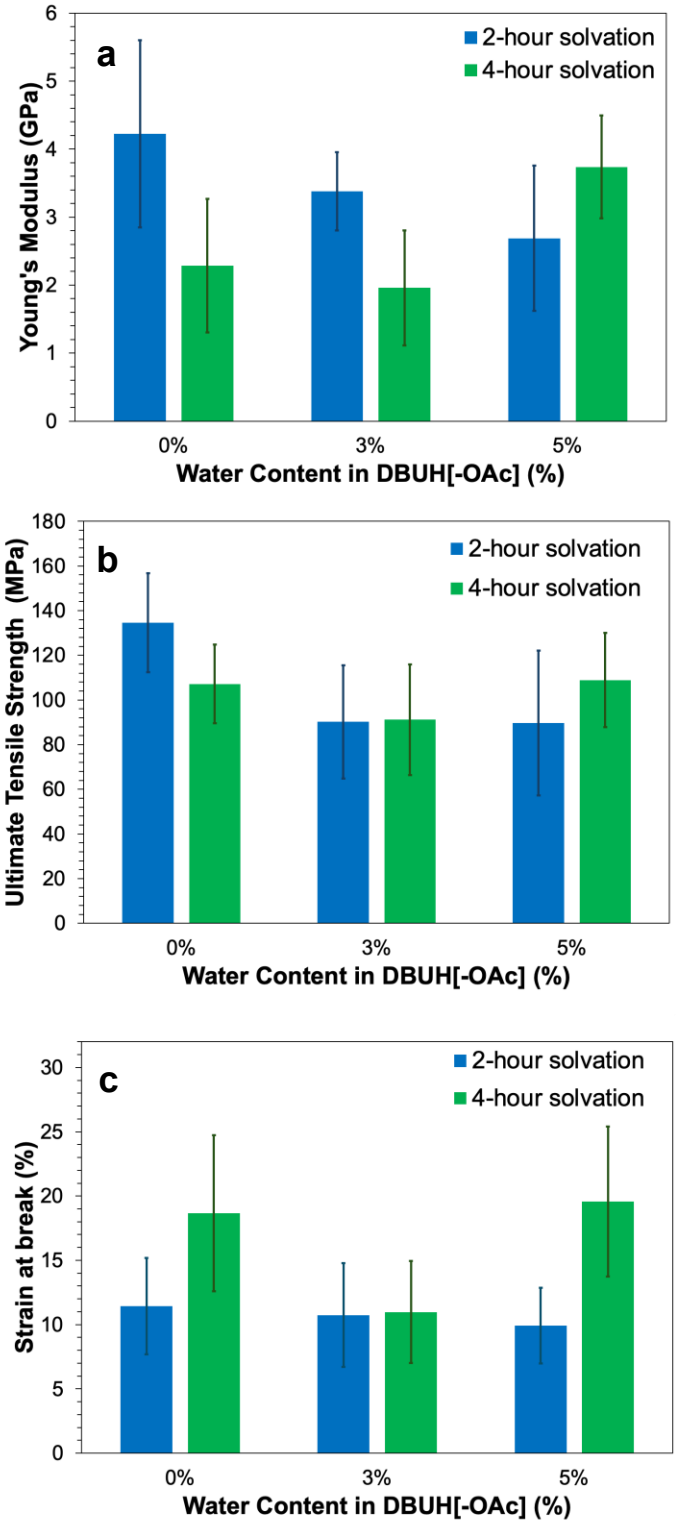


Figure 4-8: Plots of a. Young's modulus and b. Ultimate Tensile Strength and c. Strain at break for syringe-casted fibers precipitated in methanol for 24 hours.

4.4 Conclusions

Parametric experiments helped to gauge how cellulose solvation by [DBUH][-OAc] ionic liquid (IL) was affected by both solvation time and the presence of trace amounts of water in the mix. Higher water content in the IL interfered with cellulose solubility and > 5wt/% water, cellulose was virtually insoluble. Results suggest that both the presence of water and undissolved cellulose fibers contribute to variations in rheological properties. For cellulose dispersions, at a lower solvation time (2 hours), viscous energy, Ea, does not seem to be impacted dramatically with water, but the presence of undissolved fibers with increased water content raises viscosity. At greater solvation time (4 hours), both viscous energetics and viscosity are reduced with water content. Microscopy on regenerated extruded fibers (D=~500 μm) cast from higher water content (5%) slurries had rougher textures compared to those cast from lower water content slurries, but the morphological and viscosity differences do not result in statistically significant differences in the mechanical behavior of regenerated fibers. Overall, water reduced the capacity of ILs to dissolve cellulose and affected the viscosity of IL-cotton slurries. This appears to be a viable way to regulate cellulose solubility, and perhaps the purity of more complex lignocelluloses can be enhanced by selective additions of antisolvents to the IL mix.

Chapter 5 : Water/[DBUH][Acetate] Mixtures for Controlled Lignin/Cellulose Isolations from Corn Stover

5.1 Introduction

Lignin is a natural aromatic polymer, one of the most abundant biopolymers after cellulose, and accounts for 15-40% of most lignocellulose biomasses. Lignin is also among the most abundant renewable aromatic chemicals. [157] Because of the abundance of aromatic and aliphatic hydroxyl groups in lignin, it has gained traction as a renewable raw material to replace polyol, bisphenol-A, and phenol for synthesizing polyurethane, epoxy, and phenolic resins, to name a few. To address the uncertainty of petroleum-based raw materials and to improve polymer biodegradation, the replacement of oil-derived polyols with lignin is a significant way to make the polyurethane market greener. Hydroxyl (-OH) groups in lignin can either be aliphatic, showing up as side groups on linear carbon fractions, or phenolic, identified on one of lignin's aromatic monomer groups: syringyl (S-unit), guaiacyl (G-unit), and p-hydroxyphenyl (H-unit) or in lignin's carboxylic acid moieties. [113,122,161,162] The presence of aliphatic (primary and secondary) and phenolic (aromatic) hydroxyl groups determines the valorization pathways for lignin. [162] For example, lignin with a high content of primary aliphatic hydroxyl groups is most reactive with isocyanate, thus more suitable for polyurethanes, though lignin with aliphatic hydroxyl groups exhibits poor solubility in most solvents, thereby limiting accessibility to O-H groups for isocyanate reactions. Lignin with high phenolic concentrations is most effective for epoxies, and with H and S-unit lignin, suitable for phenolic resin formulations with formaldehyde. [113,296,297]

The concentration of specific hydroxyl group moieties present in lignin can be impacted by processing conditions, which may also impact the extent of delignification. [146–148] Unfortunately, lignin and cellulose extraction from lignocellulose biomasses is hindered by high levels of commingling and covalent links between lignin and hemicellulose fractions in the plant cell wall. [298,299] The type of plant also impacts the types of hydroxyl groups present for extraction. Plants

Contributions: In this study, I conducted most of the experimental and analysis efforts, while ^{31}PNMR analysis was outsourced to the Nejad group at Michigan State University.

like corn stover contain all 3 lignin phenolic monomers, making them a great starting material for extracting aromatic hydroxyl group-rich lignin. [167]

In the United States, corn makes up close to 95% of total feed grain production, but when one considers the mass collected at harvest, the fraction of corn relative to the inedible portions of the plant (called stover) is closer to 50%[300,301]. Corn stover (CS) refers to the stalks, leaves, cobs, and husk that are left behind after harvesting. As a result of the high volume of corn produced in the United States, corn stover is one of the most abundant biomass discards. [301] After harvesting, about 16-44% of the corn stover can be safely harvested, while the remainder of the corn residue is left on the field surface to supply nutrients to the soil and to prevent erosion. [302] The rate of harvested residue will change based on the total biomass yield, the harvesting method, and the risk of harvesting.[303,304] For example, though a high biomass yield results in more corn residue available to be harvested, conventional tilling practices like moldboard plowing may bury residue, reducing surface residue, thereby requiring that more of the stover be kept on the field surface for fortification. [302,305] In this system, only about 19% of corn residue can be harvested.[305] Alternatively, up to 44% of corn residue can be harvested from conservative tillage if 200 bushels per acre of corn can be harvested. [305] These factors must be considered in using corn stover as a valuable feedstock.

Lignocellulose structures are difficult to penetrate with solvents, and they have small molecules and salts that are likely to be conveyed as extractions occur. As a result, a liquid hot water (LHW) treatment has been explored as a separate step to isolate hemicellulose and other soluble inorganic components associated with the stover. During LHW treatment, raw plant material is heated in water at elevated temperatures (130-240 °C) and associated pressures in a vacuum-sealed vessel. [306,307] Under these conditions, hemicellulose swells and hydrolyzes, and the cellulose structure is opened up, leaving a lignin-and cellulose-rich lignocellulose that can then be more effectively isolated. [308] The extracted hemicellulose monomers (xylose - the most abundant, mannose, galactose, glucose, arabinose, and uronic acids) and oligomers (xylooligosaccharides) can be separated into their own feedstock stream.

LHW severity factor, (R_0), is an empirical value that is time and temperature-dependent and is used widely in the LHW treatment world to describe hydrothermal conditions. This severity factor, $\log R_0$ is assigned to each treatment condition in Table 5-1 using the following equation:

$$R_0 = t \cdot \exp\left(\frac{T_i - T_b}{\bar{\omega}}\right) \qquad \text{Equation 5-1}$$

Where t is time, T_i is the target temperature, T_b is the base temperature (100 °C), and $\bar{\omega}$ is an experimental value of 14.75, which was derived by Overend and Chornet (1987). [309] This value was determined with the assumptions that the reaction follows first-order kinetics and has an Arrhenius relationship with Temperature. [104,306,310,311] Under this assumption and from experimentation, the value of 14.75 means that for every 10 °C, the reaction rate doubles and is linked to the activation energy of hydrolytic cleavage. With this LHW pretreatment, the resulting biomass stream is prepped for more targeted isolations.

Carboxylic acid-based ionic liquids (ILs) are known to break hydrogen bonds in cellulose. [312,313] For example, the strong hydrogen bonding (H-bonding) behavior in acetate-based ILs causes major disruptions in interchain hydrogen bonding among cellulose chains. [81,314,315] Studies have also shown that carboxylic acid ILs are capable of breaking β-O-4 linkages in lignin. [204,316] The coupled H-Bond and β-O-4 linkage breaking allows the solvent to penetrate more easily, leading to more complete biomass solvation and difficult extractions of individual cellulose and lignin components.

In Chapter 4, it was observed that water's affinity for H-Bond competition with [DBUH][-OAc]) has been proven to squelch H-bond disruptions. [1–3] At ~10% water, the solvation of cellulose using [DBUH][Acetate] is significantly reduced. If water selectively reduces cellulose solvation, then using diluted [DBUH][-OAc] may more selectively extract lignin (Figure 5-1). As water fine-tunes the dissolution behavior of [DBUH][-OAc], the mixture may also reduce the extent of lignin modification, thereby fine-tuning final lignin properties.

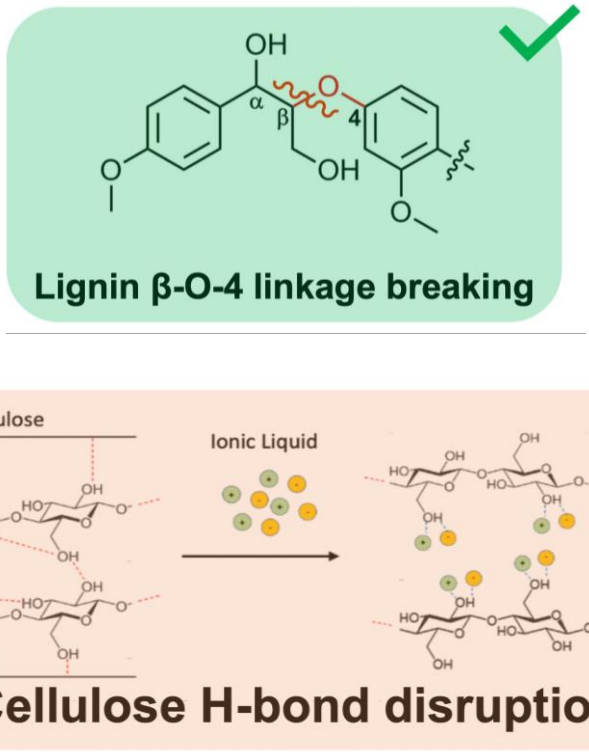


Figure 5-1: Schematic of delignification goal: lignin extraction with minimal cellulose disruption

5.2 Materials and Methods

Corn Stover (CS) was sourced from a local farm. About 20 grams of dry corn stover was soaked in a 1:1 mixture of ethanol (purchased from Thermo Fisher Scientific) and DI water (1000 mL) overnight to clean the stover. DBU and Acetic acid were purchased from Thermo Fisher Scientific.

5.2.1 Liquid Hot Water Treatment of Corn Stover

Corn stover was first ground in a coffee grinder, then sifted through a 300 μm sieve to reduce particle size since smaller particles are more tractable to LHW treatment. This step produced particles with diameters <300 μm and lengths that were <1000 μm. After sieving, 8 grams of corn stover were deposited into a 100 mL SS316 stainless steel MTI Corporation GSL-500X-XX hydrothermal reactor.The reactor was heated to the target temperature for 40 minutes and experiments were done from 130-190 °C for 30-240 minutes, yielding the following severity factors in Table 5-1:

Table 5-1: LHW conditions vs severity Factor

Time	**Temperature (**°C)	**Severity Factor**
0	0	0
130	30	2.36
150	30	2.95
170	30	3.54
170	60	3.84
170	120	4.14
170	240	4.44

5.2.2 Corn Stover Structural Changes

Scanning Electron Microscopy (SEM) was done at x60 magnification to visualize structural changes to corn stover after LHW treatment (Figure 5-2). After LHW treatment, the structures of the residual fibrils are compromised, and the swelling and fragmentation of the fibrils are more enhanced with longer times and higher temperatures (b-e). These structural changes are a sign of biomass structural openings that would result in greater access to lignin and cellulose.

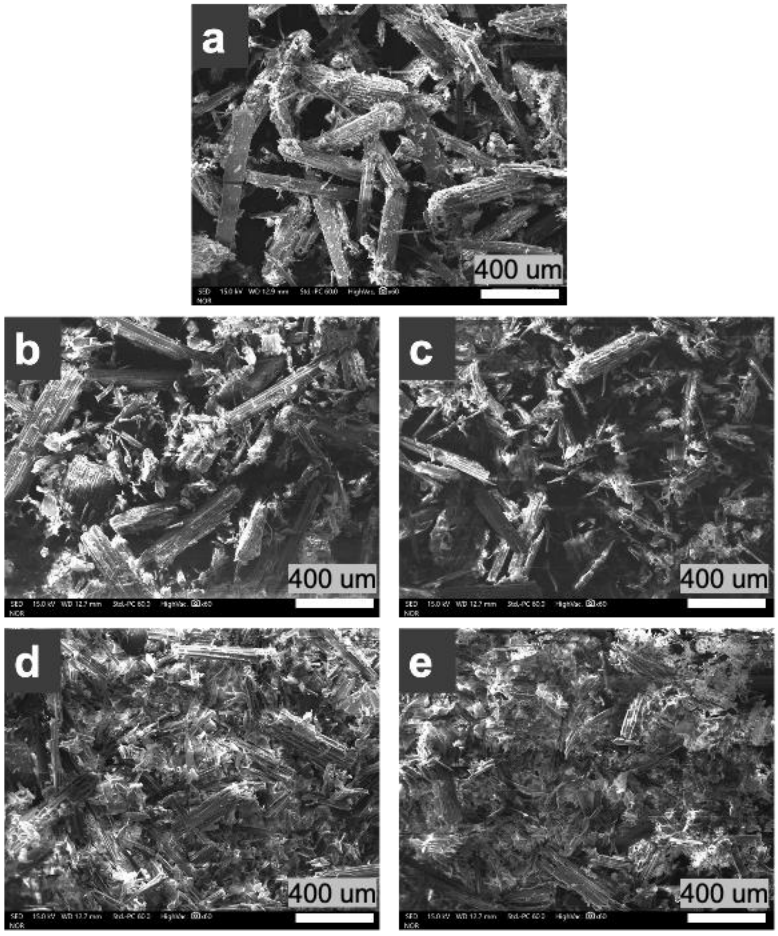


Figure 5-2: Scanning Electron Micrographs of corn stover a. before LHW treatment and after 30-minute treatments at b. 130 °C, c. 150 °C, 30 minutes, d. 170 °C, and e. 190 °C

5.2.3 Compositional Analysis of LHW-Treated Biomass and Hemicellulose Hydrolysis

Compositional analysis was conducted for treated and untreated corn stover to determine their fractions of cellulose, hemicellulose, and lignin. After hemicellulose hydrolysis into the aqueous stream, the amount of hemicellulose in the biomass is expected to decrease significantly, and the residual structure will be more available for extraction.

Compositional analysis for each biomass component was conducted using the following steps: Lignin composition - Lignin composition was determined using Klason lignin determination. [283] 2 grams of corn stover were weighed into a flask with 20 mL of 72% sulfuric acid and stirred at 150 RPM at room temperature. After 3 hours of stirring, 200 mL of DI water was added to the mixture, boiled at 100 °C for 2 hours, and then cooled. After 24 hours, the remaining lignin was washed thoroughly with hot water to remove any residual acid. The mixture was then dried at 105

°C for 2 hours (to constant weight) and weighed to determine the fraction of biomass composed of lignin.

Holocellulose Composition - Holocellulose is the portion of the biomass that comprises both cellulose and hemicellulose and was determined using steps from Hubbell & Regauskus. [318] About 3 grams of corn stover was weighed into a sealable flask with 160 mL of water and heated to 70 °C. Once the solution was at temperature, 0.67 mL of acetic acid and 0.67 grams of sodium chlorite ($NaClO_2$) were added to the mixture to create an oxidizing acidic environment. The addition of acetic acid and sodium chlorite was repeated 3 times every 2 hours. Afterwards, the remaining holocellulose was collected via vacuum filtration, rinsed with 300 mL of DI Water, and set aside for cellulose composition determination.

Alpha-Cellulose Composition - Cellulose composition was determined using steps from Ramadevi et al. [283] About 2 grams of Holocellulose was weighed into a sealable flask with 20 mL of 17.5% sodium hydroxide (NaOH), then stirred vigorously for 30 minutes at room temperature. After stirring, 33 mL of DI Water was added to the flask and stirred for 1 hour. The remaining biomass was then vacuum filtered and washed with 100 mL 8.3% sodium hydroxide, 200 mL DI Water, 15 mL acetic acid, then rinsed again with 200 mL DI Water.

Hemicellulose Composition – Hemicellulose composition was determined by taking the difference in weight between the holocellulose content and the alpha-cellulose content.

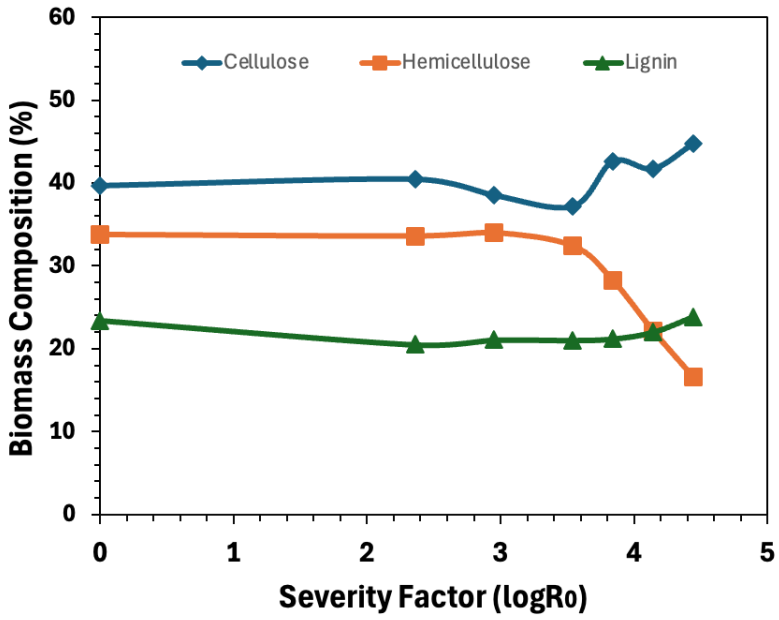


Figure 5-3: Cellulose, Lignin, and hemicellulose content as a function of severity factor (treatment condition) for CS

Compositional analysis of corn stover shows a significant reduction of hemicellulose content after hydrothermal treatment (LHW). The selective isolation of hemicellulose results in a sample where cellulose and lignin become the majority components in the residual biomass for higher purity extractions of both cellulose and lignin. The purification of the biomass mixture was also inferred using the conductivity of the LHW liquid stream as a metric for hemicellulose hydrolysis. (Figure 5-3). When hemicellulose hydrolyzes into its monomers and oligosaccharides (xylose and xylooligosacharide), acetic acid is formed from their acetyl groups, decreasing the pH of the solution, thereby increasing its conductivity (Figure 5-4). [319] Conductivity rose because of more acidic groups in the extraction fluid.

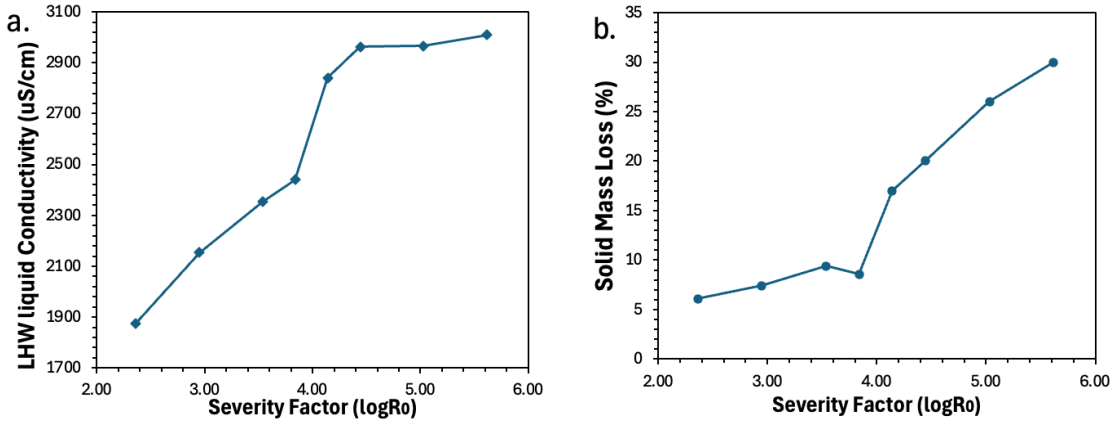


Figure 5-4: The a. mass loss of hydrothermally treated corn stover and b. conductivity of the liquid stream as a function of treatment condition

5.2.4 Ionic Liquid Water Mixtures Preparation

See 4.2.1 for [DBUH][-OAc] synthesis. For this study, 0, 5, 10, 20, 30, 50, 60, 80 w%/w% water in IL were prepared for cellulose extraction and 0-20% water in IL was prepared for lignin extraction. Abbreviations can be found in Table 5-2.

Table 5-2: Abbreviations for IL/Water treated Lignin samples

Lignin Sample Name	Water: IL content for treatment
0WIL	0:100
5WIL	5:95
10WIL	10:90
20WIL	20:80

5.2.5 Lignin/IL Processing and Initial Lignin Composition

In a 50 mL vial, a 1:10 CS: IL mixture is prepared (2 grams of corn stover in 20 grams IL). The mixtures were heated at 80 °C 0 for 3 hours at 100 RPM. After IL processing, the biomass fragments dissolved in IL/CS solution were precipitated out in 100 mL of water, vacuum filtered, and the solid fraction was set aside to dry at 105 °C for 2 hours. After drying, the reprecipitated fraction (with higher lignin exposure) was added to a vial with 30 mL of 0.5M NaOH, which is a mild alkaline treatment that liberates any lignin still in the precipitate. The liquid portion (extracted lignin + residual hemicellulose + NaOH) was then vacuum filtered using two 4-inch diameter

Whatman 1 filter paper sheets, while the cellulose-rich portion was set aside for washing with 200 mL of hot DI water to eliminate any H_2SO_4 residue. Lignin was then precipitated from the filtered liquid using 1 M H_2SO_4 titrated to a pH of 2. The precipitated mixture was then washed and vacuum filtered using two 1.5-inch-diameter Whatman No. 1 filter paper sheets. Both the cellulose-rich portion and the lignin-rich portion were dried overnight in a vacuum oven at 40 °C to constant weight (Figure 5-5)

The extraction rate was determined by measuring the weight of the extracted lignin over the grams of lignin present in untreated CS. The initial lignin fraction in untreated corn stover was determined by Klason lignin determination (See 5.2.2). [320]

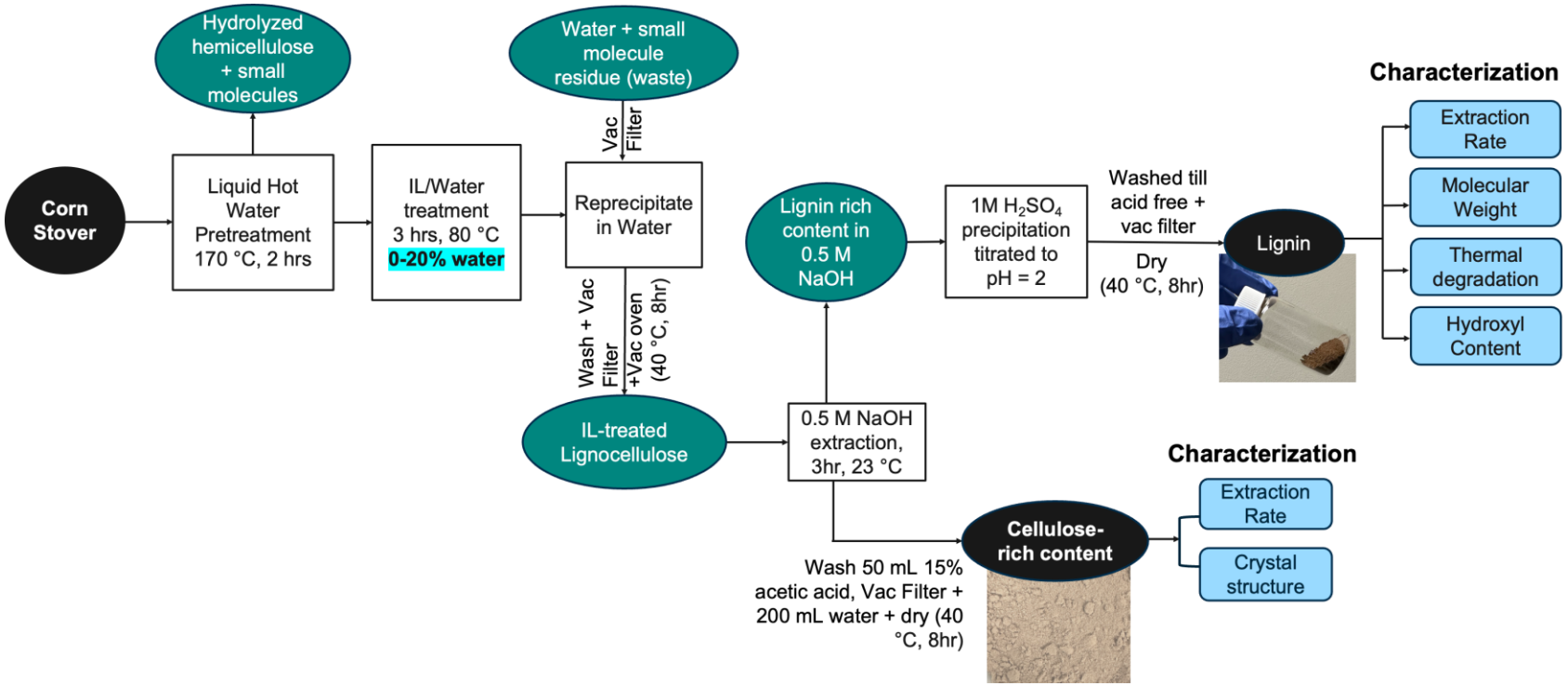


Figure 5-5: Schematic of lignin and cellulose isolation from IL/Water treatment of CS, and characterization

5.2.6 X-Ray Diffraction of Cellulose-Rich Portion of the IL Treated Corn Stover

Using a Rigaku Miniflex X-ray diffractometer, X-ray diffraction (XRD) data was extracted, covering 2θ values of 5-60° with a ramp speed of 10°/min, a CuKa X-ray source ($\lambda = 0.154$ nm), and a step size of 0.02°. The crystallinity index of the XRD spectra for each cellulose-rich portion extracted via water/IL mixtures was determined using two methods: 1) a widely used Peak Height Method (PHM) which utilizes an empirical formula to resolve %Crystallinity (%CrI) (see Section 4.2.2) and 2) a Peak Deconvolution Method (DM) which takes the ratio of integrated deconvoluted crystalline spectra over the sum of integrated crystalline and amorphous spectra.[68,321] For PHM, the baseline was first corrected using Origin, then crystallinity peaks and the empirical "amorphous" estimates were determined using the peak finder tool. For DM, the cellulose spectra were deconvoluted, and the baseline was established using the Rigaku Smart Lab II, then the Origin data analysis application was used to integrate individual amorphous and crystalline spectra.

5.2.7 Thermal Analysis

Thermogravimetric Analysis (TGA) was conducted using an IR-Perkin Elmer TGA. 8-10 mg of lignin was added to the TGA boat and was heated from 50-800 °C at 10 °C/min in an inert atmosphere with an N_2 flow rate of 40 ml/min. Dynamic weight loss with temperature and time, and total mass after heating, resolved the lignin weight after thermal degradation, fraction of inorganic impurities, and decomposition temperatures.

5.2.8 GPC

Gas Permeation Chromatography (GPC) was performed on the IL-treated lignin samples to measure particle elution time for Molecular Weight (MW) estimates. To prep lignin samples for GPC, the extracted lignin first had to be acetylated to ensure that lignin is readily soluble in THF, the solvent used for GPC. About 0.5 grams of lignin were first dried to constant weight at 80°C. Then, 0.25 grams of the dry lignin were added to a 20 -mL vial. Under a fume hood, 5 mL of Pyridine and 5 mL of acetic anhydride were added to the solid, sealed, and left to mix at room temperature for 20-24 hours, 150 RPM. After mixing, a solution of 20 mL of 0.1 mol HCl was produced in a separate flask to which the reacted lignin was slowly added and mixed for 5 minutes. The precipitated solids from this reaction were centrifuged, washed with 200 mL of water, and dried in a vacuum oven at 60 °C until constant weight. About 1mg/ml of dried, acetylated lignin

in THF was measured and filtered through a 22 mm PVDF syringe filter into a 2 mL GPC vial. Standard GPC procedures were performed and compared with a polystyrene standard (Figure 5-6).

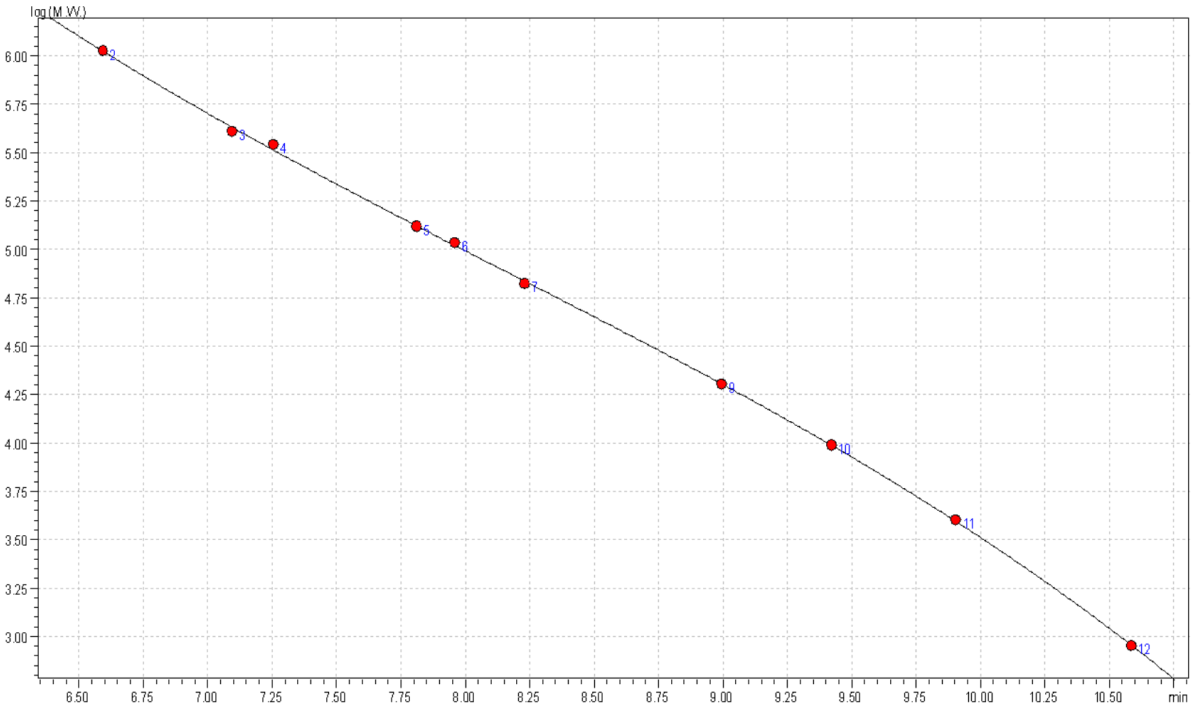


Figure 5-6: Polystyrene standard calibration curve for Gas Permeation Chromatography (GPC)

5.2.9 31P-NMR

Quantitative Phosphorous-31 Nuclear Magnetic Resonance (^{31}P-NMR) was conducted on the treated lignin samples to observe changes in hydroxy groups and hydroxy content. To prepare lignin for ^{31}P-NMR analysis, procedures from Argyropoulos [141]and Granata et al.[322] were used with modifications from Kalami et al.[114] First, a 1:6 v/v solution of pyridine and deuterated chloroform was prepared under a fume hood in a glass vial. Then about 1000 mL of the pyridine-chloroform solution was added into 3 separate vials: one containing 22.6 mg of internal standard (cyclohexanol), and the other containing 5-8 mg of relaxation agent (chromium acetylacetonate). After the internal standard and relaxation agent solutions were set aside, 500 mL of the pyridine-chloroform solution is deposited into a glass vial containing 30 mg of lignin. To ensure complete lignin solubility, 200 mL of dimethylformamide was added to the lignin solution. Immediately before analysis, 100 mL of relaxation agent solution and 100 mL of internal standard were added to the lignin solution, followed by 100 mL of the phosphitylation reagent ((2-chloro-4,4,5,5-

tetramethyl-1,3,2- dioxaphospholane). About 600-700 mL of the total solution was added to a standard NMR test tube. Samples should be run no more than an hour after preparation. The following parameters in Table 5-3 are used for ^{31}P-NMR measurements:

Table 5-3 ^{31}PNMR Parameters for IL-treated lignin

Parameters	**Value**
Number of scans	128
Phase angle 90	90 degrees
Relaxation delay	5 seconds

Each sample's hydroxyl content was determined using a procedure from Nikafshar et. al. [323] The ratio of the cyclohexanol internal standard integrated area to the integrated areas of specific spectral sections was used to quantify hydroxyl content (Table 5-4).

Table 5-4: ^{31}PNMR ppm ranges for aliphatic, phenolic, and carboxylic acid hydroxyl groups

Section name	**Spectral region (ppm)**
Aliphatic -OH groups	149.1-145.4
cyclohexanol	145.3-144.9
syringyl phenolic -OH	143.2-142.0
guaiacyl phenolic	140.5-138.6
p-hydroxyphenyl	138.5-137.3
carboxylic acids	135.9-134.0

5.3 Results and Discussion

5.3.1 Lignin and Cellulose Remain Comingled After IL Solvation of Cellulose;

Due to the intermingling of cellulose, lignin, and hemicellulose in the plant cell wall, access to both lignin and cellulose is limited, and opening the structure via LHW treatment is meant to increase access for extraction, reduce hemicellulose content, and isolate soluble salts and sugars. Solvation tests in pure [DBUH][-OAc] show that LHW treatment opens the lignocellulose

structure (Figure 5-2), allowing access to cellulose and lignin, and when dissolved in pure IL, LHW-treated corn stover (treated at 170 °C for 2 hours) had a % solvation value that was more than 4x higher than untreated corn stover (Figure 5-7). Yet still, upon solvation, both components remain comingled and are entirely dispersed into a slurry, making it very difficult to isolate cellulose and lignin individually.

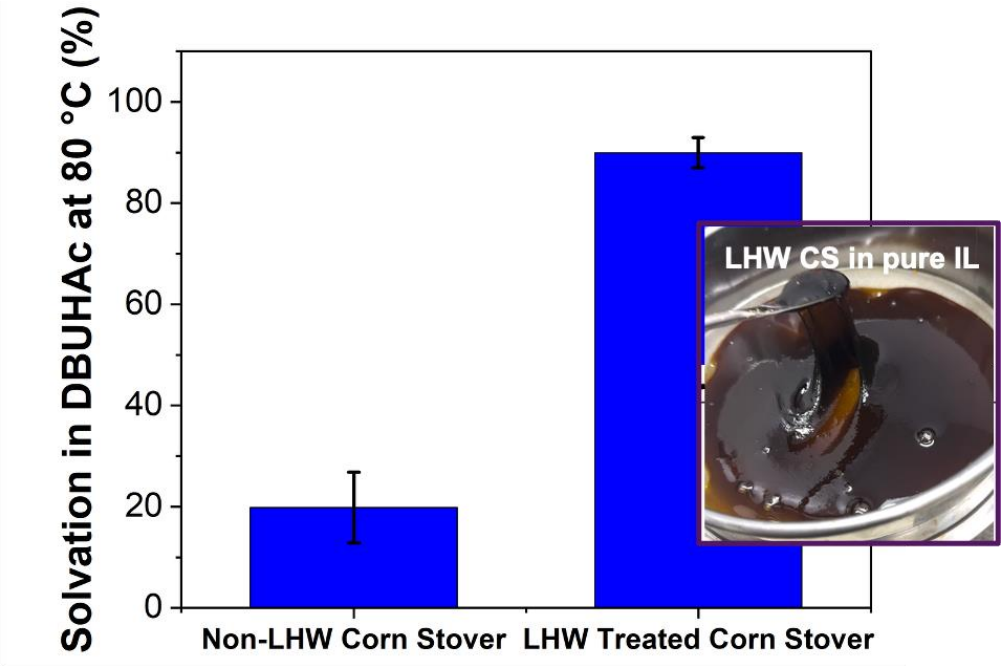


Figure 5-7: Liquid solvation in IL (80 °C for 3 hours) before and after LHW treatment (170 °C for 2 hours)

5.3.2 Cellulose Crystallinity is More Pronounced After IL-Water Treatments

Characteristic cellulose I XRD peaks in raw, untreated lignocellulose have a primary peak observed at around 22.0 °- 22.7 °, which corresponds to the (200) crystal plane (peak-1 – Figure 5-8a). [324–326] Cellulose I in lignocelluloses also has a convoluted peak (peak 2 – Figure 5-8a) at 14 ° - 16.5 °, which corresponds to overlapping $(1\bar{1}0)$ and (100) planes. [324–326]. Two methods were compared to determine crystallinity index (%CrI) trends, 1. Peak Height Method (PHM) (Figure 5-8a), and 2. Deconvolution Method (DM) (Figure 5-8b). PHM is the most broadly used method for %CrI determination in cellulose. In PHM, an empirical formula (Equation 5-2) is used:

$$\%\mathrm{CrI} = \frac{\mathrm{I_{200}} - \mathrm{I_{am}}}{\mathrm{I_{200}}} \times 100 \qquad \text{Equation 5-2}$$

Where I_{200} is the intensity of the (200) plane peak at around 22.2°, and the amorphous peak is estimated to sit between the primary (200) plane peak and the $(1\bar{1}0)$/(100) peak at around 18°. In

the deconvolution method, %CrI is determined by finding the ratio of integrated crystalline spectra over the sum of both the integrated crystalline and amorphous spectra.

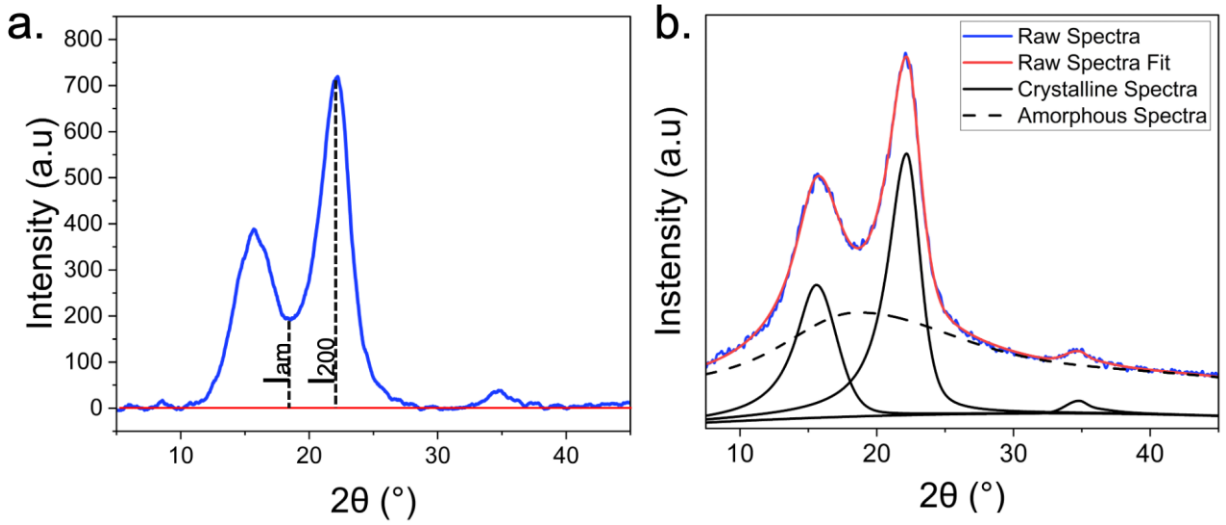


Figure 5-8: Examples of XRD spectra Crystallinity determination using two methods: a. Peak Height Method (PHM) and b. Deconvolution Method (DM).

To selectively isolate cellulose in corn stover samples, 5-80% water was introduced into the IL system. Between the PHM and DM-%CrI values resolved, the PHM values across IL/water samples were much higher, which is consistent with trends in other studies that suggest that this method consistently yields higher biomass crystallinity values and may have some inherent flaws since it does not consider all crystallinity peaks.[321,327] Using both PHM and DM as methods to compare the different corn stover samples, PHM highlights that XRD crystallinity is more pronounced for IL/water treated samples, whereas DM crystallinity differences are not as pronounced with water. While DM likely gives a holistic view of crystallinity since it considers all crystallinity spectra, PHM highlights nuances in the IL/water treatment, which demonstrates an enhanced spectra as a function of water. Both methods highlight %CrI reduction for the pure IL system.

In samples dissolved by pure IL, the cellulose structure is largely amorphous, and peak-2 is almost entirely diminished (Figure 5-9a). This diminished peak is evidence of disrupted lattice planes due to IL's interference of strong hydrogen bonds. In cellulose, the $(1\bar{1}0)$ and (100) planes are the H-

Bonded interfaces, which is why they are more susceptible to H-Bond disruptions by H-Bonding [DBUH][-OAc].[328–330] On the other hand, Van der Waals bonds dominate (200) planes. [330]

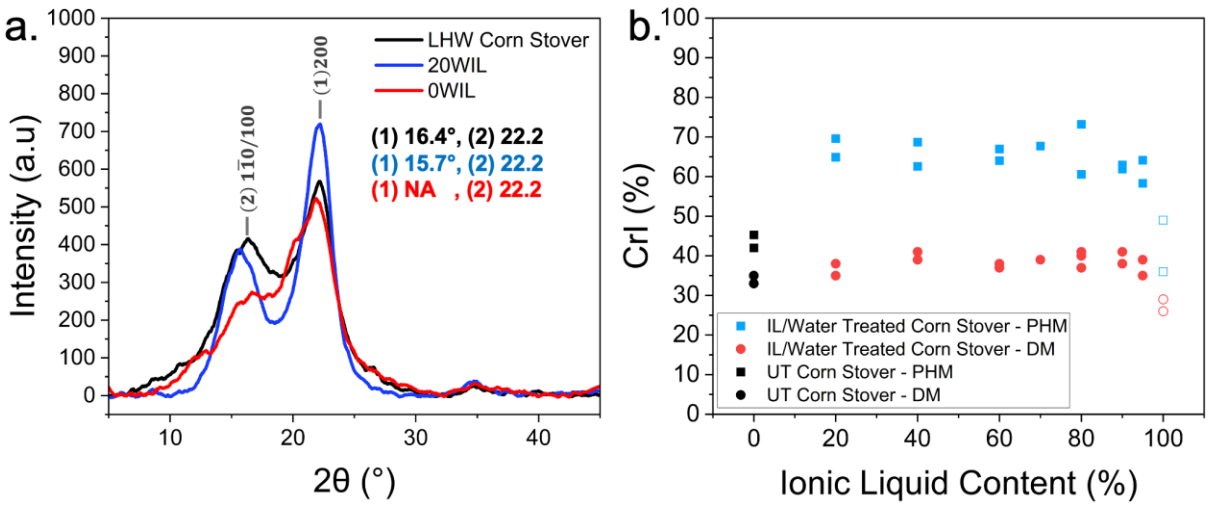


Figure 5-9: Cellulose XRD data for LHW-pretreated (black), 20% water/IL-treated (blue), and pure IL-treated (red) corn stover b. crystallinity as a function of water content of IL/Water treated corn stover, where LHW-pretreated corn stover is black, PHM (blue – square) and DM (red – circle) crystallinities. IL/water-treated samples are solid colored; pure IL-treated samples have open squares and circles.

For raw corn stover, a cellulose crystallinity of about 45% is observed using PHM and 35% using DM, and two characteristic peaks are seen at 16.4, the (1$\bar{1}$0)/(100) plane (peak-2), and at 22.2°, the (200) plane (peak-1) (Figure 5-9a). After IL/water treatments, peaks 1 and 2 are more pronounced, the intensity of peak-2 increases, and the degree of cellulose crystallinity increases by about 20% relative to the LHW corn stover for the PHM method (Figure 5-9b); the cellulose crystallinity increases by about 3-5% for the DM method. For the 20WIL sample, characteristic peaks are observed at 15.7° and 22.2° (Figure 5-9a), indicating a slight leftward shift of peak-2. This peak shift is proof of expanded lattice spacing and some disruption to the cellulose structure, but cellulose crystallinity is still observed. Other studies observed that treating lignocellulose biomasses with mild conditions increases cellulose crystallinity due to the extraction of amorphous components like lignin and hemicellulose. [98,100,331] Other IL-treated lignocelluloses also report similar disruption to the lignocellulose cellulose structure when pure IL is used. [332,333]

These results confirm not only that water/IL mixtures are benign to the exposed cellulose but also that the crystalline fraction is more pronounced due to the isolation of lignin from CS. For 80%

water in IL (20% IL), a comparable corn stover crystallinity to 20% water in IL (80% IL) is observed. This means that dilute IL mixtures can still be employed for effective lignin extraction.

Extraction rates for the four samples show comparable delignification percentages (Figure 5-10). There may be tradeoffs between complete fractionation and not enough fractionation when water is introduced. On one hand, complete fractionation causes comingling, which results in inefficient lignin isolation. On the other hand, too much water may inhibit lignin isolation, thus negatively impacting efficiency. In addition, the reality of lignin loss between processing steps impacts observed isolation efficiencies.

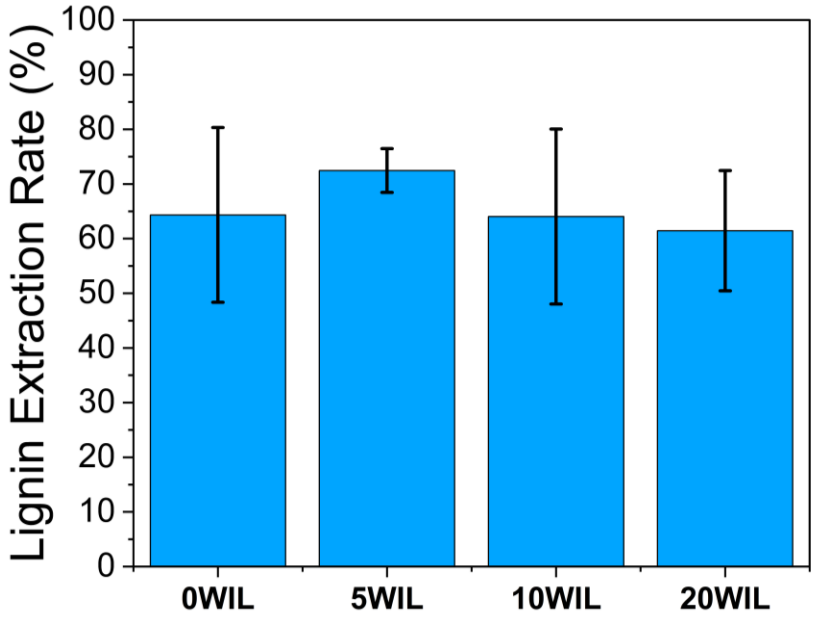


Figure 5-10: Lignin extraction rates for IL-Water mixtures: 0WIL (0% water), 5WIL (5% water), 10WIL (10% water), 20WIL (20% water)

5.3.3 With Trace Amounts of Water, Lower Elution Times and Less Lignin Impurities are Observed

Gas Permeation Chromatography (GPC) shows retention time data for IL/water-treated corn stover (Figure 5-11). Treatment duplicates were prepared for GPC and TGA analysis to confirm trends. As water content for IL treatment increases (up to 20%), the peak retention time of lignin extracted is slightly reduced, which corresponds to a subtle rise in chain length and MW of the lignin

precipitate. Using a calibration curve from a polystyrene standard (Figure 5-6), MW estimates are 2060, 2120, 3090, and 4170 g/mol for 0, 5,10, and 20 WIL, respectively.

For 0WIL, lignin depolymerization is likely maximized in comparison to water/IL mixtures. While other studies have shown that acetic acid-based IL depolymerization of lignin can be conservative, research shows that they are capable of breaking C-O bonds to delignify lignin. [197,334–336] With water, lignin depolymerization is reduced since water inhibits [DBUH][-OAc] interactions with lignin. [337,338] As a result, higher MW, less depolymerized structures are precipitated. Overall, the leftward shift of the GPC curves for water/IL-treated samples suggests evidence of slight lignin MW tuning using water (Figure 5-11).

A slight shoulder corresponding to lower MW species is also observed in GPC, which may suggest the presence of impurities, lower MW lignin, or low MW residual hemicellulose that are conveyed into the mixture during β-O-4 cleavage. Regardless, the presence of this peak suggests heterogeneity in the extracted lignin caused by low MW oligomers.

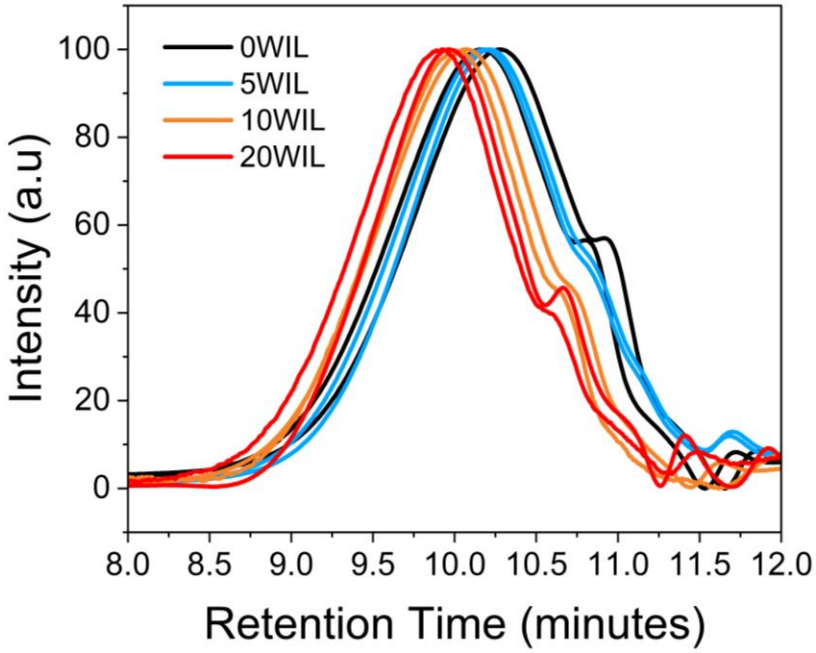


Figure 5-11: GPC Curves for IL/Water extracted lignin. Duplicate lignin samples are plotted

TGA was run to assess the degradation profile for each lignin sample. The comprehensive thermogravimetric characteristics for each IL/Water treatment type are recorded in Table 5-5. Overall, all lignin samples have similar degradation profiles and show two observed inflections in the degradation derivative peaks. These peaks are seen at ~290 °C and ~350 °C (Figure 5-12), confirming the presence of a second species seen in GPC (Figure 5-11). Past TGA studies observe that low MW species can exhibit lower degradation temperatures and sharper degradation peaks. This lower temperature peak may also be residual carbohydrates since hemicellulose and cellulose degrade at 250-300°C and have sharper degradation peaks. Again, additional analysis will be needed to determine the presence of residual carbohydrates.

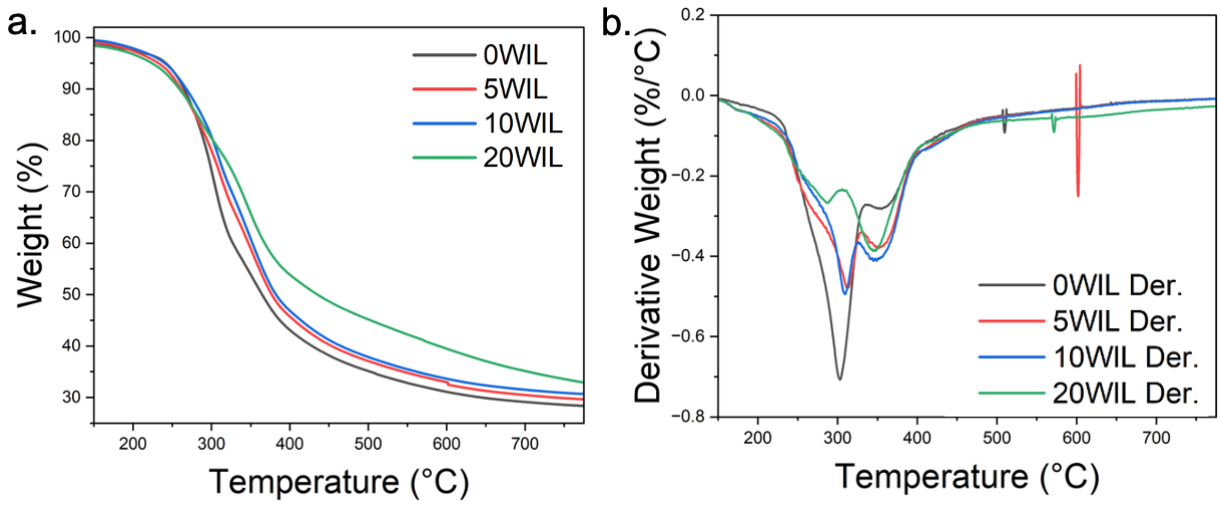


Figure 5-12: a. Degradation curves from 100-800 °C and b. Derivative of degradation curves from 100-800 °C

While 20WIL has a lower initial onset degradation temperature (at 229 °C), it has the most stable thermal profile, with lower holistic degradation rates, likely due to its higher MW. In addition, the 20WIL sample also has a slightly higher residue percentage at 800 °C, though the residue % value for all lignin samples may converge to virtually the same value at higher degradation temperatures.

Table 5-5: Comprehensive TGA values for lignin treated with Water/IL

Sample	Onset Degradation (°C)	Derivative Peak 1 (°C)	Derivative Peak 2 (°C)	Residue at 800 °C (%)
0WIL	264±23	302±9	353±9	28±8
5WIL	254±13	312±25	350±13	29±5
10WIL	260±5	309±12	347±12	31±7
20WIL	229±22	286±13	346±7	33±4

5.3.4 Analysis of Lignin Hydroxyl Content for 0WIL And 20WIL

The ^{31}PNMR spectra for 0WIL and 20WIL lignin samples can be seen in Figure 5-13, and the total hydroxyl values for each lignin type were determined using a method by Nikafshar et al. [339]. Corn stover inherently contains all three aromatic lignin monomers, carboxylic acid groups, as well as aliphatic lignin, [340] though the amounts of each functional group that is conveyed may change based on the ionic liquid mixture used.

According to the ^{31}PNMR spectra for 0WIL and 20WIL, the total hydroxyl contents for the two lignin types were 6.39 and 5.52 mmol/g, respectively, and their aliphatic -OH and phenolic -OH groups differed drastically. For 0WIL, phenolic content was greater than the aliphatic content, with values of 3.43 and 2.34 mmol/g, respectively. Comparatively, the 20WIL lignin sample saw much greater aliphatic lignin content (4.56 mmol/g) than phenolic (0.94 mmol/g). The carboxylic acid content also differed: 0.62 mmol/g for the 0WIL and 0.02 for 20WIL.

In the pure IL mixture, the high phenolic ratio, paired with its lower MW, is indicative of effective β-O-4 cleavage. [341] Comparatively, the lower phenolic content for 20WIL, paired with its greater MW, hints at low β-O-4 cleavage, even if comparable isolation rates are observed from Figures 5-10. In comparison to other IL-extracted lignin studies from Brandt et al and Wen et al, mild treatment conditions yielded lignin with high aliphatic lignin content, which is comparable to the 20WIL observations. [154,341]

For 20WIL, the recorded aliphatic content is higher than values in the literature for native corn stover lignin extracted via alkaline treatments, which report values between 1.0-3.5 mmol/g. [342–344] The high aliphatic content could be indicative of some residual hemicellulose components that were conveyed during ionic liquid treatment or NaOH extraction, given that hemicelluloses can be dissolved in NaOH. However, the 0WIL sample has aliphatic content that is almost two times lower than the 20WIL sample, likely due to higher dissolution of residual hemicellulose and effective β-O-4 cleavage. Regardless, the low phenolic content in 20WIL points to a less modified lignin structure.

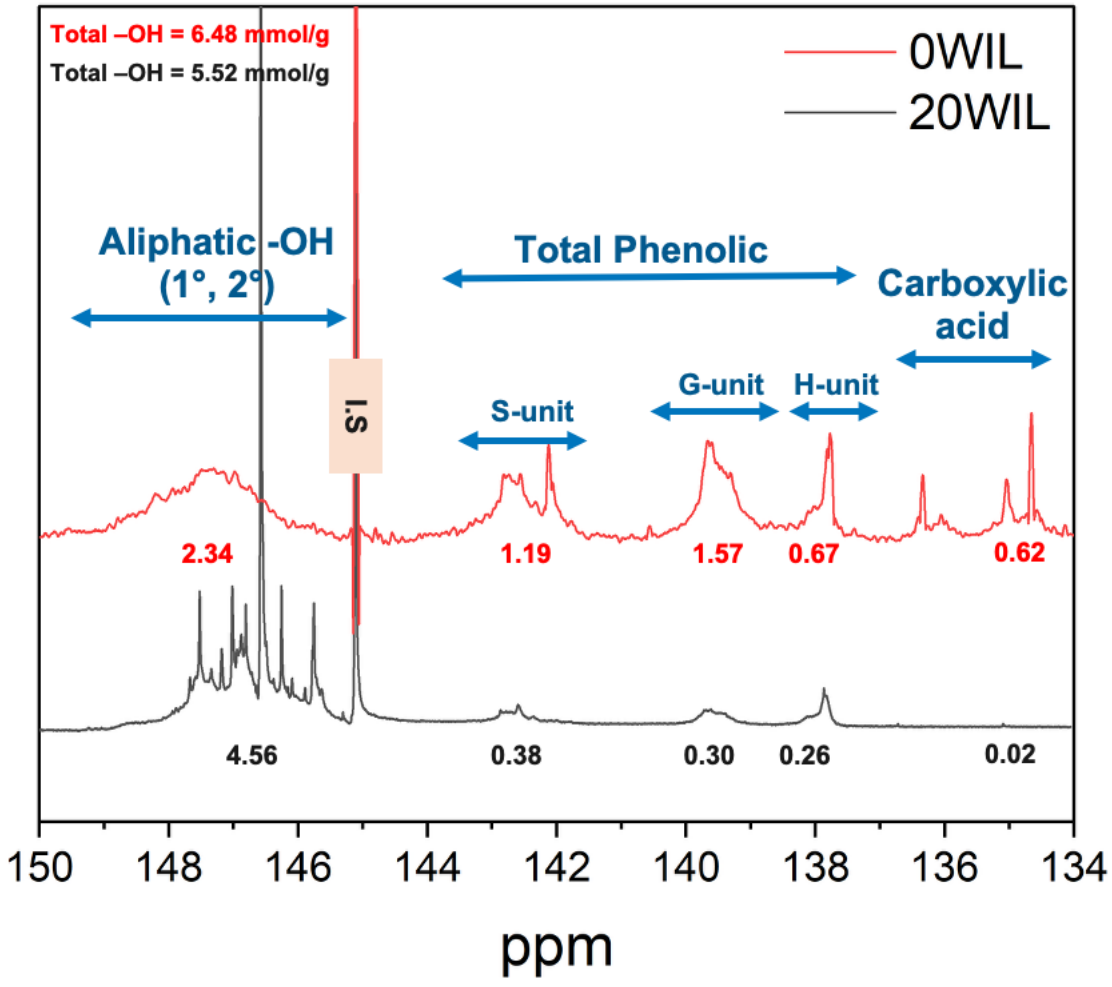


Figure 5-13: Phospourous-31 NMR spectra for 0WIL and 20WIL showcasing specific aliphatic, phenolic, and carboxylic acid regions

Both lignin samples can be utilized effectively for separate valorization pathways. For 0WIL, the high phenolic content makes it suitable for epoxidation reactions, and the high aliphatic content in 20WIL makes it a great candidate for polyurethane synthesis though complete solubility is needed for any subsequent synthesis, post-extraction. [113,296,297] It is important to note that, during ^{31}PNMR analysis, the 20WIL sample dissolved into a cloudy mixture in the pyridine: chloroform solution used for ^{31}PNMR. Given that phenolic hydroxyl-rich lignin is more susceptible to solvation in organic solvents, this cloudiness in the ^{31}PNMR solution impacts the reported value for aliphatic content more than the phenolic.[345] To make more definitive claims, effective dissolution of all samples for ^{31}PNMR analysis is needed, and careful replication between samples is paramount.

5.3.5 Lignin Solubility Analysis

If IL/Water extracted lignin is to be used in biopolymer synthesis, the solubility of lignin in common solvents must be known; having a completely soluble material ensures that the reaction mixture is completely homogeneous, thus reducing the probability of phase separation, poor reactivity, or potential structural defects and inconsistencies in physical properties. A fully soluble mixture also ensures that the properties of the reaction product can be better controlled.

Lignin solubility in acetone and DMSO was investigated because these solvents are known for their ability to dissolve lignin effectively. Solvation tests show that all lignin samples display greater solvation in DMSO (Figure 5-14). This is likely due to similar solubility parameters, δ, between DMSO and lignin. According to literature, DMSO and acetone have δ-values of 13.0 $(cal/cm^3)^{1/2}$ and 9.7 $(cal/cm^3)^{1/2,}$ respectively, whereas lignin's δ value generally falls between 13-14.2 $(cal/cm^3)^{1/2}$. This means that DMSO has a closer δ value to lignin, making lignin more susceptible to DMSO solvation.[346–348]

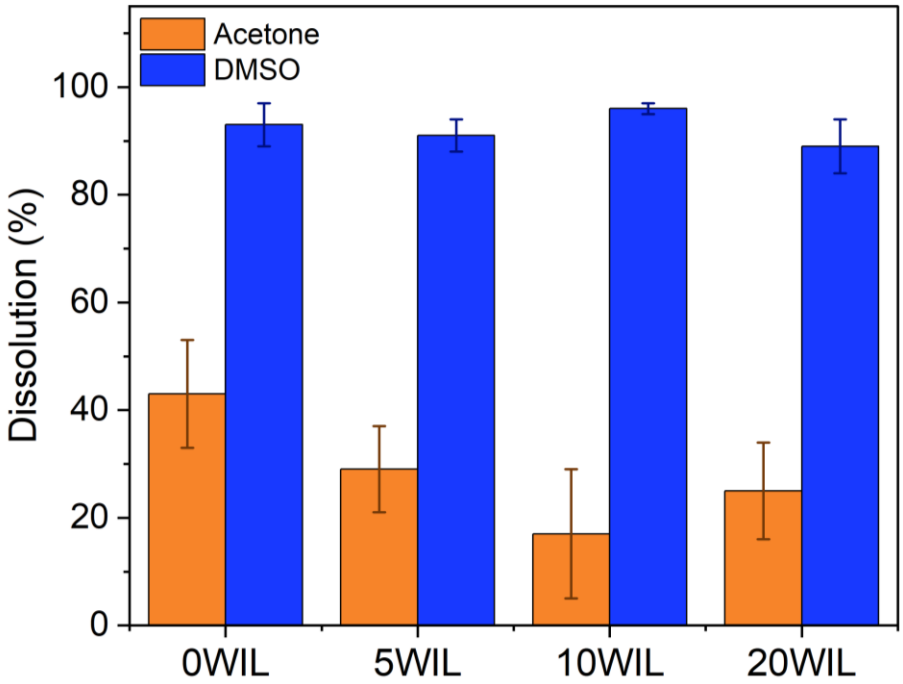


Figure 5-14: Solubility of IL/Water treated lignin samples in Acetone and DMSO

Lignin solubility is influenced by the lignin polarity, the type of solvent used, lignin functional groups, the MW of isolated lignin, amongst many other factors[349]. Lignin with a higher hydroxyl content is more polar and susceptible to solubility in polar solvents[350]. Also, lower MW lignin dissolves more readily in acetone. [151,348] As a result, acetone can be used to selectively isolate lower MW fractions for subsequent biopolymer synthesis. The most notable differences between water/IL-treated lignin samples show that the 0WIL lignin has the greatest solubility at around 43±10%. This could be because of its smaller approximate MW, since smaller MW lignin molecules are likely able to dissolve more effectively in acetone. Also, its higher phenolic content is indicative of a more polar structure, making it more susceptible to solvation in acetone.

Overall, the results confirm that there is potential to use water to reduce IL utilization, retain cellulose properties, and selectively isolate lignin. With water/IL mixtures, the MW, thermal, and hydroxyl properties of extracted lignin can also be tuned. These results suggest the potential to alter the valorization pathway of [DBUH]-OAc] extracted lignin, and its potential end-use cases, by adding water to the IL solvent.

5.4 Conclusions

The potential for selective extraction of lignin using IL/Water mixtures was studied using [DBUH][-OAc] Ionic liquid (IL). Selective lignin extraction was confirmed by assessing whether the corn stover (CS) cellulose structure was disrupted post IL/Water treatment. Using two %CrI determination methods, data revealed that the PHM gives more distinctive comparisons in XRD spectra between LHW treated corn stover and IL/water treated corn stover. For both PHM and DM methods, At 0% water (0WIL), crystallinity reduced notably and the $1\bar{1}0/100$ characteristic cellulose peak that typically shows up at $2\theta = \sim 15\ ^\circ$ was completely diminished. In comparison, IL/Water lignin samples experienced ~20% increases in crystallinity across water content (5-80%). Pure IL treatments (0WIL) saw lignin samples with an average MW value of 2061 g/mol, with non-negligible amounts of lower MW molecule species. The 0WIL lignin also has aliphatic and phenolic hydroxyl values of 2.34 and 3.4 mmol/g. Comparatively, the presence of water (20%) results in the conveyance of lignin with a higher estimated MW (4120 g/mol), and higher thermal stability than 0WIL. The 20WIL sample is also aliphatic -OH rich (4.56 mmol/g), though the high aliphatic values may be indicative of residual hemicellulose. Overall, all results confirm that the valorization pathway for lignin can be tailored by adding water to the IL mixture.

Chapter 6 : Conclusions and Future Works

In this dissertation, two plastic remediation strategies were studied, which address the problem of petro-based chemicals in our environment. To mitigate this issue, the two studies explored:

1. Using a pressure-sensitive adhesive (PSA) to address the need for plastic cleanup in aquatic environments
2. The extraction of natural biopolymers (lignin and cellulose) for biobased alternatives to synthetic, environmentally persistent polymers.

The first project explored two studies on the use of PEHA PSAs as a strategy for MP capture in aquatic environments. Essentially, both studies probe how the capturing environment (laundering additives and the presence of various polymers) inhibits or improves MP sequestering by PEHA. The second project looked at two studies that utilize [DBUH][-OAc] ionic liquid as a solvent for biopolymer extractions of lignin and cellulose, which can then be used for subsequent bioplastic synthesis.

6.1 Conclusions: PEHA Sequestering of Microplastics

In chapter 2, the impact of textile microfibers from the laundering of synthetic fabric is acknowledged. PEHA is used as a target-site preventative measure for obstructing the transition of microfibers from laundering systems to marine environments. A bimodal molecular weight mixture of 95K and 950K PEHA was formulated for MP capturing due to its efficient adhesion characteristics based on prior experience. Adhesive-coated substrates were submerged into a Nylon or PETE suspension prepared with individual laundering additives (glycerol, sodium citrate, and tergitol) to simulate laundry effluent. Quantitative analysis of both particle count and total area of MP coverage on the glass slide were determined using grey scale image analysis (Image J) as metrics for capture efficiency, and adhesion tests were conducted to understand the strength of Nylon or PETE interactions with PEHA in the presence of laundering additives. Results show that amphiphilic additives, like tergitol, interact with PEHA via hydrophobic interactions, compete for the surface of the PSA and prevent MPs from attaching to the PEHA surface. The work confirms

that soaps and detergents are not benign contaminants and will reduce binding if PEHA pressure sensitive adhesives are used for MP capture in laundry effluent.

PEHA-assisted capture is further probed in chapter 3 and addresses a gap in the literature that does not address how PSA sequestering of MP is impacted when more than 1 particle is present, which represents a more real system. Here, single polymer (mono) and multipolymer suspensions of ground particles of PE, PETE, and PP were prepared, and a bimodal 95k:950k mixture of PEHA was spray-coated onto PE foam substrates and completely immersed in a reservoir dispersed with MPs to gauge MP capture. These particles were on the larger end of the MP spectrum, and a realistic representation of mixed ensembles of particles in aqueous solution.

Capture efficiency (by particle count) was measured using the Fiji (ImageJ) Trainable Weka Segmentation plugin for MP distinction by color. Capture efficiency was determined by calculating the ratio of MPs captured over the average number of particles deposited (n=10), which corresponded to 1.5 grams of material. From 1-minute exposure tests, it was revealed that multipolymer dispersions experienced greater capture efficiencies than monopolymer dispersions across plastic types. Even PETE, a high-density particle, experienced a ~20% increase in capture efficiency. In a phenomenon known as heteroaggregation, it is postulated that multiple types of binding mechanisms are present when there is more than one plastic species in dispersions interact with the adhesive including hydrophobic affinity and secondary bonding with hydrogen bonding with the acrylate motifs. As particles are binding, the surface energetics of the adhesive are changing as is its morphological texture. Comparatively, single polymer systems have fewer binding mechanisms to work with, so available binding mechanisms are more limited. In real systems, rarely is one type of particles are present. Noting the enhanced particle capturing for multipolymer systems is promising.

6.1.1 Challenges

Several challenges exist that may curtail the deployment of polyacrylate PSAs as MP capturing tools. In laundering, the goal is to cleanse fabrics which are burdened with oils, dust, and grease that may be just as likely to be drawn to the adhesive surface reducing its potential to capture the fabric fragments that are discharged during washing. Also, since users can change the conditions of laundering environments by altering the operating temperature, concentration of detergent, and

duration of a run, several factors may reduce the overall efficacy of the adhesive for binding particles. For example, PSA tackiness is reduced in colder temperatures; the adhesive hardens, which may cause a decline in how effectively particles bind with the adhesive.

I also found that PEHA itself is a polymer with some latent swelling in water and can be prone to coalesce on the substrate surface with longer exposure times in aqueous solution. It has already been noted in chapter 2 that amphiphilic polymers may act as plasticizers that, at higher concentrations, may weaken the adhesive, causing it to wash into the water. As a minimum, any migration of the adhesive on the substrate complicated analysis of particle counts, and so short time exposures less than 5 minutes in aqueous solution were commonly used. Turbulent currents in marine environments may also contribute to PSA erosion. Once this happens, MPs and nanoplastics can be re-introduced into the liquid stream, nullifying the effect of the capture. It's also possible to engineer the adhesive for higher stability in water. More research is also needed to determine what durations and environmental conditions are most optimal for PEHA, given that I had performed more idealized experiments in DI water vs ground water or seawater. In addition, it may be possible to deposit and covalently bond adhesive onto substrate surfaces to prevent the adhesive from washing away. For glass substrates, UV radical polymerization of the polymers and the use of silane coupling agents can induce strong covalent siloxane bonds to a glass substrate. [351]

6.1.2 Future Direction – Life of Sequestered Microplastics After Collection

Regardless of the method of collection, after collecting MPs, something must be done with the sequestered plastic. The circular economy would ideally use the captured particulates in some new form. Two approaches may be explored for handling post-collection MPs: recycling and biodegradation.

Within a circular economy, plastic waste may be a valuable raw material that can either be used for second-generation polymers or less desirably, for energy. With homogeneous mixtures of MPs, the chemical recycling of polymers into their chemical monomers and/or oligomers for second-generation plastic synthesis may be achievable, but for heterogeneous mixtures, it may be more complicated. [352,353] Because isolated MP streams are often complicated mixtures of several MP types, they cannot easily be separated for use as second-generation plastic feedstocks. We would

also need to isolate the adhesive from the particulates. Going forward, methods must be explored that ideally do not require the separation of different plastic species. Alternatively, pyrolyzing mixed MP residues can be converted into smaller chains and small molecules, potentially for new polymer synthesis or for waste-to-energy applications without first separating the MPs. [354]

Also, in recent years, the microbial degradation of synthetic plastics has been achieved. Fungi and bacteria can be specialized via evolution or through intentional genetic mutations. [355,356] These specialized microbes secrete compatible extracellular enzymes that hydrolyze polymer chains, which are taken up by microbial cells as carbon sources, then turned into harmless substances like water (H_2O), carbon dioxide (CO_2), and biomass. [357,358] Microbial considerations are a great next step for the future of fully mitigating pervasive plastic pollution but again, one would still need to contain the by-products of these deterioration processes if one was producing volatile monomers from the original polymer mixtures.

6.2 Conclusion: Ionic Liquid/Water Mediated Lignocellulose Extraction

The replacement of petrochemicals with lignocellulose components is one way sustainable polymer synthesis can address the problem with persistent petrochemical polymers. In chapters 4 and 5, [DBUH][-OAc] ionic liquid was synthesized for cellulose and lignin extraction. In both chapters, water was used as a tool for regulating biopolymer solvation. Since water has hydrogen bonding characteristics, it competes with [DBU][-OAc] hydrogen bond displacements in cellulose. Chapter 4 resolved how cellulose solvation is impacted in IL/Water mixtures. The results from Chapter 4 show that cellulose solubility increases the separation potential between lignin and cellulose in IL/water systems, and the subsequent rheological behaviors of dissolved slurries are dependent on time, temperature, and water content. At 7% water in IL, cellulose solvation was reduced significantly due to the H-bonding competition between water and the IL. In pure IL, cellulose dissolves entirely at 80 °C (2 hours). From 3-5% water in ionic liquid mixtures, the presence of undissolved residual fibers resulted in higher viscosities and, when precipitated, fewer changes in crystal formation in regenerated cellulose fibers than when pure the IL dissolved the entire structure.

In chapter 5, targeted lignin extractions from the more complicated lignocellulose form of corn plant residuals called corn stover (CS) were also conducted using IL/water mixtures. The

inhibitory properties of water resolved in chapter 4 were leveraged in chapter 5 for lignin-specific extractions. For targeted lignin isolations containing sufficient amounts of water, the solubility of the ionic liquid was tuned so that cellulose was conserved while lignin solvation persisted. Cellulose changes were measured and observed using microscopy and crystallinity as metrics for structural changes due to the IL exposure. In untreated lignocellulose, cellulose has 2 diffractions associated with the crystal at 2θ = 14- 16.5 °, convoluted $(1\bar{1}0)$ & (110) plane and 22.0 °- 22.7 °, a (200) plane. When the water-containing IL mixtures were used to dissolve the biomass, it was noted that there was a ~20% increase in crystallinity, corresponding to a more cellulose in the sample and containing less amorphous materials like lignin. As the water content in the Ionic liquid was raised, the extracted lignin fraction retained higher MW lignin. This is attributed to the fact that water inhibits depolymerization, though [DBU][-OAc] ions can still participate in lignin extraction.

In this study, not only was targeted lignin extraction proved, but higher-purity, higher-thermal-stability lignin was extracted when water was added to the ionic liquid when exposed to the stover. Lignin isolated after extraction using water-containing IL solutions noted high aliphatic hydroxyl content, while samples extracted from pure ionic liquid noted higher phenolic content. This observation might influence how the lignin residues might be used as reactive intermediates in future polymer production.

6.2.1 Challenges

The most notable challenge associated with IL-mediated lignocellulose extraction is that large-scale use is limited. While ionic liquids have been touted as greener alternatives to Kraft lignin processing due to their low vapor pressure in the melt, IL-based processing is more expensive due to the cost of producing the superbase starting materials , but still can be toxic to living organisms, and have low biodegradability. [359] Also, the need for further acids and bases for lignin precipitation means the use of more chemicals for processing. Lastly, ILs require large amounts of water for biomass washing and any losses of ionic liquid that are not recycled require replenishment. To harness the power of ionic liquids for industrial use, and to circumvent possible environmental, energetic, and economic wrenches, it would great to find more powerful ionic liquids that function at lower concentration. It is also paramount that scientists understand any latent toxicity issues.

Scalability is also an issue when considering total polyol replacements with lignin for polymer synthesis. Lignin is a heterogeneous polymer and has inherent variability depending on its biomass source, resulting in different concentrations of functional hydroxyl groups, aliphatic and phenolic, and different aromatic monomers: syringyl (S-unit), guaiacyl (G-unit), and hydroxyphenyl (H-unit). While pure ionic liquid processing can reduce lignin heterogeneity by producing phenolic-rich lignin, it makes processing more expensive. Comparatively, while ionic liquid mixtures are effective even with 20% water/IL solutions, the tradeoff is poorer homogeneity and consequently lower reactivity in comparison to pure ionic liquid extracted lignin. Also, though biobased polyols consume less synthetic feedstocks for polymer production, the cradle-to-gate energy cost for biomass extraction and use may be greater than that of crude-oil polyols. Further work is needed to work on the value proposition.

6.2.2 Future Direction: Ionic Liquid Recycling

Though [DBUH][-OAc] ionic liquids are less costly than Imidazolium-based ILs, ILs are much more expensive than other extraction methods like organosolv and alkaline extraction methods. After antisolvent liberation of IL, the resulting mixture can be rotary evaporated to remove water and isolate the IL, though the resulting IL mixture may have impurities. If recycled ILs are to be used for subsequent lignocellulose extractions, impurities may negatively impact the efficacy of extraction. For future utilizations of recycled ILs, the effect of reuse on IL yield, impurity level, degradation of the IL from constant heating cycles, and extraction efficacy should be investigated

6.2.3 Future Direction: Lignin Characterization for Residual Carbohydrates

After Lignin isolation using IL/Water mixtures, GPC, TGA, and ^{31}P-NMR suggested the presence of low-MW species that can either be fragmented lignin or residual carbohydrates like hemicellulose and cellulose. To confirm any trends observed by the pure IL and water/IL mediated extractions of lignin, extensive characterization must be done on the extracted lignin samples. The National Renewable Energy Laboratory (NREL) has developed a standard for carbohydrate determination, which involves acid hydrolysis to break down residual hemicelluloses and cellulose into chemical components, followed by High-Performance Liquid Chromatography (HPLC). [320] In HPLC, characteristic components like xylose, mannose, furfural, acetic acid, etc. for hemicellulose and glucose for cellulose can be determined. [360,361] Proton NMR (^{1}H-NMR) and

carbon NMR (^{13}C-NMR) can also be used to further deduce chemical structures like crosslinking and confirm the extent of β-O-4 cleavage.[362,363]

6.2.4 Future Direction: Exploring Intrinsic IL Modifications by Altering Acid Pka

In making polyol-based polymers, smaller MW lignin with high hydroxyl reactivity is better. Because of this, effective lignin bond breaking is important. Other studies have shown that highly acidic ionic liquids can break lignin bonds easily. The deprotonated strong acidic moiety activates the lignin for subsequent β-O-4 bond cleavage by the superbase moiety (See Figure 1-11). [193] The sensitivity of this bond is mostly due to the strong dissociation between the cation and anion that allows them to function as independent ions for their individual roles in β-O-4 cleavage. In IL pairings between strong acids (i.e sulfuric acid) and a superbase, since the acid dissociates easily, the ion pair interaction is generally weaker, meaning that the ions can act more independently. [185] In ion pairs using weaker acids (i.e a carboxylic acid), the ions interact more intimately since the anion stabilizes the proton on the protonated superbase (Figure 6-1). While the mechanism for strong acid-IL β-O-4 bond cleavage is understood, less is known about how lignin bond breaking may be enhanced by carboxylic acid ionic liquids.

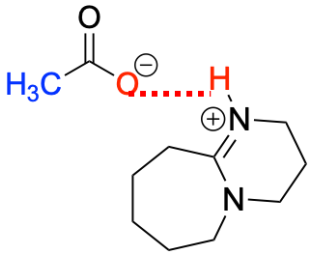


Figure 6-1: Schematic of DBU Acetate hydrogen bonding interactions between the carboxylate anion (conjugate base) and the DBUH+ cation (conjugate acid)

From these ion-pair interactions, it can be hypothesized that if ions act more independently by lowering the pKa of the acid moiety, β-O-4 linkage breakage is easier and more efficient. In scout tests that were initiated (Appendix B), three DBU-Carboxylate IL derivatives with varying acid pKas – DBU-Acetate (DBU-OAc)> DBU-Glycolate (DBU-Gly) > DBU-Malonate (DBU-Mal) (Figure 6-2)– were explored for their lignin extraction. They were made but the lignocellulosic biomass process did not produce enough statistically significant results to warrant further exploration.

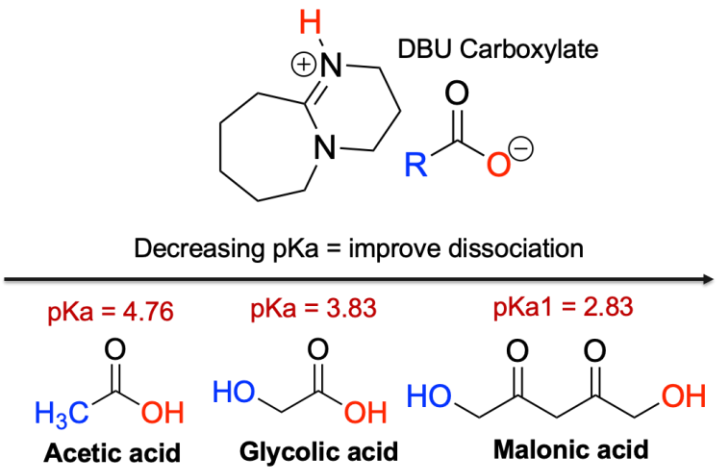


Figure 6-2: DBU Carboxylates examples made from acid with varying pKas

6.3 Closing statement

Plastic pollution remediation is a lofty feat that requires intentional and strategic interventions in preventing accumulation in our waterways, plastic cleanup, and biodegradable plastic innovation. As persistent petro-based plastics continue to be ubiquitous parts of our modern world, it is paramount that society address their accumulation at equivalent rates to their production and discarding. This body of work aims to address just a few of the many scientific mitigations available for microplastic capture and biodegradable plastic synthesis, but only scratches the surface of a larger problem – the reality that plastic waste production is exponential. To meet mitigation demands, scientists, policy makers, industries, and citizens must make plastic pollution prevention a priority.

Appendix A: Supplemental Instructions for "Water Regulates [DBUH][-OAc] Solvation of Cellulose and can Fine-Tune its Rheological Behavior"

A.1 Matlab Code for Cross Model Curve Fitting for Zero Shear Viscosity

The following code (Figure A-1) was generated and used to extract zero shear viscosity, η_0, which was used to generate Arrhenius plots for viscous energy (in slope-intercept form – Figure 4-5)

Import data from text file

```
opts = delimitedTextImportOptions("NumVariables", 3);

% Specify range and delimiter
opts.DataLines = [3, inf];
opts.Delimiter = "\t";

% Specify column names and types
opts.VariableNames = ["VarName1", "viscosity", "shearRate"];
opts.VariableTypes = ["double", "double", "double"];

% Specify file level properties
opts.ExtraColumnsRule = "ignore";
opts.EmptyLineRule = "read";

% Import the vscosity vs shear rate data
tbl = readtable("DBUH Ac - 5% water - 5% cotton dissolved - 60 degC - rate 0-100 - t1.txt", opts);
```

Convert to output type

```
shearRate = tbl.shearRate; % read shear rate
%G1 = tbl.G1;
%G11 = tbl.G11;
Et_comp = tbl.viscosity; % read viscosity

% establishing x-axis range
i = 1;
k = 0;
while k < 0
   k = shearRate(i);
   i = i + 1;
end
shearRate = shearRate(i:end);
Et_comp = Et_comp(i:end);

Et_comp = smoothdata(Et_comp,'movmedian',3);
shearRate = smoothdata(shearRate,'movmedian',3);

%cross model function from curve fit tool fitted to viscosity vs shear rate data
[CrossM, Cross_gof] = Cross_Model(shearRate, Et_comp);
```

Appendix Figure A-1: This code inputs the raw data from viscosity vs shear rate data and matches the data to an appropriate cross model curve fit

The cross-model function in Figure A-1 was generated from the curve fitting tool where "n0/((1+p*x)^(1-n))" was modified from Equation 4-3 and the variables are as follows:

n0 = η_0 (zero-shear viscosity)
p = $\eta 0/\tau^*$ (τ^* is the critical shear stress)
n = n (the viscous constant based on curve-fitted data vs. shear rate)

Figure A-2 shows the auto-generated function for the cross model.

```
function [fitresult, gof] = Cross_Model(Freq, Et_comp)
```

```
%CREATEFIT(FREQ,ET_COMP)
%  Create a fit.
%
%  Data for 'Cross_model' fit:
%      X Input : Freq
%      Y Output: Et_comp
%  Output:
%      fitresult : a fit object representing the fit.
%      gof : structure with goodness-of fit info.
%
%  See also FIT, CFIT, SFIT.

%  Auto-generated by MATLAB on 21-Feb-2022 16:01:17
```

Fit: 'Cross_model'.

```
[xData, yData] = prepareCurveData( Freq, Et_comp );

% Set up fittype and options.
ft = fittype( 'n0/(1+(p*x)^(1-n))', 'independent', 'x', 'dependent', 'y' );
opts = fitoptions( 'Method', 'NonlinearLeastSquares' );
opts.Display = 'Off';
opts.Lower = [0 0 0];
opts.StartPoint = [0.485375648722841 0.8002804688888 0.421761282626275];

% Fit model to data.
[fitresult, gof] = fit( xData, yData, ft, opts );

% Plot fit with data.
figure( 'Name', 'Cross_model' );
h = loglog(xData, yData,'s' );
hold on
plot(fitresult);
legend( h, 'Eta (Pa*s) vs. ShearRate (1/s)', 'Cross_model', 'Location', 'NorthEast', 'Interpreter', 'none' );
% Label axes
xlabel( 'ShearRate (1/s)', 'Interpreter', 'none' );
ylabel( 'Eta (Pa*s)', 'Interpreter', 'none' );
grid on
```

Appendix Figure A-2: A plot fit is created using the MATLAB curve-fitting package using the equation for the cross model "n0/((1+p*x)^(1-n))"

The parameters in Figure A-3 were extracted from the code in Figure A-1. All the parameters can be extracted from "CrossM" in the MATLAB workspace.

```
General model:
val(x) = n0/(1+(p*x)^(1-n))
Coefficients (with 95% confidence bounds):
  n =      0.4305  (0.3837, 0.4774)
  n0 =       15.19  (15.08, 15.3)
  p =    0.002314  (0.001932, 0.002696)
```

Appendix Figure A-3: Predicted values of η_0 (n0), $\eta 0/\tau^*$ (p) where τ^* is the critical shear stress, and the viscous constant (n) based on curve fitted data.vs shear rate.

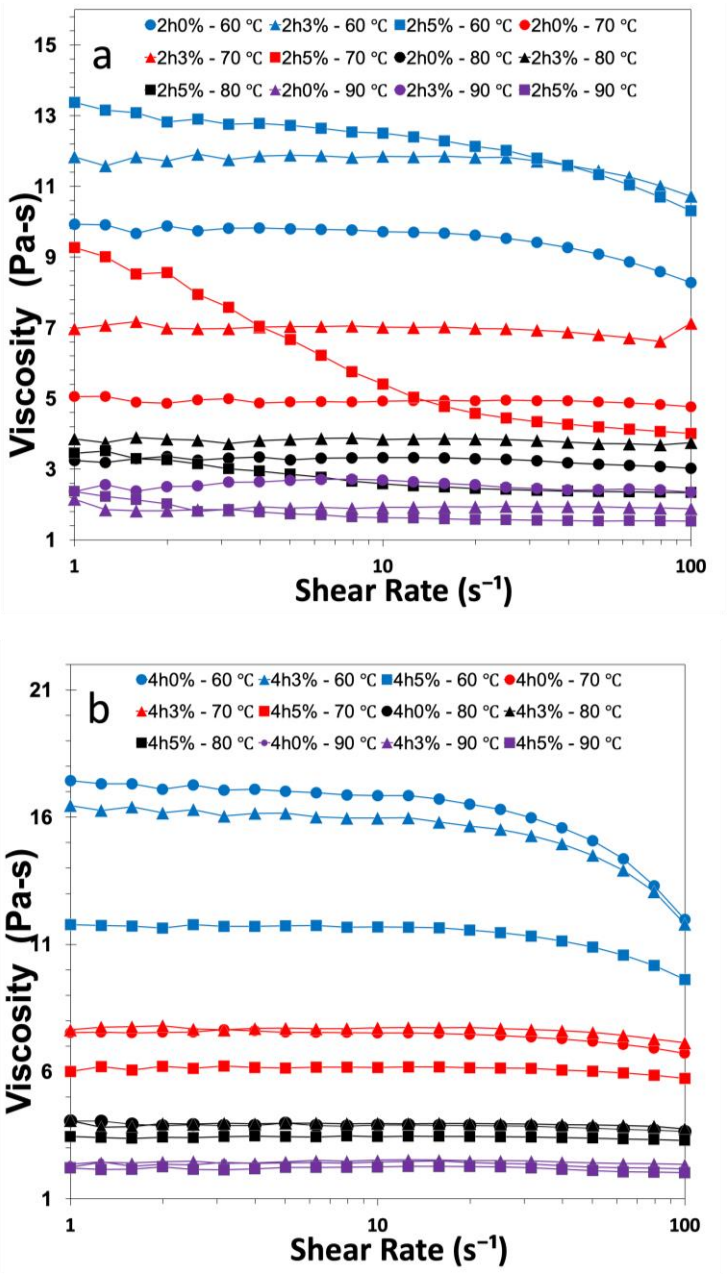
The n0 value in Figure A-3 was used to generate Arrhenius curves (lnη0 vs 1/T) seen in Figure 4-5

A.2 Viscosity vs Strain Rates 2 and 4 Hours and All Rheology Temperatures

The following results are viscosity vs strain rate measurements for all rheology conditions:

2h0%, 2h3%, 2hr5% at 60, 70, 80, 90 °C oven temperature and

4h0%, 4h3%, 4hr5% at 60, 70, 80, 90 °C oven temperature.



Appendix Figure A-4: Viscosity vs shear rate for a. 2-hr solvation solutions and b. 4-hr solvation solution

Appendix B: Preliminary Work on the Impact of Reducing the Acid pKa on Ionic Liquid-Mediated Lignin Extraction

B.1 Preliminary Work

Three ionic liquids, DBU Acetate, DBU Glycolate, and DBU Malonate, were synthesized and used for lignin and cellulose extraction. The pKa's of the acid moieties are as follows: 4.76 (acetic acid), 3.83 (glycolic acid), 2.83 (malonic acid), and structures of each acid moiety can be found in Chapter 6. Ideally, as pKa decreases, lignin extraction should be enhanced. In ionic liquids with low pKa acid moieties, both the conjugate acid and base participate in β-O-4 linkage breaking and act as separate entities (see Chapter 6 for mechanism). For example, for imidazolium hydrogen sulfate [C_3SO_3HMIM][HSO_4], which has an acid moiety with a pKa1 of 1.92 in water, the acid and base are completely dissociated, allowing them to act independently and efficiently in their mechanistic roles in β-O-4 linkage breaking (see Chapter 6).[193] Preliminary results for DBU-Carboxylate dissolutions of corn stover were conducted to understand the effects of pKa on lignin extraction via β-O-4 linkage breaking.

B.2 Materials

Corn stover was obtained from a local farm; 20 grams were cleaned in 500 mL of equal parts water and ethanol, then dried at 105 °C. Ionic Liquid chemicals: 1-8 Diazobicycloundecene (DBU), glycolic acid, acetic acid, and malonic acid were purchased from Thermo Fisher Scientific. Corn stover was obtained from a local Michigan Farm, and Sulfuric acid and Sodium hydroxide were purchased from Millipore Sigma. Pyridine, deuterated chloroform, cyclohexanol (98%), Dimethylformamide (DMF), chromium acetate relaxation agent, and the phosphorylation reagent (2-chloro-4,4,5,5-tetramethyl-1,3,2-dioxaphospholane) were purchased from Millipore Sigma.

B.3 Ionic Liquid Synthesis

Three ionic liquids were synthesized: DBUAcetate, (DBUAc) DBUGlycolate (DBUGly), and DBUMalonate (DBUMal). The three acids were chosen to assess how decreasing pKa may impact lignin characteristics. The pKa1 for the acids of interest were 4.76 and 3.83 for acetic acid and glycolic acid, respectively, and a pKa_1 of 2.83 for malonic acid. A 1:1 molar ratio of DBU and the acid of choice was mixed and left to react in an ice bath for 3 hours at 100 RPM. After the ionic liquid is made, the result is a viscous liquid. Water is removed from the mixture via rotary evaporator at 80°C.

B.4 Cellulose XRD

See section 5.5 for cellulose XRD

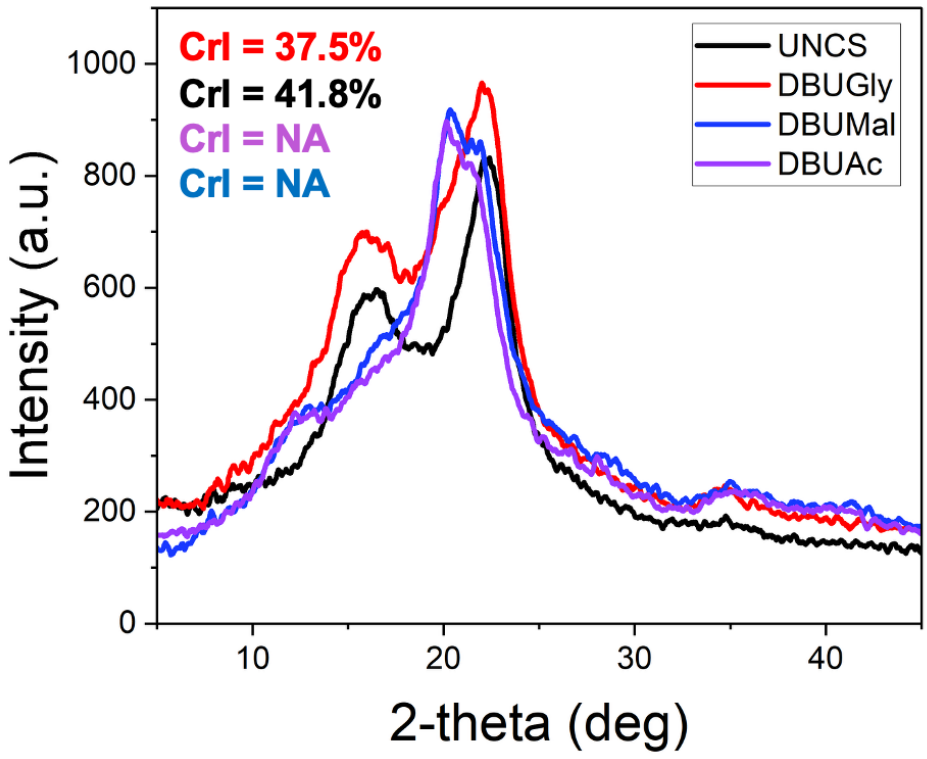
B.5 Lignin Characterization

See Chapter 5 for procedures.

B.6 Preliminary Results

B.6.1 Cellulose Structural Changes are Inconclusive but Suggest That DBU Glycolate may Maintain Cellulose Structure

Since acetic acid, glycolic acid, and malonic acid three acid types are carboxylic acids, each acid type contains hydroxy groups which have hydrogen-bonding characteristics. Cellulose is a structure that has chains that are mainly held together by hydrogen bonds; this means that cellulose can be easily disrupted by DBU-Carboxylates via hydrogen bond displacements. Due to hydrogen bond displacements, dissolved cellulose remains comingled with lignin, compromising lignin selectivity. Figure E-1 shows Xray diffraction peaks for untreated cellulose (black), as well as corn stover dissolved in [DBUH][-OAc] (purple), DBUGly (red), and DBUMal (blue).

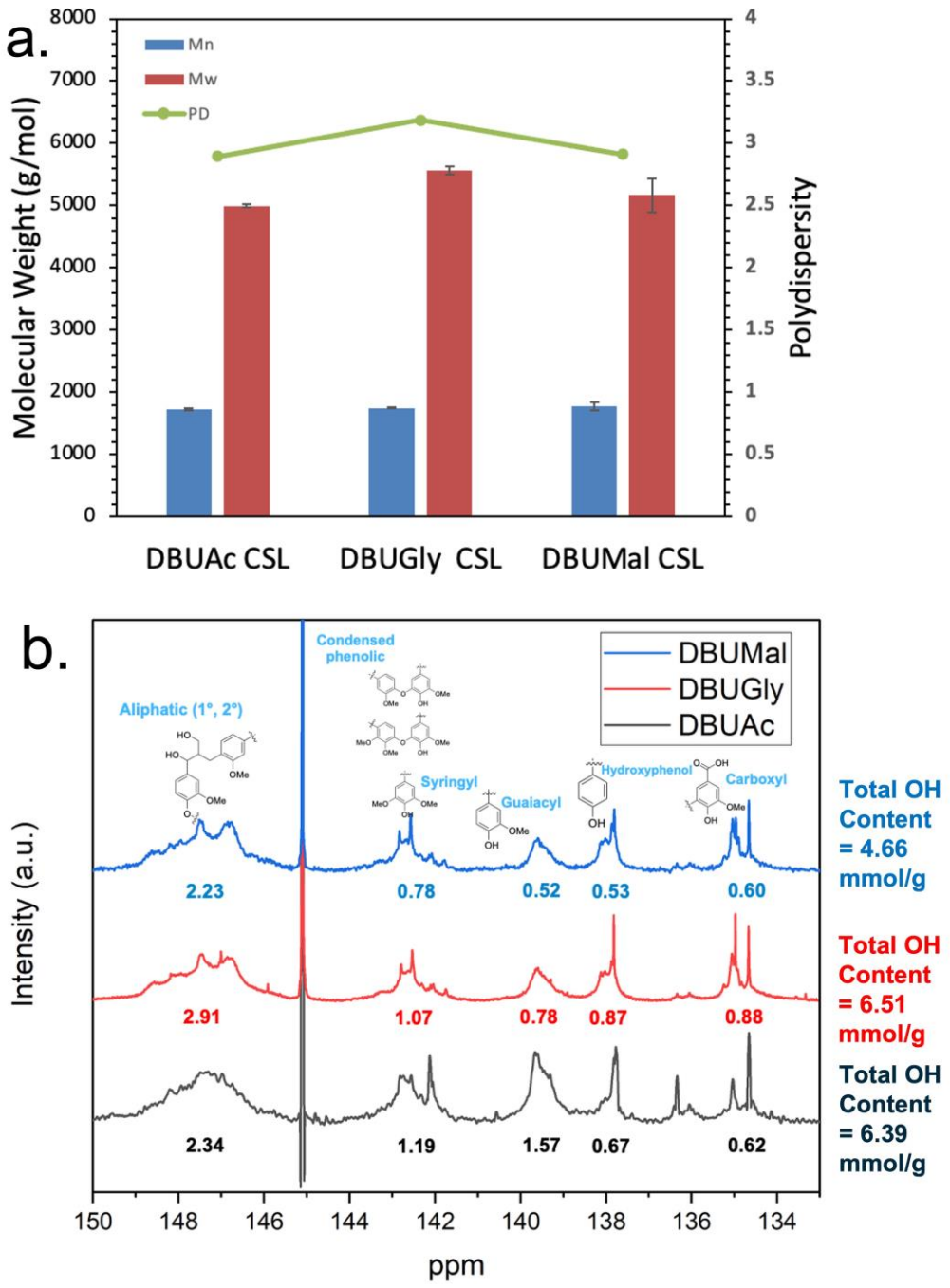


Appendix Figure B-1: Cellulose XRD data of DBU-Carboxylates treated corn stover where UNCS is non-IL treated CS

Biomass structures show significant reduction in crystallinity across all treatment types due to the disruption of hydrogen bonds which is also indicative of low selectivity.

DBU-carboxylates do not behave like non-carboxylate ionic liquids because the carboxylate anion does not behave as an independent ion and strongly interacts with the DBUH+ cation through hydrogen-bond stabilization of the deprotonated DBUH+ proton. As a result, hydrogen-bonding disruptions dominate even with low pKa as seen in Figure E-1.

The muddling of pKa effects by strong hydrogen bonding behavior also seems to muddle expected trends in lignin. Expected trends are as follows as functions of lowering pKa: low molecular weight, higher hydroxy content due to enhanced β-O-4 breaking. Those trends are not seen in molecular weight measurements or PNMR measurements (Figure E-3). In fact, molecular weights do not differ greatly between ionic liquids; the molecular weight values for extracted lignin hover around 5000-5500 g/mol for Mw and 1600 g/mol for Mn.



Appendix Figure B-2: a. Mn, Mw and Polydispersity index of DBU-Carboxylate Lignin samples with b. corresponding PNMR curves with hydroxyl content

In addition, a higher hydroxy content is actually seen for [DBUH][-OAc] (6.39 mmol/g) and DBUGly (6.51 mmol/g) in comparison to DBUMal (4.66 mmol/g), even though DBUMal has a lower pKa1. Since Malonic acid is a diacid, the H-bond effect between malonate and DBUH+ may be greater, thus impacting its ability to act as a lone ion. Essentially, H-bonding effects need to be

squelched in order to confirm whether β-O-4 breaking trends with pKa of the carboxylic acid moiety. Chapter 4 and 5 show how the addition of water lowers H-bond disruptions of cellulose. In future works, It is possible to employ this same method – the addition of water – to elucidate pKa effects.

B.7 Summary of Preliminary Observations and Future Considerations

In this work on modified Ionic liquids, data seem to show notable changes in lignin hydroxy content for the different ionic liquids, but no clear trend with pKa is observed. For DBU Carboxylates, hydrogen bonding has a greater impact on lignin extraction than pKa differences. Ideally, as in the case in chapter 4, water can be used as an antisolvent to prevent the solvation of cellulose and so that characteristic differences from pKa-modified ionic liquids may be better observed. For future experiments, >10% of water should be added to each ionic liquid type to reduce the impact of hydrogen bond disruptions. It can be hypothesized that as water is added, lowering the pKa of the acid moiety would result in lignin with lower molecular weight and higher hydroxyl content. This is because, as water reduces H-Bond disruption, pKa differences would be more pronounced; with a more pronounced pKa effect, DBU deprotonation of the acid is more efficient, resulting in more distinct separation of the two ions for participating in lignin bond breakage

Bibliography

(1) *New Research Highlights the Problem of Microplastic Pollution*. Global Environmental Health Newsletter. https://www.niehs.nih.gov/research/programs/geh/geh_newsletter/2023/8/articles/new_research_highlights_the_problem_of_microplastic_pollution (accessed 2026-01-26).

(2) Ghobish, S. A.; Motti, C. A.; Bissember, A. C.; Vamvounis, G. Microplastics in the Marine Environment: Challenges and the Shift towards Sustainable Plastics and Plasticizers. *J. Hazard. Mater.* **2025**, *491*, 137945. https://doi.org/10.1016/j.jhazmat.2025.137945.

(3) *Production, use, and fate of all plastics ever made | Science Advances*. https://www.science.org/doi/10.1126/sciadv.1700782 (accessed 2026-01-27).

(4) Mercola, J. From Bakelite to Biohazard: The Century-Long Rise of Microplastics. *Cureus* **2025**. https://doi.org/10.7759/cureus.99627.

(5) Soares, S.; Serralha, F.; Paz, M. C.; Carriço, N.; Galatanu, S.-V. Unveiling the Data: An Analysis of Plastic Waste with Emphasis on the Countries of the E^3UDRES2 Alliance. *Heliyon* **2024**, *10* (7), e28375. https://doi.org/10.1016/j.heliyon.2024.e28375.

(6) Chamas, A.; Moon, H.; Zheng, J.; Qiu, Y.; Tabassum, T.; Jang, J. H.; Abu-Omar, M.; Scott, S. L.; Suh, S. Degradation Rates of Plastics in the Environment. *ACS Sustain. Chem. Eng.* **2020**, *8* (9), 3494–3511. https://doi.org/10.1021/acssuschemeng.9b06635.

(7) Fotopoulou, K. N.; Karapanagioti, H. K. Degradation of Various Plastics in the Environment. In *Hazardous Chemicals Associated with Plastics in the Marine Environment*; Takada, H., Karapanagioti, H. K., Eds.; Springer International Publishing: Cham, 2019; pp 71–92. https://doi.org/10.1007/698_2017_11.

(8) Babaremu, K. O.; Okoya, S. A.; Hughes, E.; Tijani, B.; Teidi, D.; Akpan, A.; Igwe, J.; Karera, S.; Oyinlola, M.; Akinlabi, E. T. Sustainable Plastic Waste Management in a Circular Economy. *Heliyon* **2022**, *8* (7), e09984. https://doi.org/10.1016/j.heliyon.2022.e09984.

(9) Tan, A. F. J.; Yu, S.; Wang, C.; Yeoh, G. H.; Teoh, W. Y.; Yip, A. C. K. Reimagining Plastics Waste as Energy Solutions: Challenges and Opportunities. *Npj Mater. Sustain.* **2024**, *2* (1), 2. https://doi.org/10.1038/s44296-024-00007-x.

(10) US EPA, O. *Microplastics Research*. https://www.epa.gov/water-research/microplastics-research (accessed 2026-06-23).

(11) Arredondo-Navarro, A.; Gallardo-Owens, D.; Scott, J.; Farias, S.; Wang, X.; Cochran, W.; Hayek, E. E.; Minghetti, M.; Cerrato, J. M.; Gonzalez-Estrella, J. Thermal Oxidation, Ultraviolet Radiation, and Mechanical Abrasion - Understanding Mechanisms of Microplastic Generation and Chemical Transformation. *Microplastics Nanoplastics* **2026**, *6* (1), 26. https://doi.org/10.1186/s43591-026-00178-5.

(12) *UNECE to reduce microplastic emissions thanks to the adoption of abrasion limits for all new tyres for cars and vans | UNECE*. https://unece.org/sustainable-development/press/unece-reduce-microplastic-emissions-thanks-adoption-abrasion-limits (accessed 2026-06-23).

(13) hostmaster@performanceplustire.com. *How Long Does a Tire Take to Decompose in Landfills*. https://www.performanceplustire.com/Blog/How-Long-Does-a-Tire-Take-to-Decompose-in-Landfills (accessed 2026-06-25).
(14) Han, Z.; Xiong, J.; Zhou, J.; Wang, Z.; Hu, T.; Xu, J. Microplastics Removal from Stormwater Runoff by Bioretention Cells: A Review. *J. Environ. Sci.* **2025**, *154*, 73–90. https://doi.org/10.1016/j.jes.2024.07.007.
(15) Kutralam-Muniasamy, G.; Shruti, V. C.; Pérez-Guevara, F.; Roy, P. D. Microplastic Diagnostics in Humans: "The 3Ps" Progress, Problems, and Prospects. *Sci. Total Environ.* **2023**, *856*. https://doi.org/10.1016/j.scitotenv.2022.159164.
(16) Leslie, H. A.; van Velzen, M. J. M.; Brandsma, S. H.; Vethaak, A. D.; Garcia-Vallejo, J. J.; Lamoree, M. H. Discovery and Quantification of Plastic Particle Pollution in Human Blood. *Environ. Int.* **2022**, *163*. https://doi.org/10.1016/j.envint.2022.107199.
(17) Sharma, R. K.; Kumari, U.; Kumar, S. Impact of Microplastics on Pregnancy and Fetal Development: A Systematic Review. *Cureus 16* (5), e60712. https://doi.org/10.7759/cureus.60712.
(18) Xu, H.; Chen, C.; Pang, Z.; Zhang, G.; Zhang, W.; Kan, H. Effects of Microplastics Concentration on Plant Root Traits and Biomass: Experiment and Meta-Analysis. *Ecotoxicol. Environ. Saf.* **2024**, *285*, 117038. https://doi.org/10.1016/j.ecoenv.2024.117038.
(19) Padervand, M.; Lichtfouse, E.; Robert, D.; Wang, C. Removal of Microplastics from the Environment. A Review. *Environ. Chem. Lett.* **2020**, *18* (3), 807–828. https://doi.org/10.1007/s10311-020-00983-1.
(20) Sajjad, M.; Huang, Q.; Khan, S.; Khan, M. A.; Liu, Y.; Wang, J.; Lian, F.; Wang, Q.; Guo, G. Microplastics in the Soil Environment: A Critical Review. *Environ. Technol. Innov.* **2022**, *27*, 102408. https://doi.org/10.1016/j.eti.2022.102408.
(21) Casoli, G.; Rumkumar, S. *Plastic Pollution in the Oceans: A Systemic Analysis—Status Quo and Possible Sustainable Solutions, in: Mare Plasticum - The Plastic Sea*; Springer International Publishing: Cham, Switzerland, 2020; p 243.
(22) Gies, E. A.; LeNoble, J. L.; Noël, M.; Etemadifar, A.; Bishay, F.; Hall, E. R.; Ross, P. S. Retention of Microplastics in a Major Secondary Wastewater Treatment Plant in Vancouver, Canada. *Mar. Pollut. Bull.* **2018**, *133*, 553–561. https://doi.org/10.1016/j.marpolbul.2018.06.006.
(23) Hossain, N.; Bhuiyan, M. A.; Pramanik, B. K.; Nizamuddin, S.; Griffin, G. Waste Materials for Wastewater Treatment and Waste Adsorbents for Biofuel and Cement Supplement Applications: A Critical Review. *J. Clean. Prod.* **2020**, *255*. https://doi.org/10.1016/j.jclepro.2020.120261.
(24) Hsu 許強, C. S.; Robinson, P. R. Petrochemicals. In *Petroleum Science and Technology: Downstream*; Hsu, C. S., Robinson, P. R., Eds.; Springer Nature Switzerland: Cham, 2024; pp 243–291. https://doi.org/10.1007/978-3-031-46645-8_9.
(25) Crawford, C. B.; Quinn, B. Physiochemical Properties and Degradation. In *Microplastic Pollutants*; Elsevier, 2017; pp 57–100. https://doi.org/10.1016/B978-0-12-809406-8.00004-9.
(26) Polymeric Implants. **2012**, 397–411. https://doi.org/10.1016/B978-0-444-53349-4.00230-2.
(27) Kapustin, N. O.; Grushevenko, D. A. Analysis of the "Circular Plastics Economy" Phenomena and Its Long-Term Implications for Demand for Petroleum Market. *Environ. Sci. Pollut. Res.* **2023**, *30* (36), 85889–85902. https://doi.org/10.1007/s11356-023-28441-9.

(28) Sharma, B.; Shrestha, A. Petroleum Dependence in Developing Countries with an Emphasis on Nepal and Potential Keys. *Energy Strategy Rev.* **2023**, *45*, 101053. https://doi.org/10.1016/j.esr.2023.101053.
(29) Petroleum. In *Veterinary Toxicology*; Academic Press, 2025; pp 665–682. https://doi.org/10.1016/B978-0-443-29007-7.00029-7.
(30) Sharma, K.; Shah, G.; Singhal, K.; Soni, V. Comprehensive Insights into the Impact of Oil Pollution on the Environment. *Reg. Stud. Mar. Sci.* **2024**, *74*, 103516. https://doi.org/10.1016/j.rsma.2024.103516.
(33) Yang, M.; Zhang, J.; Sun, Z.; Sun, D. All-Natural Plant-Derived Polyurethane as a Substitute of a Petroleum-Based Polymer Coating Material. *J. Agric. Food Chem.* **2024**, *72* (12), 6444–6453. https://doi.org/10.1021/acs.jafc.4c00141.
(34) *Bioplastics Market Size To Reach $44.77 Billion By 2030*. https://www.grandviewresearch.com/press-release/global-bioplastics-market (accessed 2026-01-26).
(35) Sobeih, M. O.; Sawalha, S.; Hamed, R.; Ali, F.; Kim, M. P. Starch-Derived Bioplastics: Pioneering Sustainable Solutions for Industrial Use. *Materials* **2025**, *18* (8), 1762. https://doi.org/10.3390/ma18081762.
(36) Giaveri, S.; Schmitt, A. M.; Roset Julià, L.; Scamarcio, V.; Murello, A.; Cheng, S.; Menin, L.; Ortiz, D.; Patiny, L.; Bolisetty, S.; Mezzenga, R.; Maerkl, S. J.; Stellacci, F. Nature-Inspired Circular-Economy Recycling for Proteins: Proof of Concept. *Adv. Mater. Deerfield Beach Fla* **2021**, *33* (44), 2104581. https://doi.org/10.1002/adma.202104581.
(37) Qing, Y.; Sabo, R.; Wu, Y.; Cai, Z. *High Performance Cellulose Nanofibril Composite Films*; BioResources; 2012; Vol. 7, pp 3064–3075.
(38) Jõul, P.; Ho, T. T.; Kallavus, U.; Konist, A.; Leiman, K.; Salm, O.-S.; Kulp, M.; Koel, M.; Lukk, T. Characterization of Organosolv Lignins and Their Application in the Preparation of Aerogels. *Materials* **2022**, *15* (8), 2861. https://doi.org/10.3390/ma15082861.
(39) Chazovachii, P. T.; Rieland, J. M.; Sheffey, V. V.; Jugovic, T. M. E.; Zimmerman, P. M.; Eniola-Adefeso, O.; Love, B. J.; McNeil, A. J. Using Adhesives to Capture Microplastics from Water. *ACS EST Eng.* **2021**, *1* (12), 1698–1704. https://doi.org/10.1021/acsestengg.1c00272.
(40) Jugovic, T. M. E.; Thurber, H. E.; Robo, M. T.; Ji, W.; Clough, M. E.; McNeil, A. J.; Zimmerman, P. M. Predicting Polyacrylate–Microplastic Interactions with Atomistic Simulation. *Phys. Chem. Chem. Phys.* **2025**. https://doi.org/10.1039/D5CP03631C.
(41) Rieland, J. M.; Hu, Z.; Deese, J. S.; Love, B. J. Pressure Sensitive Adhesives for Quantifying Microplastic Isolation. *Sep. Purif. Technol.* **2023**, *307*, 122819. https://doi.org/10.1016/j.seppur.2022.122819.
(42) Zhang, J.; Xu, J.; Chen, W.; Chen, Y.; Pan, Z.; Wu, W. Adhesion-Driven Removal of Microplastics From Aquatic Systems by Using Microgel Glues. *Adv. Sci. n/a* (n/a), e75293. https://doi.org/10.1002/advs.75293.
(43) Amparo, N. A.; Leyble, D. C.; Trajeco, M. A.; Mercado, M. A.; Mangrobang, M. Sala: An Autonomous Water Trash Skimmer Using Path Planning Algorithm, 2023. https://doi.org/10.13140/RG.2.2.32203.60965.
(44) Cho, S.; Park, S. J.; Lee, Y. J.; Lee, Y. J.; Lee, Y. A.; Kim, H.; Kim, S. J.; Chung, S.; Moon, M. Capillary Skimming of Floating Microplastics via a Water-Bridged Ratchet. *Adv. Sci.* **2024**, *12* (1), 2408623. https://doi.org/10.1002/advs.202408623.

(45) *Rivers • The Interceptor • The Ocean Cleanup*. The Ocean Cleanup. https://theoceancleanup.com/rivers/ (accessed 2025-12-29).
(46) Brewer, A.; Dror, I.; Berkowitz, B. The Mobility of Plastic Nanoparticles in Aqueous and Soil Environments: A Critical Review. *ACS EST Water* **2021**, *1* (1), 48–57. https://doi.org/10.1021/acsestwater.0c00130.
(47) Creton, C. Pressure-Sensitive Adhesives: An Introductory Course. *MRS Bull.* **2003**, *28* (6), 434–439. https://doi.org/10.1557/mrs2003.124.
(48) Ramkumar, M.; Ji, W.; Thurber, H. E.; Clough, M. E.; Chirdon, S.; McNeil, A. J. Enhancing Microplastic Capture Efficiencies with Adhesive Coatings on Stainless-Steel Filters. *RSC Appl. Polym.* **2024**, *2* (3), 456–460. https://doi.org/10.1039/d3lp00282a.
(49) Comyn, J. Theories of Adhesion. In *Handbook of Adhesives and Sealants*; Elsevier, 2006; Vol. 2, pp 1–50. https://doi.org/10.1016/S1874-5695(06)80012-6.
(50) Moore, G. *What is surface energy and how does it affect adhesive bonding?*. Permabond. https://permabond.com/what-is-surface-energy/ (accessed 2026-06-20).
(51) *Mactac | What You Didn't Know About Surface Energy: The Basis of Bonding*. https://www.mactac.com/TapeTalk10 (accessed 2026-06-20).
(52) *Tech Tip: How do I measure the surface tension of plastics?* https://www.tstar.com/blog/tech-tip-how-do-i-measure-the-surface-tension-of-plastics (accessed 2026-06-25).
(53) Kalchgruber, L.; Hahn, M.; Schwenzfeier, K. A.; Rester, M.; Weissensteiner, C.; Mears, L. L. E.; Valtiner, M. Unraveling a Molecular Adhesion Mechanism at Complex Polymer–Metal Interfaces. *ACS Appl. Mater. Interfaces* **2024**, *16* (45), 62970–62978. https://doi.org/10.1021/acsami.4c13314.
(54) Hor, J. L.; Wang, H.; Fakhraai, Z.; Lee, D. Effects of Polymer–Nanoparticle Interactions on the Viscosity of Unentangled Polymers under Extreme Nanoconfinement during Capillary Rise Infiltration. *Soft Matter* **2018**, *14* (13), 2438–2446. https://doi.org/10.1039/C7SM02465G.
(55) Hu, K.; Li, Q.; Ji, X. Polymer Entanglement-Induced Hydrogel Adhesion. *Gels* **2024**, *10* (12), 822. https://doi.org/10.3390/gels10120822.
(56) Lee, J.; Kim, R. E.; Lee, J.; Lee, J.; Kim, S.; Kim, J.; Kang, D.; Kwon, Y.; Kim, D.; Lee, A.; Kim, H. S. Surface Roughness Engineering of Mechanical Interlocking for Enhanced Metal–Polymer Adhesion in Additive Manufacturing. *Virtual Phys. Prototyp.* **2026**, *21* (1), e2653924. https://doi.org/10.1080/17452759.2026.2653924.
(57) Matos-Pérez, C. R.; White, J. D.; Wilker, J. J. Polymer Composition and Substrate Influences on the Adhesive Bonding of a Biomimetic, Cross-Linking Polymer. *J. Am. Chem. Soc.* **2012**, *134* (22), 9498–9505. https://doi.org/10.1021/ja303369p.
(58) Chen, S.; Zhang, K.; Li, Z.; Wu, Y.; Zhu, B.; Zhu, J. Hydrogen-Bonded Supramolecular Adhesives: Synthesis, Responsiveness, and Application. *Supramol. Mater.* **2023**, *2*, 100032. https://doi.org/10.1016/j.supmat.2023.100032.
(59) *Polyacrylate | Synthesis, Copolymersization, Monomers | Britannica*. https://www.britannica.com/science/polyacrylate (accessed 2026-06-25).
(60) Chen, Q.; Shang, H.; Cheng, B.; Lu, C.; Wang, Y.; Zhang, Y.; Shao, T. Quantifying Triboelectric Series of Polymers Based on the Measurement of Triboelectrification with NaCl Solution. *Chem. Eng. J.* **2024**, *488*, 150871. https://doi.org/10.1016/j.cej.2024.150871.
(61) Li, M.; Zhang, J.; Chen, G.; Liu, Y.; Xie, D.; Li, M.; Zhang, Y.; Song, J.; Luo, Z. Strong and Tough Adhesive Hydrogel Based on Polyacrylate/Carboxylated Cellulose

Nanofibers/Zr4+ for High-Sensitivity Motion Monitoring and Controlled Transdermal Drug Delivery. *Int. J. Biol. Macromol.* **2025**, *303*, 140657. https://doi.org/10.1016/j.ijbiomac.2025.140657.
(62) *Polyacrylate Adhesive - QinanX New Material*. https://qinanxgroup.com/polyacrylate-adhesive/ (accessed 2026-06-17).
(63) Fitzgerald, D. M.; Colson, Y. L.; Grinstaff, M. W. Synthetic Pressure Sensitive Adhesives for Biomedical Applications. *Prog. Polym. Sci.* **2023**, *142*, 101692. https://doi.org/10.1016/j.progpolymsci.2023.101692.
(64) *Poly 2-Ethylhexyl Acrylate: Comprehensive Analysis Of Synthesis, Properties, And Industrial Applications*. https://eureka.patsnap.com/materials/poly-2-ethylhexyl-acrylate (accessed 2026-04-13).
(65) D, S. Handbook of Pressure Sensitive Adhesive Technology. **1989**. https://doi.org/10.1007/978-1-4757-0866-0.
(66) Luo, W.; Chen, W.; Liu, D.; Huang, X.; Ma, B. Effect of Temperature and Humidity on Mechanical Properties and Constitutive Modeling of Pressure-Sensitive Adhesives. *Sci. Rep.* **2024**, *14* (1). https://doi.org/10.1038/s41598-024-64960-2.
(67) Hassan, S. S.; Williams, G. A.; Jaiswal, A. K. Emerging Technologies for the Pretreatment of Lignocellulosic Biomass. *Bioresour. Technol.* **2018**, *262*, 310–318. https://doi.org/10.1016/j.biortech.2018.04.099.
(68) Park, S.; Baker, J. O.; Himmel, M. E.; Parilla, P. A.; Johnson, D. K. Cellulose Crystallinity Index: Measurement Techniques and Their Impact on Interpreting Cellulase Performance. *Biotechnol. Biofuels* **2010**, *3*, 10. https://doi.org/10.1186/1754-6834-3-10.
(69) Wang, J. X.; Asano, S.; Kudo, S.; Hayashi, J. I. Deep Delignification of Woody Biomass by Repeated Mild Alkaline Treatments with Pressurized O2. *ACS Omega* **2020**, *5* (45), 29168–29176. https://doi.org/10.1021/acsomega.0c03953.
(70) Østby, H.; Várnai, A. Hemicellulolytic Enzymes in Lignocellulose Processing. *Essays Biochem.* **2023**, *67* (3), 531–547. https://doi.org/10.1042/EBC20220154.
(71) Balart, R.; Garcia-Garcia, D.; Fombuena, V.; Quiles-Carrillo, L.; Arrieta, M. P. Biopolymers from Natural Resources. *Polymers* **2021**, *13* (15), 2532. https://doi.org/10.3390/polym13152532.
(72) Vasile, C.; Baican, M. Lignins as Promising Renewable Biopolymers and Bioactive Compounds for High-Performance Materials. *Polymers* **2023**, *15* (15), 3177. https://doi.org/10.3390/polym15153177.
(73) Suryatapa, D. Organic Farming: A Sustainable Agricultural System. In *Encyclopedia of Sustainable Technologies (Second Edition)*; Abraham, M. A., Ed.; Elsevier: Oxford, 2024; pp 544–557. https://doi.org/10.1016/B978-0-323-90386-8.00088-7.
(74) Trogen, M.; Kilpeläinen, P.; Pitkänen, L.; Sawada, D.; Fliri, L.; Schlapp-Hackl, I.; Hummel, M. Cellulose–Xylan Composite Fibres as Precursors for Carbon Fibres. *RSC Adv.* **2025**, *15* (56), 48061–48071. https://doi.org/10.1039/D5RA07682J.
(75) Wang, Y.; Qi, J.; Zhang, M.; Xu, T.; Zheng, C.; Yuan, Z.; Si, C. Cellulose-Based Aerogels, Films, and Fibers for Advanced Biomedical Applications. *Chem. Eng. J.* **2024**, *497*, 154434. https://doi.org/10.1016/j.cej.2024.154434.
(76) Yang, Q.; Saito, T.; Berglund, L. A.; Isogai, A. Cellulose Nanofibrils Improve the Properties of All-Cellulose Composites by the Nano-Reinforcement Mechanism and Nanofibril-Induced Crystallization. *Nanoscale* **2015**, *7* (42), 17957–17963. https://doi.org/10.1039/c5nr05511c.

(77) Sun, L.; Chen, J. Y.; Jiang, W.; Lynch, V. Crystalline Characteristics of Cellulose Fiber and Film Regenerated from Ionic Liquid Solution. *Carbohydr. Polym.* **2015**, *118*, 150–155. https://doi.org/10.1016/j.carbpol.2014.11.008.
(78) Sengupta, A. K. Rayon Fibres. In *Manufactured Fibre Technology*; Gupta, V. B., Kothari, V. K., Eds.; Springer Netherlands: Dordrecht, 1997; pp 480–513. https://doi.org/10.1007/978-94-011-5854-1_17.
(79) *What is Viscose Fabric: Properties, How its Made and Where*. Sewport. https://sewport.com/fabrics-directory/viscose-fabric (accessed 2026-06-22).
(80) McCall, E. R.; Jurgens, J. F. Chemical Composition of Cotton. *Text. Res. J. 211 19-21* **1951**, *21* (1), 19–21.
(81) Liang, Y.; Hawkins, J. E.; Ries, M. E.; Hine, P. J. Dissolution of Cotton by 1-Ethyl-3-Methylimidazolium Acetate Studied with Time–Temperature Superposition for Three Different Fibre Arrangements. *Cellulose* **2021**, *28* (2), 715–727. https://doi.org/10.1007/s10570-020-03576-x.
(82) Yu, Z.; Yang, Y. Carbon Footprint of Global Cotton Production. *Resour. Environ. Sustain.* **2025**, *20*, 100214. https://doi.org/10.1016/j.resenv.2025.100214.
(83) Law, R. C. 5. Applications of Cellulose Acetate 5.1 Cellulose Acetate in Textile Application. *Macromol. Symp.* **2004**, *208* (1), 255–266. https://doi.org/10.1002/masy.200450410.
(84) Portela, R.; Leal, C. R.; Almeida, P. L.; Sobral, R. G. Bacterial Cellulose: A Versatile Biopolymer for Wound Dressing Applications. *Microb. Biotechnol.* **2019**, *12* (4), 586–610. https://doi.org/10.1111/1751-7915.13392.
(85) Rahman, M. S.; Hasan, M. S.; Nitai, A. S.; Nam, S.; Karmakar, A. K.; Ahsan, M. S.; Shiddiky, M. J. A.; Ahmed, M. B. Recent Developments of Carboxymethyl Cellulose. *Polymers* **2021**, *13* (8). https://doi.org/10.3390/polym13081345.
(86) Bellesia, T.; Carullo, D.; Fachin, A.; Soltanzadeh, M.; Ghaani, M.; Ascrizzi, G. I.; Piazza, L.; Farris, S. Microfibrillated Cellulose Films from Agri-Food Wastes and Plant Residues for Food Packaging Applications – A Comparative Investigation. *Food Packag. Shelf Life* **2026**, *54*, 101728. https://doi.org/10.1016/j.fpsl.2026.101728.
(87) Hindi, S.; Al-Shareef, A. Microcrystalline Cellulose: Its Processing and Pharmaceutical Specifications. **2023**, *1*, 26–38.
(88) Khoshnevisan, K.; Maleki, H.; Samadian, H.; Shahsavari, S.; Sarrafzadeh, M. H.; Larijani, B.; Dorkoosh, F. A.; Haghpanah, V.; Khorramizadeh, M. R. Cellulose Acetate Electrospun Nanofibers for Drug Delivery Systems: Applications and Recent Advances. *Carbohydr. Polym.* **2018**, *198*, 131–141. https://doi.org/10.1016/j.carbpol.2018.06.072.
(89) Hassan, N. S.; Jalil, A. A.; Hitam, C. N. C.; Vo, D. V. N.; Nabgan, W. Biofuels and Renewable Chemicals Production by Catalytic Pyrolysis of Cellulose: A Review. *Environ. Chem. Lett.* **2020**, *18* (5), 1625–1648. https://doi.org/10.1007/s10311-020-01040-7.
(90) Jiang, Z.; Ngai, T. Recent Advances in Chemically Modified Cellulose and Its Derivatives for Food Packaging Applications: A Review. *Polymers* **2022**, *14* (8). https://doi.org/10.3390/polym14081533.
(91) Spörl, J. M.; Beyer, R.; Abels, F.; Cwik, T.; Müller, A.; Hermanutz, F.; Buchmeiser, M. R. Cellulose-Derived Carbon Fibers with Improved Carbon Yield and Mechanical Properties. *Macromol. Mater. Eng.* **2017**, *302* (10), 1700195. https://doi.org/10.1002/mame.201700195.

(92) Nam, S.; French, A. D.; Condon, B. D.; Concha, M. Segal Crystallinity Index Revisited by the Simulation of X-Ray Diffraction Patterns of Cotton Cellulose Iβ and Cellulose II. *Carbohydr. Polym.* **2016**, *135*, 1–9. https://doi.org/10.1016/j.carbpol.2015.08.035.
(93) Kullmann, R.; Delbianco, M.; Roth, C.; Weikl, T. R. Role of van Der Waals, Electrostatic, and Hydrogen-Bond Interactions for the Relative Stability of Cellulose Iβ and II Crystals. *J. Phys. Chem. B* **2024**, *128* (49), 12114–12121. https://doi.org/10.1021/acs.jpcb.4c06841.
(94) Gong, J.; Li, J.; Xu, J.; Xiang, Z.; Mo, L. Research on Cellulose Nanocrystals Produced from Cellulose Sources with Various Polymorphs. *RSC Adv.* **2017**, *7* (53), 33486–33493. https://doi.org/10.1039/c7ra06222b.
(95) Rana, Md. M.; De la Hoz Siegler, H. Influence of Ionic Liquid (IL) Treatment Conditions in the Regeneration of Cellulose with Different Crystallinity. *J. Mater. Res.* **2023**, *38* (2), 328–336. https://doi.org/10.1557/s43578-022-00797-7.
(96) Rana, Md. M.; De la Hoz Siegler, H. Influence of Ionic Liquid (IL) Treatment Conditions in the Regeneration of Cellulose with Different Crystallinity. *J. Mater. Res.* **2023**, *38* (2), 328–336. https://doi.org/10.1557/s43578-022-00797-7.
(97) Deng, Z.; Xia, A.; Liao, Q.; Zhu, X.; Huang, Y.; Fu, Q. Laccase Pretreatment of Wheat Straw: Effects of the Physicochemical Characteristics and the Kinetics of Enzymatic Hydrolysis. *Biotechnol. Biofuels* **2019**, *12* (1), 159. https://doi.org/10.1186/s13068-019-1499-3.
(98) Chen, W.; Yi, J.; Zhao, C.; Shi, Y.; Kang, Q.; Lu, J.; Zhu, J. Low-Temperature EDA/Urea Pretreatment Improves Enzymatic Hydrolysis of Corn Stover through Changing Physical and Chemical Structure. *Biomass Convers. Biorefinery* **2024**, *14* (18), 23195–23206. https://doi.org/10.1007/s13399-023-04335-1.
(99) Silva, N.; Silva, N.; Mulinari, D. Influence of Sequential Acid-Alkali Treatment on Palm Biomass Waste Properties. *J. Nat. Fibers* **2022**, *19* (14), 7502–7516. https://doi.org/10.1080/15440478.2021.1951421.
(100) Wang, Y.; Cai, D.; Jiang, Y.; Mei, X.; Ren, W.; Sun, M.; Su, C.; Cao, H.; Zhang, C.; Qin, P. Rapid Fractionation of Corn Stover by Microwave-Assisted Protic Ionic Liquid [TEA][HSO4] for Fermentative Acetone–Butanol–Ethanol Production. *Biotechnol. Biofuels Bioprod.* **2024**, *17* (1), 62. https://doi.org/10.1186/s13068-024-02499-0.
(101) Gautam, D.; Rana, V.; Sharma, S.; Kumar Walia, Y.; Kumar, K.; Umar, A.; Ibrahim, A. A.; Baskoutas, S. Hemicelluloses: A Review on Extraction and Modification for Various Applications. *ChemistrySelect* **2025**, *10* (24), e06050. https://doi.org/10.1002/slct.202406050.
(102) Monteiro, C. R. M.; Ávila, P. F.; Pereira, M. A. F.; Pereira, G. N.; Bordignon, S. E.; Zanella, E.; Stambuk, B. U.; de Oliveira, D.; Goldbeck, R.; Poletto, P. Hydrothermal Treatment on Depolymerization of Hemicellulose of Mango Seed Shell for the Production of Xylooligosaccharides. *Carbohydr. Polym.* **2021**, *253*, 117274. https://doi.org/10.1016/j.carbpol.2020.117274.
(103) Wang, X.; He, J.; Pang, S.; Yao, S.; Zhu, C.; Zhao, J.; Liu, Y.; Liang, C.; Qin, C. High-Efficiency and High-Quality Extraction of Hemicellulose of Bamboo by Freeze-Thaw Assisted Two-Step Alkali Treatment. *Int. J. Mol. Sci.* **2022**, *23* (15), 8612. https://doi.org/10.3390/ijms23158612.

(104) Ji, G.; Zhang, B.; Niu, Q.; Liu, Y.; Yang, Q. Enhancement of Liquid Hot Water Pretreatment on Corn Stover with Ball Milling to Improve Total Sugar Yields. *Sustainability* **2023**, *15* (23), 16426–16426. https://doi.org/10.3390/su152316426.
(105) Deng, W.; Feng, Y.; Fu, J.; Guo, H.; Guo, Y.; Han, B.; Jiang, Z.; Kong, L.; Li, C.; Liu, H.; Nguyen, P. T. T.; Ren, P.; Wang, F.; Wang, S.; Wang, Y.; Wang, Y.; Wong, S. S.; Yan, K.; Yan, N.; Yang, X.; Zhang, Y.; Zhang, Z.; Zeng, X.; Zhou, H. Catalytic Conversion of Lignocellulosic Biomass into Chemicals and Fuels. *Green Energy Environ.* **2023**, *8* (1), 10–114. https://doi.org/10.1016/j.gee.2022.07.003.
(106) Huang, L.-Z.; Ma, M.-G.; Ji, X.-X.; Choi, S.-E.; Si, C. Recent Developments and Applications of Hemicellulose From Wheat Straw: A Review. *Front. Bioeng. Biotechnol.* **2021**, *9*, 690773. https://doi.org/10.3389/fbioe.2021.690773.
(107) Scheller, H. V.; Ulvskov, P. Hemicelluloses. *Annu. Rev. Plant Biol.* **2010**, *61*, 263–289. https://doi.org/10.1146/annurev-arplant-042809-112315.
(108) Huang, C.; Yu, Y.; Li, Z.; Yan, B.; Pei, W.; Wu, H. The Preparation Technology and Application of Xylo-Oligosaccharide as Prebiotics in Different Fields: A Review. *Front. Nutr.* **2022**, *9*. https://doi.org/10.3389/fnut.2022.996811.
(109) Chen, Y.; Xie, Y.; Ajuwon, K. M.; Zhong, R.; Li, T.; Chen, L.; Zhang, H.; Beckers, Y.; Everaert, N. Xylo-Oligosaccharides, Preparation and Application to Human and Animal Health: A Review. *Front. Nutr.* **2021**, *8*, 731930. https://doi.org/10.3389/fnut.2021.731930.
(110) Peng, X.; Ren, J.; Sun, R. An Efficient Method for the Synthesis of Hemicellulosic Derivatives with Bifunctional Groups in Butanol/Water Medium and Their Rheological Properties. *Carbohydr. Polym.* **2011**, *83* (4), 1922–1928. https://doi.org/10.1016/j.carbpol.2010.10.064.
(111) Kumar, A.; Anushree; Kumar, J.; Bhaskar, T. Utilization of Lignin: A Sustainable and Eco-Friendly Approach. *J. Energy Inst.* **2020**, *93* (1), 235–271. https://doi.org/10.1016/j.joei.2019.03.005.
(112) Panesar, S. S.; Jacob, S.; Misra, M.; Mohanty, A. K. Functionalization of Lignin: Fundamental Studies on Aqueous Graft Copolymerization with Vinyl Acetate. *Ind. Crops Prod.* **2013**, *46*, 191–196. https://doi.org/10.1016/j.indcrop.2012.12.031.
(113) Nikafshar, S.; Wang, J.; Dunne, K.; Sangthonganotai, P.; Nejad, M. Choosing the Right Lignin to Fully Replace Bisphenol A in Epoxy Resin Formulation. *ChemSusChem* **2021**, *14* (4), 1184–1195. https://doi.org/10.1002/cssc.202002729.
(114) Kalami, S.; Chen, N.; Borazjani, H.; Nejad, M. Comparative Analysis of Different Lignins as Phenol Replacement in Phenolic Adhesive Formulations. *Ind. Crops Prod.* **2018**, *125*, 520–528. https://doi.org/10.1016/j.indcrop.2018.09.037.
(115) Li, C.; Jin, H.; Hou, M.; Guo, X.; Xiao, T.; Cao, X.; Jia, W.; Fatehi, P.; Shi, H. Fractionated Lignin as a Polyol in Polyurethane Fabrication. *Int. J. Biol. Macromol.* **2024**, *256*. https://doi.org/10.1016/j.ijbiomac.2023.128290.
(116) Gondaliya, A.; Nejad, M. Lignin as a Partial Polyol Replacement in Polyurethane Flexible Foam. *Mol. Basel Switz.* **2021**, *26* (8), 2302. https://doi.org/10.3390/molecules26082302.
(117) Ghorbani, M.; Liebner, F.; van Herwijnen, H. W. G.; Pfungen, L.; Krahofer, M.; Budjav, E.; Konnerth, J. Lignin Phenol Formaldehyde Resoles: The Impact of Lignin Type on Adhesive Properties. *BioResources* **2016**, *11* (3), 6727–6741. https://doi.org/10.15376/biores.11.3.6727-6741.

(118) Mendiburu-Valor, E.; Larraza, I.; Echeverria-Altuna, O.; Harismendy, I.; Peña-Rodriguez, C.; Eceiza, A. Thermoset Polyurethanes from Biobased and Recycled Components. *J. Polym. Environ.* **2023**, *31* (11), 4946–4959. https://doi.org/10.1007/s10924-023-02891-1.
(119) Shin, E. J.; Prasad, C.; Choi, H. Y. Recent Advances in Thermoplastic Polyurethane-Based Composites, Properties, Synthesis and Its Applications. *J. Ind. Eng. Chem.* **2026**, *156*, 150–191. https://doi.org/10.1016/j.jiec.2025.09.009.
(120) Ci, Y.; Lv, D.; Yang, X.; Du, H.; Tang, Y. High-Performance Cellulose/Thermoplastic Polyurethane Composites Enabled by Interaction-Modulated Cellulose Regeneration. *Carbohydr. Polym.* **2024**, *346*. https://doi.org/10.1016/j.carbpol.2024.122611.
(121) Das, A.; Mahanwar, P. A Brief Discussion on Advances in Polyurethane Applications. *Adv. Ind. Eng. Polym. Res.* **2020**, *3* (3), 93–101. https://doi.org/10.1016/j.aiepr.2020.07.002.
(122) Gondaliya, A.; Nejad, M. Lignin as a Partial Polyol Replacement in Polyurethane Flexible Foam. *Mol. Basel Switz.* **2021**, *26* (8), 2302. https://doi.org/10.3390/molecules26082302.
(123) Figueiredo, J. de C.; Gomes, F. J. B.; Redmond, E. F. A.; Bujanovic, B.; Lelis, R. C. C.; Santana, M. F.; Mickles, C. Synthesis and Application of Kraft Lignin-Based Polyurethane Coatings for Functional Paper Packaging Materials. *Polymers* **2026**, *18* (7). https://doi.org/10.3390/polym18070787.
(124) Das, A.; Mahanwar, P. A Brief Discussion on Advances in Polyurethane Applications. *Adv. Ind. Eng. Polym. Res.* **2020**, *3* (3), 93–101. https://doi.org/10.1016/j.aiepr.2020.07.002.
(125) Pohl, M.; Danieli, E.; Leven, M.; Leitner, W.; Blümich, B.; Müller, T. E. Dynamics of Polyether Polyols and Polyether Carbonate Polyols. *Macromolecules* **2016**, *49* (23), 8995–9003. https://doi.org/10.1021/acs.macromol.6b01601.
(126) Kapuge Dona, N. L.; Smith, R. C. Tailoring Polymer Properties Through Lignin Addition: A Recent Perspective on Lignin-Derived Polymer Modifications. *Molecules* **2025**, *30* (11), 2455. https://doi.org/10.3390/molecules30112455.
(127) Jin, F.-L.; Li, X.; Park, S.-J. Synthesis and Application of Epoxy Resins: A Review. *J. Ind. Eng. Chem.* **2015**, *29*, 1–11. https://doi.org/10.1016/j.jiec.2015.03.026.
(128) Liu, S.; Chevali, V. S.; Xu, Z.; Hui, D.; Wang, H. A Review of Extending Performance of Epoxy Resins Using Carbon Nanomaterials. *Compos. Part B Eng.* **2018**, *136*, 197–214. https://doi.org/10.1016/j.compositesb.2017.08.020.
(129) He, X.; Ji, Y.; Zhao, Y.; Guan, Z.; Cao, D.; Luo, Z.; Li, S. Phase Structure and Mechanical Properties of Epoxy Resin Modified with Hydroxyl-Terminated Poly(Methylphenylsiloxane). *Polymers* **2026**, *18* (13). https://doi.org/10.3390/polym18131569.
(130) Kireev, V. V.; Bilichenko, Y. V.; Borisov, R. S.; Mu, J.; Kuznetsov, D. A.; Eroshenko, A. V.; Filatov, S. N.; Sirotin, I. S. Synthesis of Bisphenol A Based Phosphazene-Containing Epoxy Resin with Reduced Viscosity. *Polymers* **2019**, *11* (12), 1914. https://doi.org/10.3390/polym11121914.
(131) *Lignin carbon fiber: The path for quality, TAPPI JOURNAL March 2017*. https://imisrise.tappi.org/TAPPI/Products/17/MAR/17MAR107.aspx (accessed 2026-07-16).
(132) *Carbon Fiber Market Size, Share & Trends, Forecast, 2034*. https://www.fortunebusinessinsights.com/industry-reports/carbon-fiber-market-101719 (accessed 2026-07-16).

(133) Huang, X. Fabrication and Properties of Carbon Fibers. *Materials* **2009**, *2* (4), 2369–2403. https://doi.org/10.3390/ma2042369.
(134) Wang, S.; Bai, J.; Innocent, M. T.; Wang, Q.; Xiang, H.; Tang, J.; Zhu, M. Lignin-Based Carbon Fibers: Formation, Modification and Potential Applications. *Green Energy Environ.* **2022**, *7* (4), 578–605. https://doi.org/10.1016/j.gee.2021.04.006.
(135) Paul, R. M.; Naskar, A. *Low-Cost Bio-Based Carbon Fibers for High Temperature Processing*; Final Technical Report, 1373688; 2017; p Final Technical Report, 1373688. https://doi.org/10.2172/1373688.
(136) Jang, M.; Park, J.; Choi, J.; Kim, S.-S. Plasticized Melt Spinning of Lignin Precursor Fibers and Carbonization Assisted by Electron Beam Irradiation. *ACS Sustain. Chem. Eng.* **2025**, *13* (4), 1617–1627. https://doi.org/10.1021/acssuschemeng.4c08229.
(137) Rougé, J.; Beaucamp, A.; Collins, M. N. Wet-Spinning and Carbonisation of Water Coagulated Lignin/Bio-Based Thermoplastic Polyurethane Precursor Fibres. *Compos. Part Appl. Sci. Manuf.* **2025**, *199*, 109196. https://doi.org/10.1016/j.compositesa.2025.109196.
(138) Parot, M.; Rodrigue, D.; Stevanovic, T. Electrospinning of Softwood Organosolv Lignin without Polymer Addition. *ACS Sustain. Chem. Eng.* **2023**, *11* (2), 607–616. https://doi.org/10.1021/acssuschemeng.2c05233.
(139) Team, P. I. *Lignin-based carbon fiber technology landscape 2026*. Patsnap. https://www.patsnap.com/resources/blog/articles/lignin-based-carbon-fiber-technology-landscape-2026/ (accessed 2026-07-16).
(140) Liu, F.; Wang, Q.; Zhai, G.; Xiang, H.; Zhou, J.; Jia, C.; Zhu, L.; Wu, Q.; Zhu, M. Continuously Processing Waste Lignin into High-Value Carbon Nanotube Fibers. *Nat. Commun.* **2022**, *13* (1), 5755. https://doi.org/10.1038/s41467-022-33496-2.
(141) Argyropoulos, D. D. S.; Crestini, C.; Dahlstrand, C.; Furusjö, E.; Gioia, C.; Jedvert, K.; Henriksson, G.; Hulteberg, C.; Lawoko, M.; Pierrou, C.; Samec, J. S. M.; Subbotina, E.; Wallmo, H.; Wimby, M. Kraft Lignin: A Valuable, Sustainable Resource, Opportunities and Challenges. *ChemSusChem* **2023**, *16* (23), e202300492. https://doi.org/10.1002/cssc.202300492.
(142) Duret, E.; de Moura, L. C. R.; Morales, A.; Labidi, J.; Robles, E.; Charrier-El Bouhtoury, F. Efficient Lignin Precipitation from Softwood Black Liquor Using Organic Acids for Sustainable Valorization. *Polymers* **2025**, *17* (7), 926. https://doi.org/10.3390/polym17070926.
(143) Naqvi, M.; Yan, J.; Dahlquist, E. Black Liquor Gasification Integrated in Pulp and Paper Mills: A Critical Review. *Bioresour. Technol.* **2010**, *101* (21), 8001–8015. https://doi.org/10.1016/j.biortech.2010.05.013.
(144) Jiju, P. S.; Patel, A. K.; Shruthy, N. S.; Shalu, S.; Dong, C.-D.; Singhania, R. R. Sustainability through Lignin Valorization: Recent Innovations and Applications Driving Industrial Transformation. *Bioresour. Bioprocess.* **2025**, *12* (1), 88. https://doi.org/10.1186/s40643-025-00929-x.
(145) Wu, F.-P.; Qiu, L.-L.; Zhao, Y.-P.; Fu, Z.-P.; Liang, J.; Xiao, J.; Li, J.; Liu, F.-J.; Cao, J.-P. Self-Hydrogen Transfer Hydrogenolysis of β-O-4 Bonds in Lignin Model Compounds over NiCu/Al2O3 Catalyst. *Fuel* **2024**, *372*, 132094. https://doi.org/10.1016/j.fuel.2024.132094.
(146) Mukesh, C.; Huang, G.; Qin, H.; Liu, Y.; Ji, X. Insight into Lignin Oxidative Depolymerization in Ionic Liquids and Deep Eutectic Solvents. *Biomass Bioenergy* **2024**, *188*, 107305. https://doi.org/10.1016/j.biombioe.2024.107305.

(147) Andriani, F.; Lawoko, M. Oxidative Carboxylation of Lignin: Exploring Reactivity of Different Lignin Types. *Biomacromolecules* **2024**, *25* (7), 4246–4254. https://doi.org/10.1021/acs.biomac.4c00326.
(148) Karlsson, M.; Romson, J.; Elder, T.; Emmer, Å.; Lawoko, M. Lignin Structure and Reactivity in the Organosolv Process Studied by NMR Spectroscopy, Mass Spectrometry, and Density Functional Theory. *Biomacromolecules* **2023**, *24* (5), 2314–2326. https://doi.org/10.1021/acs.biomac.3c00186.
(149) Sadeghifar, H.; Ragauskas, A. Technical Lignin Fractionation: A Powerful Tool for Lignin Structure Homogenization and Its Application.
(150) Antonsson, S.; Henriksson, G.; Johansson, M.; Lindström, M. E. Low *M*w-Lignin Fractions Together with Vegetable Oils as Available Oligomers for Novel Paper-Coating Applications as Hydrophobic Barrier. *Ind. Crops Prod.* **2008**, *27* (1), 98–103. https://doi.org/10.1016/j.indcrop.2007.08.006.
(151) Domínguez-Robles, J.; Tamminen, T.; Liitiä, T.; Peresin, M. S.; Rodríguez, A.; Jääskeläinen, A.-S. Aqueous Acetone Fractionation of Kraft, Organosolv and Soda Lignins. *Int. J. Biol. Macromol.* **2018**, *106*, 979–987. https://doi.org/10.1016/j.ijbiomac.2017.08.102.
(152) Nitsos, C.; Stoklosa, R.; Karnaouri, A.; Vörös, D.; Lange, H.; Hodge, D.; Crestini, C.; Rova, U.; Christakopoulos, P. Isolation and Characterization of Organosolv and Alkaline Lignins from Hardwood and Softwood Biomass. *ACS Sustain. Chem. Eng.* **2016**, *4* (10), 5181–5193. https://doi.org/10.1021/acssuschemeng.6b01205.
(153) Prinsen, P.; Rencoret, J.; Gutiérrez, A.; Liitiä, T.; Tamminen, T.; Colodette, J. L.; Berbis, M. Á.; Jiménez-Barbero, J.; Martínez, Á. T.; Del Río, J. C. Modification of the Lignin Structure during Alkaline Delignification of Eucalyptus Wood by Kraft, Soda-AQ, and Soda-O_2 Cooking. *Ind. Eng. Chem. Res.* **2013**, *52* (45), 15702–15712. https://doi.org/10.1021/ie401364d.
(154) Brandt, A.; Chen, L.; Dongen, B. E. van; Welton, T.; P. Hallett, J. Structural Changes in Lignins Isolated Using an Acidic Ionic Liquid Water Mixture. *Green Chem.* **2015**, *17* (11), 5019–5034. https://doi.org/10.1039/C5GC01314C.
(155) Sun, Y.-C.; Liu, X.-N.; Wang, T.-T.; Xue, B.-L.; Sun, R.-C. Green Process for Extraction of Lignin by the Microwave-Assisted Ionic Liquid Approach: Toward Biomass Biorefinery and Lignin Characterization. *ACS Sustain. Chem. Eng.* **2019**, *7* (15), 13062–13072. https://doi.org/10.1021/acssuschemeng.9b02166.
(156) Nair, L. G.; Agrawal, K.; Verma, P. Organosolv Pretreatment: An in-Depth Purview of Mechanics of the System. *Bioresour. Bioprocess.* **2023**, *10* (1), 50. https://doi.org/10.1186/s40643-023-00673-0.
(157) Li, T.; Takkellapati, S. The Current and Emerging Sources of Technical Lignins and Their Applications. *Biofuels Bioprod. Biorefining Biofpr* **2018**, *0*, 1–32. https://doi.org/10.1002/bbb.1913.
(158) de la Torre, M. J.; Moral, A.; Hernández, M. D.; Cabeza, E.; Tijero, A. Organosolv Lignin for Biofuel. *Ind. Crops Prod.* **2013**, *45*, 58–63. https://doi.org/10.1016/j.indcrop.2012.12.002.
(159) Labauze, H.; Cachet, N.; Benjelloun-Mlayah, B. Acid-Based Organosolv Lignin Extraction from Wheat Straw: Kinetic and Structural Analysis. *Ind. Crops Prod.* **2022**, *187*, 115328. https://doi.org/10.1016/j.indcrop.2022.115328.

(160) Peng, M.; Nakabayashi, M.; Kim, K.; Kamiya, K.; Qian, E. W. Lignin Depolymerization with Alkaline Ionic Liquids and Ethylene Glycol in a Continuous Flow Reactor. *Fuel* **2023**, *335*, 126960. https://doi.org/10.1016/j.fuel.2022.126960.
(161) Antonino, L. D.; Gouveia, J. R.; de Sousa Júnior, R. R.; Garcia, G. E. S.; Gobbo, L. C.; Tavares, L. B.; dos Santos, D. J. Reactivity of Aliphatic and Phenolic Hydroxyl Groups in Kraft Lignin towards 4,4′ MDI. *Molecules* **2021**, *26* (8), 2131. https://doi.org/10.3390/molecules26082131.
(162) Jacobs, B.; Graulus, G.-J.; Bernaerts, K. V.; Verberckmoes, A. Comprehensive Characterization of Sustainably Synthesized Lignin-Based Polyols towards Thermoset Materials. *Mater.* **2025**, *9*, 101279. https://doi.org/10.1016/j.nxmate.2025.101279.
(163) Antonino, L. D.; Gouveia, J. R.; de Sousa Júnior, R. R.; Garcia, G. E. S.; Gobbo, L. C.; Tavares, L. B.; dos Santos, D. J. Reactivity of Aliphatic and Phenolic Hydroxyl Groups in Kraft Lignin towards 4,4′ MDI. *Molecules* **2021**, *26* (8), 2131. https://doi.org/10.3390/molecules26082131.
(164) Río, J. C. del; Rencoret, J.; Gutiérrez, A.; Elder, T.; Kim, H.; Ralph, J. Lignin Monomers from beyond the Canonical Monolignol Biosynthetic Pathway: Another Brick in the Wall. *ACS Sustain. Chem. Eng.* **2020**, *8*, 4997–5012. https://doi.org/10.1021/acssuschemeng.0c01109.
(165) Wang, Z.; Zhang, Z.; Wang, H.; Deuss, P. J. Tuning Lignin Properties by Mild Ionic-Liquid-Mediated Selective Alcohol Incorporation. *Chem Catal.* **2022**, *2* (6), 1407–1427. https://doi.org/10.1016/j.checat.2022.04.005.
(166) Suota, M. J.; da Silva, T. A.; Zawadzki, S. F.; Sassaki, G. L.; Hansel, F. A.; Paleologou, M.; Ramos, L. P. Chemical and Structural Characterization of Hardwood and Softwood LignoForce™ Lignins. *Ind. Crops Prod.* **2021**, *173*, 114138. https://doi.org/10.1016/j.indcrop.2021.114138.
(167) Yuan, S.; Li, B.; Chang, L.; Guo, H.; Ding, L.; Hou, J.; Zhang, S.; Zang, C.; Zheng, L.; Yang, W.; Guan, H. Characterization and Antioxidant Activity of Differentiated Fractionation Lignin from Corn Stover. *Int. J. Biol. Macromol.* **2025**, *303*, 140538. https://doi.org/10.1016/j.ijbiomac.2025.140538.
(168) Kačík, F.; Kačíková, D. STRUCTURAL CHARACTERIZATION OF LIGNIN BY SYRINGYL TO GUAIACYL RATIO AND MOLECULAR MASS DETERMINATION.
(169) A Systematic Study on the Processes of Lignin Extraction and Nanodispersion to Control Properties and Functionality. *Green Chem.* **2024**, *26* (6), 2967–2984. https://doi.org/10.1039/d3gc04299e.
(170) Wannid, P.; Hararak, B.; Padee, S.; Klinsukhon, W.; Suwannamek, N.; Raita, M.; Champreda, V.; Prahsarn, C. Fiber Melt Spinning and Thermo-Stabilization of Para-Rubber Wood Lignin: An Approach for Fully Biomass Precursor Preparation. *ACS Omega* **2023**, *8* (37), 33891–33903. https://doi.org/10.1021/acsomega.3c04590.
(171) Zhang, Y.; Stepanova, S.; Van Aelst, K.; Sels, B. F. Consider Lignin's Hydroxyl Groups Content and Type, Its Molecular Weight and Content When Converting It into Epoxy Resin. *Curr. Opin. Green Sustain. Chem.* **2023**, *40*, 100750. https://doi.org/10.1016/j.cogsc.2022.100750.
(172) Abolore, R. S.; Jaiswal, S.; Jaiswal, A. K. A Comprehensive Review on Sustainable Lignin Extraction Techniques, Modifications, and Emerging Applications. *Ind. Crops Prod.* **2025**, *235*, 121696. https://doi.org/10.1016/j.indcrop.2025.121696.

(173) Li, X.; Yang, J.; He, W.; Zhao, S.; Fang, Z.; Guo, K.; Li, Y. A Review: Using Ionic Liquids for Lignin Extraction from Lignocellulose and High-Value Utilization. *Molecules* **2025**, *30* (12), 2514. https://doi.org/10.3390/molecules30122514.
(174) Liu, X.; Li, Y.; M. Ewulonu, C.; Ralph, J.; Xu, F.; Zhang, Q.; Wu, M.; Huang, Y. Mild Alkaline Pretreatment for Isolation of Native-Like Lignin and Lignin-Containing Cellulose Nanofibers (LCNF) from Crop Waste. *ACS Sustain. Chem. Eng.* **2019**, *7* (16), 14135–14142. https://doi.org/10.1021/acssuschemeng.9b02800.
(175) da Costa Lopes, A. M.; João, K. G.; Rubik, D. F.; Bogel-Łukasik, E.; Duarte, L. C.; Andreaus, J.; Bogel-Łukasik, R. Pre-Treatment of Lignocellulosic Biomass Using Ionic Liquids: Wheat Straw Fractionation. *Bioresour. Technol.* **2013**, *142*, 198–208. https://doi.org/10.1016/j.biortech.2013.05.032.
(176) Introduction: Ionic Liquids. *Chem. Rev.* **2017**, *117* (10), 6633–6635. https://doi.org/10.1021/acs.chemrev.7b00246.
(177) Silah, H.; Kul, D.; Uslu, B. Why Are Ionic Liquids so Unique? – A Review on Ionic Liquids and Hemoglobin Modified Electrodes as Electrochemical Sensing Platforms. *Electrochimica Acta* **2025**, *532*, 146504. https://doi.org/10.1016/j.electacta.2025.146504.
(178) Philippi, F.; Welton, T. Targeted Modifications in Ionic Liquids – from Understanding to Design. *Phys. Chem. Chem. Phys.* **2021**, *23* (12), 6993–7021. https://doi.org/10.1039/D1CP00216C.
(179) Chatterjee, R.; Bhukta, S.; Dandela, R. Super Base Derived Ionic Liquids: A Useful Tool in Organic Synthesis. *http://www.eurekaselect.com*.
(180) Liu, F.; Guo, J.; Zhao, P.; Gu, Y.; Gao, J.; Liu, M. Facile Synthesis of DBU-Based Protic Ionic Liquid for Efficient Alcoholysis of Waste Poly(Lactic Acid) to Lactate Esters. *Polym. Degrad. Stab.* **2019**, *167*, 124–129. https://doi.org/10.1016/j.polymdegradstab.2019.06.028.
(181) Rafaela Rocha Pinto; Silvana Matteddi; Martin Aznar. Synthesis and Physical Properties of Three Protic Ionic Liquids with the Ethylammonium Cation. *Chem. Eng. Trans.* **2015**, *43*, 1165–1170. https://doi.org/10.3303/CET1543195.
(182) Damilano, G.; Kalebić, D.; Binnemans, K.; Dehaen, W. One-Pot Synthesis of Symmetric Imidazolium Ionic Liquids N,N-Disubstituted with Long Alkyl Chains. *RSC Adv.* **2020**, *10* (36), 21071–21081. https://doi.org/10.1039/D0RA03358H.
(183) Gregorio, G. F. D.; Weber, C. C.; Gräsvik, J.; Welton, T.; Brandt, A.; Hallett, J. P. Mechanistic Insights into Lignin Depolymerisation in Acidic Ionic Liquids. *Green Chem.* **2016**, *18* (20), 5456–5465. https://doi.org/10.1039/C6GC01295G.
(184) Achinivu, E. C. Protic Ionic Liquids for Lignin Extraction—A Lignin Characterization Study. *Int. J. Mol. Sci.* **2018**, *19* (2), 428. https://doi.org/10.3390/ijms19020428.
(185) Jing, Y.; Mu, X.; Han, Z.; Liu, C.; Zhang, D. Mechanistic Insight into β–O–4 Linkage Cleavage of Lignin Model Compound Catalyzed by a SO3H-Functionalized Imidazolium Ionic Liquid: An Unconventional E1 Elimination. *Mol. Catal.* **2019**, *463*, 140–149. https://doi.org/10.1016/j.mcat.2018.12.002.
(186) Shill, K.; Padmanabhan, S.; Xin, Q.; Prausnitz, J. M.; Clark, D. S.; Blanch, H. W. Ionic Liquid Pretreatment of Cellulosic Biomass: Enzymatic Hydrolysis and Ionic Liquid Recycle. *Biotechnol. Bioeng.* **2011**, *108* (3), 511–520. https://doi.org/10.1002/bit.23014.
(187) Alvarez-Vasco, C.; Ma, R.; Quintero, M.; Guo, M.; Geleynse, S.; Ramasamy, K. K.; Wolcott, M.; Zhang, X. Unique Low-Molecular-Weight Lignin with High Purity Extracted from Wood by Deep Eutectic Solvents (DES): A Source of Lignin for Valorization. *Green Chem.* **2016**, *18* (19), 5133–5141. https://doi.org/10.1039/C6GC01007E.

(188) Khakalo, A.; Tanaka, A.; Korpela, A.; Orelma, H. Delignification and Ionic Liquid Treatment of Wood toward Multifunctional High-Performance Structural Materials. *ACS Appl. Mater. Interfaces* **2020**, *12* (20), 23532–23542. https://doi.org/10.1021/acsami.0c02221.
(189) Li, Z. DBU-Based Ionic Liquids. *Encycl. Ion. Liq.* **2020**, 1–10.
(190) Dissanayake, N.; Thalangamaarachchige, V. D.; Quitevis, E.; Abidi, N. Effect of Alkyl Chain Length on Dissolution and Regeneration Behavior of Cotton in 1-Alkyl-3-Methylimidazolium Acetate Ionic Liquids. *Molecules* **2025**, *30* (13). https://doi.org/10.3390/molecules30132711.
(191) Mehmood Asim, A.; Uroos, M.; Muhammad, N. Extraction of Lignin and Quantitative Sugar Release from Biomass Using Efficient and Cost-Effective Pyridinium Protic Ionic Liquids. *RSC Adv.* **2020**, *10* (72), 44003–44014. https://doi.org/10.1039/D0RA09098K.
(192) Arefmanesh, M.; Vuong, T. V.; Mobley, J. K.; Alinejad, M.; Master, E. R.; Nejad, M. Bromide-Based Ionic Liquid Treatment of Hardwood Organosolv Lignin Yielded a More Reactive Biobased Polyol. *Ind. Eng. Chem. Res.* **2020**, *59* (42), 18740–18747. https://doi.org/10.1021/acs.iecr.0c03718.
(193) Jing, Y.; Mu, X.; Han, Z.; Liu, C.; Zhang, D. Mechanistic Insight into β–O–4 Linkage Cleavage of Lignin Model Compound Catalyzed by a SO3H-Functionalized Imidazolium Ionic Liquid: An Unconventional E1 Elimination. *Mol. Catal.* **2019**, *463*, 140–149. https://doi.org/10.1016/j.mcat.2018.12.002.
(194) Hauru, L. K. J.; Hummel, M.; King, A. W. T.; Kilpeläinen, I.; Sixta, H. Role of Solvent Parameters in the Regeneration of Cellulose from Ionic Liquid Solutions. *Biomacromolecules* **2012**, *13* (9), 2896–2905. https://doi.org/10.1021/bm300912y.
(195) Gong, L.; Feng, D.; Liu, J.; Yu, Y.; Wang, J. Ionic Liquid Depolymerize the Lignocellulose for the Enzymatic Extraction of Feruloylated Oligosaccharide from Corn Bran. *Food Chem. X* **2022**, *15*, 100381. https://doi.org/10.1016/j.fochx.2022.100381.
(196) Olsson, C.; Idström, A.; Nordstierna, L.; Westman, G. Influence of Water on Swelling and Dissolution of Cellulose in 1-Ethyl-3-Methylimidazolium Acetate. *Carbohydr. Polym.* **2014**, *99*, 438–446. https://doi.org/10.1016/j.carbpol.2013.08.042.
(197) Wang, H.; Maxim, M. L.; Gurau, G.; Rogers, R. D. Microwave-Assisted Dissolution and Delignification of Wood in 1-Ethyl-3-Methylimidazolium Acetate. *Bioresour. Technol.* **2013**, *136*, 739–742. https://doi.org/10.1016/j.biortech.2013.03.064.
(198) Rizvi, S.; Gade, H. M. Imidazolium-Based Ionic Liquids as Cellulose Solvents: Mechanism and Molecular Insights. *Biomass Bioenergy* **2025**, *196*. https://doi.org/10.1016/j.biombioe.2025.107758.
(199) Haward, S. J.; Sharma, V.; Butts, C. P.; McKinley, G. H.; Rahatekar, S. S. Shear and Extensional Rheology of Cellulose/Ionic Liquid Solutions. *Biomacromolecules* **2012**, *13* (5), 1688–1699. https://doi.org/10.1021/bm300407q.
(200) Araldi da Silva, B.; de Sousa Cunha, R.; Valério, A.; De Noni Junior, A.; Hotza, D.; Gómez González, S. Y. Electrospinning of Cellulose Using Ionic Liquids: An Overview on Processing and Applications. *Eur. Polym. J.* **2021**, *147*. https://doi.org/10.1016/j.eurpolymj.2021.110283.
(201) Kirchberg, A.; Meier, M. A. R. Regeneration of Cellulose from a Switchable Ionic Liquid: Toward More Sustainable Cellulose Fibers. *Macromol. Chem. Phys.* **2021**, *222* (6), 2000433. https://doi.org/10.1002/macp.202000433.

(202) Zhang, Y.; Huo, F.; Wang, Y.; Xia, Y.; Tan, X.; Zhang, S.; He, H. Theoretical Elucidation of β-O-4 Bond Cleavage of Lignin Model Compound Promoted by Sulfonic Acid-Functionalized Ionic Liquid. *Front. Chem.* **2019**, *7*. https://doi.org/10.3389/fchem.2019.00078.
(203) Wang, H.; Tucker, M.; Ji, Y. Recent Development in Chemical Depolymerization of Lignin: A Review. *J. Appl. Chem.* **2013**, *2013*, 1–9. https://doi.org/10.1155/2013/838645.
(204) Yu, H.; Xue, Z.; Shi, R.; Zhou, F.; Mu, T. Lignin Dissolution and Lignocellulose Pretreatment by Carboxylic Acid Based Deep Eutectic Solvents. *Ind. Crops Prod.* **2022**, *184*, 115049. https://doi.org/10.1016/j.indcrop.2022.115049.
(205) Jugovic, T. Advances in the Modeling of Synthesis, Design and Properties of Polymers. **2023**.
(206) Palacios-Marín, A. V.; Jabbar, A.; Tausif, M. Fragmented Fiber Pollution from Common Textile Materials and Structures during Laundry. *Text. Res. J.* **2022**, *92* (13–14), 2265–2275. https://doi.org/10.1177/00405175221090971.
(207) Azanaw, A.; Birlie, B.; Teshome, B.; Jemberie, M. Textile Effluent Treatment Methods and Eco-Friendly Resolution of Textile Wastewater. *Case Stud. Chem. Environ. Eng.* **2022**, *6*. https://doi.org/10.1016/j.cscee.2022.100230.
(208) Tiffin, L.; Hazlehurst, A.; Sumner, M.; Taylor, M. Reliable Quantification of Microplastic Release from the Domestic Laundry of Textile Fabrics. *J. Text. Inst.* **2022**, *113* (4), 558–566. https://doi.org/10.1080/00405000.2021.1892305.
(209) Allen, E.; Henninger, C. E.; Garforth, A.; Asuquo, E. Microfiber Pollution: A Systematic Literature Review to Overcome the Complexities in Knit Design to Create Solutions for Knit Fabrics. *Environ. Sci. Technol.* **2024**, *58* (9), 4031–4045. https://doi.org/10.1021/acs.est.3c05955.
(210) Wang, C.; Song, J.; Nunes, L. M.; Zhao, H.; Wang, P.; Liang, Z.; Arp, H. P. H.; Li, G.; Xing, B. Global Microplastic Fiber Pollution from Domestic Laundry. *J. Hazard. Mater.* **2024**, *477*. https://doi.org/10.1016/j.jhazmat.2024.135290.
(211) Carr, S. A.; Liu, J.; Tesoro, A. G. Transport and Fate of Microplastic Particles in Wastewater Treatment Plants. *Water Res.* **2016**, *91*, 174–182. https://doi.org/10.1016/j.watres.2016.01.002.
(212) Bové, H.; Bongaerts, E.; Slenders, E.; Bijnens, E. M.; Saenen, N. D.; Gyselaers, W.; Van Eyken, P.; Plusquin, M.; Roeffaers, M. B. J.; Ameloot, M.; Nawrot, T. S. Ambient Black Carbon Particles Reach the Fetal Side of Human Placenta. *Nat. Commun.* **2019**, *10* (1). https://doi.org/10.1038/s41467-019-11654-3.
(213) Schmaltz, E.; Melvin, E. C.; Diana, Z.; Gunady, E. F.; Rittschof, D.; Somarelli, J. A.; Virdin, J.; Dunphy-Daly, M. M. Plastic Pollution Solutions: Emerging Technologies to Prevent and Collect Marine Plastic Pollution. *Environ. Int.* **2020**, *144*. https://doi.org/10.1016/j.envint.2020.106067.
(214) Simon, M.; Vianello, A.; Vollertsen, J. Removal of > 10 Mm Microplastic Particles from Treated Wastewater by a Disc Filter. *Water Switz.* **2019**, *11* (9). https://doi.org/10.3390/w11091935.
(215) Sun, J.; Dai, X.; Wang, Q.; van Loosdrecht, M. C. M.; Ni, B. J. Microplastics in Wastewater Treatment Plants: Detection, Occurrence and Removal. *Water Res.* **2019**, *152*, 21–37. https://doi.org/10.1016/j.watres.2018.12.050.
(216) Talvitie, J.; Heinonen, M.; Pääkkönen, J. P.; Vahtera, E.; Mikola, A.; Setälä, O.; Vahala, R. Do Wastewater Treatment Plants Act as a Potential Point Source of Microplastics?

Preliminary Study in the Coastal Gulf of Finland, Baltic Sea. *Water Sci. Technol.* **2015**, *72* (9), 1495–1504. https://doi.org/10.2166/wst.2015.360.
(217) Ben-David, E. A.; Habibi, M.; Haddad, E.; Hasanin, M.; Angel, D. L.; Booth, A. M.; Sabbah, I. Microplastic Distributions in a Domestic Wastewater Treatment Plant: Removal Efficiency, Seasonal Variation and Influence of Sampling Technique. *Sci. Total Environ.* **2021**, *752*. https://doi.org/10.1016/j.scitotenv.2020.141880.
(218) *Standards for the Use or Disposal of Sewage Sludge; Agency Response to the National Research Council Report on Biosolids Applied to Land and the Results of EPA's Review of Existing Sewage Sludge Regulations*. Federal Register. https://www.federalregister.gov/documents/2003/04/09/03-8654/standards-for-the-use-or-disposal-of-sewage-sludge-agency-response-to-the-national-research-council (accessed 2026-02-02).
(219) Luogo, B. D. P.; Salim, T.; Zhang, W.; Hartmann, N. B.; Malpei, F.; Candelario, V. M. Reuse of Water in Laundry Applications with Micro-and Ultrafiltration Ceramic Membrane. *Membranes* **2022**, *12* (2). https://doi.org/10.3390/membranes12020223.
(220) Akarsu, C.; Deniz, F. Electrocoagulation/Electroflotation Process for Removal of Organics and Microplastics in Laundry Wastewater. *CLEAN – Soil Air Water* **2021**, *49*, 2000146–2000146.
(221) Li, J.; Dagnew, M.; Ray, M. B. Effect of Coagulation on Microfibers in Laundry Wastewater. *Environ. Res.* **2022**, *212*. https://doi.org/10.1016/j.envres.2022.113401.
(222) Gulmez, C.; Atakisi, O. Investigation of Compatibility of Lipase with Commercial Detergents, Surfactants and Oxidizing Agent as a Detergent Additive. *Int. J. Chem. Technol.* **2022**, *6* (1), 33–38. https://doi.org/10.32571/ijct.1085417.
(223) Kiki, C.; Qiu, Y.; Wang, Q.; Ifon, B. E.; Qin, D.; Chabi, K.; Yu, C. P.; Zhu, Y. G.; Sun, Q. Induced Aging, Structural Change, and Adsorption Behavior Modifications of Microplastics by Microalgae. *Environ. Int.* **2022**, *166*. https://doi.org/10.1016/j.envint.2022.107382.
(224) Silva, A. B.; Bastos, A. S.; Justino, C. I. L.; da Costa, J. P.; Duarte, A. C.; Rocha-Santos, T. A. P. Microplastics in the Environment: Challenges in Analytical Chemistry - A Review. *Anal. Chim. Acta* **2018**, *1017*, 1–19. https://doi.org/10.1016/j.aca.2018.02.043.
(225) Helping Hands Cleaning Services. How Much Laundry Detergent Should I Use. **2024**.
(226) O'Callaghan, J. M.; McNamara, H.; Copley, M. P.; Hanrahan, J. P.; Morris, M. A.; Steytler, D. C.; Heenan, R. K.; Holmes, J. D. Swelling of Ionic and Nonionic Surfactant Micelles by High Pressure Gases. *Langmuir* **2010**, *26* (11), 7725–7731. https://doi.org/10.1021/la904464k.
(227) Baglioni, M.; Sekine, F. H.; Ogura, T.; Chen, S. H.; Baglioni, P. Nanostructured Fluids for Polymeric Coatings Removal: Surfactants Affect the Polymer Glass Transition Temperature. *J. Colloid Interface Sci.* **2022**, *606*, 124–134. https://doi.org/10.1016/j.jcis.2021.07.078.
(228) Sarkar, A.; Jayaram, R. V. A Comparative Study of Properties of Acrylic Based Water-Borne Polymers Using Various Surfactants for Adhesive Applications. *Polym. Sci. - Ser. B* **2018**, *60* (5), 629–637. https://doi.org/10.1134/S1560090418050147.
(229) Jing, D.; Bao, C.; Dong, Z.; Meng, X.; Han, X.; Li, G.; Chen, J. Study on the Compounding Optimization of Surfactants and Synergistic Effects on the Wettability of Bituminous Coal. *Sci. Rep.* **2024**, *14* (1). https://doi.org/10.1038/s41598-024-61266-1.
(230) Comyn, J. *Theories of Adhesion*; 2020; pp 1–50.

(231) *The plastic we can't see is changing the ocean | | UN News*. https://news.un.org/en/audio/2026/06/1167638 (accessed 2026-06-27).
(232) *World Oceans Day 2020: New IAEA Research Records Dramatic Increase in Microplastic Pollution in Eastern Tropical Pacific Ocean*. http://www.iaea.org/newscenter/news/world-oceans-day-2020-new-iaea-research-records-dramatic-increase-in-microplastic-pollution-in-eastern-tropical-pacific-ocean (accessed 2026-04-22).
(233) Gallo, F.; Fossi, C.; Weber, R.; Santillo, D.; Sousa, J.; Ingram, I.; Nadal, A.; Romano, D. Marine Litter Plastics and Microplastics and Their Toxic Chemicals Components: The Need for Urgent Preventive Measures. *Environ. Sci. Eur.* **2018**, *30* (1), 13. https://doi.org/10.1186/s12302-018-0139-z.
(234) Yang, H.; Chen, G.; Wang, J. Microplastics in the Marine Environment: Sources, Fates, Impacts and Microbial Degradation. *Toxics* **2021**, *9* (2), 41. https://doi.org/10.3390/toxics9020041.
(235) Nelms, S. E.; Barnett, J.; Brownlow, A.; Davison, N. J.; Deaville, R.; Galloway, T. S.; Lindeque, P. K.; Santillo, D.; Godley, B. J. Microplastics in Marine Mammals Stranded around the British Coast: Ubiquitous but Transitory? *Sci. Rep.* **2019**, *9* (1), 1075. https://doi.org/10.1038/s41598-018-37428-3.
(236) Merrill, G. B.; Hermabessiere, L.; Rochman, C. M.; Nowacek, D. P. Microplastics in Marine Mammal Blubber, Melon, & Other Tissues: Evidence of Translocation. *Environ. Pollut.* **2023**, *335*, 122252. https://doi.org/10.1016/j.envpol.2023.122252.
(237) Song, J.; Wang, C.; Li, G. Defining Primary and Secondary Microplastics: A Connotation Analysis. *ACS EST Water* **2024**, *4* (6), 2330–2332. https://doi.org/10.1021/acsestwater.4c00316.
(238) El Hadri, H.; Gigault, J.; Maxit, B.; Grassl, B.; Reynaud, S. Nanoplastic from Mechanically Degraded Primary and Secondary Microplastics for Environmental Assessments. *NanoImpact* **2020**, *17*, 100206. https://doi.org/10.1016/j.impact.2019.100206.
(239) Huber, M.; Archodoulaki, V.-M.; Pomakhina, E.; Pukánszky, B.; Zinöcker, E.; Gahleitner, M. Environmental Degradation and Formation of Secondary Microplastics from Packaging Material: A Polypropylene Film Case Study. *Polym. Degrad. Stab.* **2022**, *195*, 109794. https://doi.org/10.1016/j.polymdegradstab.2021.109794.
(240) Huber, M.; Archodoulaki, V.-M.; Pomakhina, E.; Pukánszky, B.; Zinöcker, E.; Gahleitner, M. Environmental Degradation and Formation of Secondary Microplastics from Packaging Material: A Polypropylene Film Case Study. *Polym. Degrad. Stab.* **2022**, *195*, 109794. https://doi.org/10.1016/j.polymdegradstab.2021.109794.
(241) Guo, B.; Ma, P. X. Synthetic Biodegradable Functional Polymers for Tissue Engineering: A Brief Review. *Sci. China Chem.* **2014**, *57* (4), 490–500. https://doi.org/10.1007/s11426-014-5086-y.
(242) Yin, Y.; Wai Woo, M. Transitioning of Petroleum-Based Plastic Food Packaging to Sustainable Bio-Based Alternatives. **2024**. https://doi.org/10.1039/D4FB00028E.
(243) Dumon, M. Plastics and Polymers Today, Some Questions, a Particular Viewpoint. *Waste Manag. Bull.* **2025**, *3* (3), 100226. https://doi.org/10.1016/j.wmb.2025.100226.
(244) Namazi, H. Polymers in Our Daily Life. *BioImpacts BI* **2017**, *7* (2), 73–74. https://doi.org/10.15171/bi.2017.09.
(245) Adetuyi, B. O.; Mathew, J. T.; Inobeme, A.; Falana, Y. O.; Adetunji, C. O.; Shahnawaz, M.; Oyewole, O. A.; K.I.T., E.; Yerima, M. B. Sources, Uses and Transport of Secondary

Microplastics from Land to Marine Environment. In *Microplastic Pollution*; Shahnawaz, Mohd., Adetunji, C. O., Dar, M. A., Zhu, D., Eds.; Springer Nature: Singapore, 2024; pp 35–49. https://doi.org/10.1007/978-981-99-8357-5_3.
(246) Dawson, A. L.; Li, J. Y. Q.; Kroon, F. J. Plastics for Dinner: Store-Bought Seafood, but Not Wild-Caught from the Great Barrier Reef, as a Source of Microplastics to Human Consumers. *Environ. Adv.* **2022**, *8*, 100249. https://doi.org/10.1016/j.envadv.2022.100249.
(247) Sui, Y.; You, X.; Xu, X.; Guo, G.; Sheng, H.; Huang, L. Harmonious Assessment of Mesh Effect in Water Sieve Sampling for Fibrous Microplastics Abundance. *Environ. Res.* **2025**, *271*, 121056. https://doi.org/10.1016/j.envres.2025.121056.
(248) Abuwatfa, W. H.; Al-Muqbel, D.; Al-Othman, A.; Halalsheh, N.; Tawalbeh, M. Insights into the Removal of Microplastics from Water Using Biochar in the Era of COVID-19: A Mini Review. *Case Stud. Chem. Environ. Eng.* **2021**, *4*, 100151. https://doi.org/10.1016/j.cscee.2021.100151.
(249) Lawal, T. D.; Jugovic, T.; Josephs, G.; Zimmerman, P. M.; Love, B. J. Surfactants Can Compete with Microplastics for Surfaces Using Adhesives as Substrates for Microplastic Sequestration. *Environ. Pollut. Barking Essex 1987* **2025**, *364* (Pt 2), 125372. https://doi.org/10.1016/j.envpol.2024.125372.
(250) Schindelin, J.; Arganda-Carreras, I.; Frise, E.; Kaynig, V.; Longair, M.; Pietzsch, T.; Preibisch, S.; Rueden, C.; Saalfeld, S.; Schmid, B.; Tinevez, J.-Y.; White, D. J.; Hartenstein, V.; Eliceiri, K.; Tomancak, P.; Cardona, A. Fiji - an Open Source Platform for Biological Image Analysis. *Nat. Methods* **2012**, *9* (7), 10.1038/nmeth.2019. https://doi.org/10.1038/nmeth.2019.
(251) Arganda-Carreras, I.; Kaynig, V.; Rueden, C.; Eliceiri, K. W.; Schindelin, J.; Cardona, A.; Sebastian Seung, H. Trainable Weka Segmentation: A Machine Learning Tool for Microscopy Pixel Classification. *Bioinformatics* **2017**, *33* (15), 2424–2426. https://doi.org/10.1093/bioinformatics/btx180.
(252) Medina Faull, L. E.; Zaliznyak, T.; Taylor, G. T. From the Caribbean to the Arctic, the Most Abundant Microplastic Particles in the Ocean Have Escaped Detection. *Mar. Pollut. Bull.* **2024**, *202*, 116338. https://doi.org/10.1016/j.marpolbul.2024.116338.
(253) Uurasjärvi, E.; Hartikainen, S.; Setälä, O.; Lehtiniemi, M.; Koistinen, A. Microplastic Concentrations, Size Distribution, and Polymer Types in the Surface Waters of a Northern European Lake. *Water Environ. Res.* **2020**, *92* (1), 149–156. https://doi.org/10.1002/wer.1229.
(254) Zhao, S.; Kvale, K. F.; Zhu, L.; Zettler, E. R.; Egger, M.; Mincer, T. J.; Amaral-Zettler, L. A.; Lebreton, L.; Niemann, H.; Nakajima, R.; Thiel, M.; Bos, R. P.; Galgani, L.; Stubbins, A. The Distribution of Subsurface Microplastics in the Ocean. *Nature* **2025**, *641* (8061), 51–61. https://doi.org/10.1038/s41586-025-08818-1.
(255) Fu, S.-Y.; Feng, X.-Q.; Lauke, B.; Mai, Y.-W. Effects of Particle Size, Particle/Matrix Interface Adhesion and Particle Loading on Mechanical Properties of Particulate–Polymer Composites. *Compos. Part B Eng.* **2008**, *39* (6), 933–961. https://doi.org/10.1016/j.compositesb.2008.01.002.
(256) Bowling, R. A. A Theoretical Review of Particle Adhesion. In *Particles on Surfaces 1: Detection, Adhesion, and Removal*; Mittal, K. L., Ed.; Springer US: Boston, MA, 1988; pp 129–142. https://doi.org/10.1007/978-1-4615-9531-1_10.

(257) Katainen, J.; Paajanen, M.; Ahtola, E.; Pore, V.; Lahtinen, J. Adhesion as an Interplay between Particle Size and Surface Roughness. *J. Colloid Interface Sci.* **2006**, *304* (2), 524–529. https://doi.org/10.1016/j.jcis.2006.09.015.
(258) Parrella, F.; Brizzolara, S.; Holzner, M.; Mitrano, D. M. Impact of Heteroaggregation between Microplastics and Algae on Particle Vertical Transport. *Nat. Water* **2024**, *2* (6), 541–552. https://doi.org/10.1038/s44221-024-00248-z.
(259) Hakim, A.; Tanu, F. Z.; Alam, S. S. Interaction, Adhesion and Aggregation of Microplastic/Nanoplastic Particles: Effects of Plastic Polymer Type. *Asian J. Water Environ. Pollut.* **2023**, *20* (5), 17–24. https://doi.org/10.3233/AJW230061.
(260) Bradley, M.; Lazim, A. M.; Eastoe, J. Stimulus-Responsive Heteroaggregation of Colloidal Dispersions: Reversible Systems and Composite Materials. *Polymers* **2011**, *3* (3), 1036–1050. https://doi.org/10.3390/polym3031036.
(261) Sharma, V. K.; Ma, X.; Guo, B.; Zhang, K. Environmental Factors-Mediated Behavior of Microplastics and Nanoplastics in Water: A Review. *Chemosphere* **2021**, *271*, 129597. https://doi.org/10.1016/j.chemosphere.2021.129597.
(262) Clint, J. H.; Wicks, A. C. Adhesion under Water: Surface Energy Considerations. *Int. J. Adhes. Adhes.* **2001**, *21* (4), 267–273. https://doi.org/10.1016/S0143-7496(00)00029-4.
(263) *Better Adhesive Bonding Begins with Ensuring Material Surface Energy*. Plasma Surface Treating. https://www.enerconind.com/plasma-treating/library-resource/better-adhesive-bonding-begins-with-ensuring-material-surface-energy/ (accessed 2026-04-07).
(264) Modified 12/11/2020, L. *2-ETHYLHEXYL ACRYLATE inhibited*. MIDSIS-TROCS. https://midsis.rempec.org/en/find-chemical/2-ethylhexyl-acrylate-inhibited (accessed 2026-04-07).
(265) Smith, R. E. Surface Energy Data for PP: Polypropylene, CAS #s 9003-08-0 (Atactic) and 25085-53-4 (Isotactic).
(266) Smith, R. E. Surface Energy Data for PET: Poly(Ethylene Terephthalate), CAS # 25038-59-9.
(267) Smith, R. E. Surface Energy Data for PE: Polyethylene, CAS # 9002-88-4.
(268) King, P. *Polypropylene Properties & Polypropylene Characteristics Explained*. Palmetto Industries. https://www.palmetto-industries.com/polypropylene-properties/ (accessed 2026-04-13).
(269) Lei, Z.; Dai, C.; Hallett, J.; Shiflett, M. Introduction: Ionic Liquids for Diverse Applications. *Chem. Rev.* **2024**, *124* (12), 7533–7535. https://doi.org/10.1021/acs.chemrev.4c00291.
(270) Etale, A.; Onyianta, A. J.; Turner, S. R.; Eichhorn, S. J. Cellulose: A Review of Water Interactions, Applications in Composites, and Water Treatment. *Chem. Rev.* **2023**, *123* (5), 2016–2048. https://doi.org/10.1021/acs.chemrev.2c00477.
(271) Xiao, Z.; Liu, M.; Bi, W.; Chen, D. D. Y. Ionic Liquid as Hydrogen Bond Acceptor in the Extraction of Nutritional Natural Products. *Food Chem.* **2023**, *412*. https://doi.org/10.1016/j.foodchem.2023.135589.
(272) Long, Y.; Li, Y.; Cao, R.; Qin, C.; Wang, B.; Wu, H.; Nie, Y. Molecular Insight into the Dissolution-Degradation Process of Cellulose Bunch in Ionic Liquids. *J. Mol. Liq.* **2024**, *414*. https://doi.org/10.1016/j.molliq.2024.126191.
(273) Yoneda, Y.; Bacher, M.; Hettegger, H.; Böhmdorfer, S.; Potthast, A.; Rosenau, T. Electron-Beaming of Cellulose Solutions in 3-Alkyl-1-Methylimidazolium Acetate Ionic

Liquids: Side Reactions of the Acetate Anions. *Cellulose* **2025**, *32* (9), 5263–5274. https://doi.org/10.1007/s10570-025-06465-3.
(274) Tan, X.; Chen, L.; Li, X.; Xie, F. Effect of Anti-Solvents on the Characteristics of Regenerated Cellulose from 1-Ethyl-3-Methylimidazolium Acetate Ionic Liquid. *Int. J. Biol. Macromol.* **2019**, *124*, 314–320. https://doi.org/10.1016/j.ijbiomac.2018.11.138.
(275) Onwukamike, K. N.; Tassaing, T.; Grelier, S.; Grau, E.; Cramail, H.; Meier, M. A. R. Detailed Understanding of the DBU/CO2 Switchable Solvent System for Cellulose Solubilization and Derivatization. *ACS Sustain. Chem. Eng.* **2018**, *6* (1), 1496–1503. https://doi.org/10.1021/acssuschemeng.7b04053.
(276) Ci, Y.; Chen, T.; Li, F.; Zou, X.; Tang, Y. Cellulose Dissolution and Regeneration Behavior via DBU-Levulinic Acid Solvents. *Int. J. Biol. Macromol.* **2023**, *252*. https://doi.org/10.1016/j.ijbiomac.2023.126548.
(277) Solhi, L.; Guccini, V.; Heise, K.; Solala, I.; Niinivaara, E.; Xu, W.; Mihhels, K.; Kröger, M.; Meng, Z.; Wohlert, J.; Tao, H.; Cranston, E. D.; Kontturi, E. Understanding Nanocellulose-Water Interactions: Turning a Detriment into an Asset. *Chem. Rev.* **2023**, *123* (5), 1925–2015. https://doi.org/10.1021/acs.chemrev.2c00611.
(278) Nazari, B.; Utomo, N. W.; Colby, R. H. The Effect of Water on Rheology of Native Cellulose/Ionic Liquids Solutions. *Biomacromolecules* **2017**, *18* (9), 2849–2857. https://doi.org/10.1021/acs.biomac.7b00789.
(279) Lengvinaitė, D.; Kvedaraviciute, S.; Bielskutė, S.; Klimavicius, V.; Balevicius, V.; Mocci, F.; Laaksonen, A.; Aidas, K. Structural Features of the [C4mim][Cl] Ionic Liquid and Its Mixtures with Water: Insight from a1H NMR Experimental and QM/MD Study. *J. Phys. Chem. B* **2021**, *125* (48), 13255–13266. https://doi.org/10.1021/acs.jpcb.1c08215.
(280) Tarasova, E.; Savale, N.; Ausmaa, P. M.; Krasnou, I.; Krumme, A. Rheology and Dissolution Capacity of Cellulose in Novel [mTBNH][OAc] Ionic Liquid Mixed with Green Co-Solvents. *Rheol. Acta* **2024**, *63* (2), 167–178. https://doi.org/10.1007/s00397-024-01433-3.
(281) Dziubinska-Kühn, K.; Croese, J.; Pupier, M.; Matysik, J.; Viger-Gravel, J.; Karg, B.; Kowalska, M. Structural Analysis of Water in Ionic Liquid Domains – A Low Pressure Study. *J. Mol. Liq.* **2021**, *334*. https://doi.org/10.1016/j.molliq.2021.116447.
(282) Rezaie, F.; Kowsari, M. H. Capturing the Effect of Anion Type on the Intermolecular Interactions between Water and Imidazolium-Based Ionic Liquids: A Comparative DFT Study. *J. Phys. Chem. B* **2025**, *129* (4), 1343–1359. https://doi.org/10.1021/acs.jpcb.4c06749.
(283) Ramadevi, P.; Sampathkumar, D.; Srinivasa, C. V.; Bennehalli, B. *EFFECT OF ALKALI TREATMENT ON WATER ABSORPTION OF SINGLE CELLULOSIC ABACA FIBER*; BioResources; 2012; Vol. 7, pp 3515–3524. https://doi.org/10.15376/biores.7.3.3515-3524.
(284) Azizan, A.; Darim, R. A.; Azmi, I. S.; Jalil, R.; Manaf, S. F. A. Understanding Crystallinity Indexes Benchmarking Concept from Optimized Parametric Ionic Liquid Pretreatment Using 1-Ethyl-3-Methylimidazolium Acetate [EMIM]Ac on Oil Palm Biomass. *J. Ion. Liq.* **2025**, *5* (1). https://doi.org/10.1016/j.jil.2025.100136.
(285) Rieland, J. M.; Nikafshar, S.; Hu, Z.; Nejad, M.; Love, B. J. Ionic Liquid-Mediated Biopolymer Extraction from Coffee Fruit. *Macromol. Mater. Eng.* **2023**, *308* (12), 2300145–2300145. https://doi.org/10.1002/mame.202300145.
(286) Achinivu, E. C.; Blankenship, B. W.; Baral, N. R.; Choudhary, H.; Kakumanu, R.; Mohan, M.; Baidoo, E. E. K.; Scown, C. D.; George, A.; Simmons, B. A.; Gladden, J.

Biomass Pretreatment with Distillable Ionic Liquids for an Effective Recycling and Recovery Approach. *Chem. Eng. J.* **2024**, *479*. https://doi.org/10.1016/j.cej.2023.147824.
(287) MATLAB. **2022**.
(288) Cross, M. M. Relation between Viscoelasticity and Shear-Thinning Behaviour in Liquids. *Rheol. Acta* **1979**, *18* (5), 609–614. https://doi.org/10.1007/BF01520357.
(289) Lavygin, I. A.; Chistoff, S. F. Temperature Dependence of the Viscosity of Polymer Melts and Liquid-Liquid Transitions. *Polym. Sci. USSR* **1985**, *27* (6), 1478–1485. https://doi.org/10.1016/0032-3950(85)90296-5.
(290) Campbell, G. A.; Radhakrishnan, J. S.; Wetzel, M. D. Comparing the Power Law Constant (n) for Mono- and Bi-Dispersed Filled Slurries: Using Percolation Theory Concepts. *Rheol. Acta* **2020**, *59*, 583–599. https://doi.org/10.1007/s00397-020-01214-8/Published.
(291) ASTM D3822-07: Standard Test Method for Tensile Properties of Single Textile Fibers. *ASTM* **2010**, *07.01*, 10–10.
(292) Gwyddion. **2025**.
(293) Matroodi, F.; Bottari, C.; Rossi, B.; Mannu, A.; Paolantoni, M.; Mele, A. Hydration Water and Ionic Aggregation in Aqueous Solutions of Imidazolium-Based Protic Ionic Liquids. *J. Mol. Liq.* **2024**, *395*. https://doi.org/10.1016/j.molliq.2023.123881.
(294) Fazio, B.; Triolo, A.; Di Marco, G. Local Organization of Water and Its Effect on the Structural Heterogeneities in Room-Temperature Ionic Liquid/H2O Mixtures; John Wiley and Sons Ltd, 2008; Vol. 39, pp 233–237. https://doi.org/10.1002/jrs.1825.
(295) Li, J.; Nawaz, H.; Wu, J.; Zhang, J.; Wan, J.; Mi, Q.; Yu, J.; Zhang, J. All-Cellulose Composites Based on the Self-Reinforced Effect. *Compos. Commun.* **2018**, *9*, 42–53. https://doi.org/10.1016/j.coco.2018.04.008.
(296) Podschun, J.; Saake, B.; Lehnen, R. Reactivity Enhancement of Organosolv Lignin by Phenolation for Improved Bio-Based Thermosets. *Eur. Polym. J.* **2015**, *67*, 1–11. https://doi.org/10.1016/j.eurpolymj.2015.03.029.
(297) Arefmanesh, M.; Vuong, T. V.; Mobley, J. K.; Alinejad, M.; Master, E. R.; Nejad, M. Bromide-Based Ionic Liquid Treatment of Hardwood Organosolv Lignin Yielded a More Reactive Biobased Polyol. *Ind. Eng. Chem. Res.* **2020**, *59* (42), 18740–18747. https://doi.org/10.1021/acs.iecr.0c03718.
(298) Kang, X.; Kirui, A.; Dickwella Widanage, M. C.; Mentink-Vigier, F.; Cosgrove, D. J.; Wang, T. Lignin-Polysaccharide Interactions in Plant Secondary Cell Walls Revealed by Solid-State NMR. *Nat. Commun.* **2019**, *10* (1), 347. https://doi.org/10.1038/s41467-018-08252-0.
(299) Liu, J.; Kim, J. I.; Cusumano, J. C.; Chapple, C.; Venugopalan, N.; Fischetti, R. F.; Makowski, L. The Impact of Alterations in Lignin Deposition on Cellulose Organization of the Plant Cell Wall. *Biotechnol. Biofuels* **2016**, *9*, 126. https://doi.org/10.1186/s13068-016-0540-z.
(300) Ruan, Z.; Wang, X.; Liu, Y.; Liao, W. Chapter 3 - Corn. In *Integrated Processing Technologies for Food and Agricultural By-Products*; Pan, Z., Zhang, R., Zicari, S., Eds.; Academic Press, 2019; pp 59–72. https://doi.org/10.1016/B978-0-12-814138-0.00003-4.
(301) *Corn and Other Feed Grains - Feed Grains Sector at a Glance | Economic Research Service*. https://www.ers.usda.gov/topics/crops/corn-and-other-feed-grains/feed-grains-sector-at-a-glance (accessed 2026-01-28).

(302) Sharifnasab, H.; Soltani, E.; Karami, H.; Grądecka-Jakubowska, K.; Gancarz, M. Meta-Analysis of Tillage Methods and Their Influence on Wheat Productivity. *Int. Agrophysics* **2024**, *38* (4), 345–351. https://doi.org/10.31545/intagr/190044.
(303) Udali, A.; Chung, W.; Talbot, B.; Grigolato, S. Managing Harvesting Residues: A Systematic Review of Management Treatments around the World. *For. Int. J. For. Res.* **2025**, *98* (2), 117–135. https://doi.org/10.1093/forestry/cpae041.
(304) Spinelli, R.; Magagnotti, N.; Aminti, G.; De Francesco, F.; Lombardini, C. The Effect of Harvesting Method on Biomass Retention and Operational Efficiency in Low-Value Mountain Forests. *Eur. J. For. Res.* **2016**, *135* (4), 755–764. https://doi.org/10.1007/s10342-016-0970-y.
(305) *Crop residue management*. https://extension.umn.edu/corn-harvest/crop-residue-management (accessed 2026-07-14).
(306) Li, M.; Cao, S.; Meng, X.; Studer, M.; Wyman, C. E.; Ragauskas, A. J.; Pu, Y. The Effect of Liquid Hot Water Pretreatment on the Chemical-Structural Alteration and the Reduced Recalcitrance in Poplar. *Biotechnol. Biofuels* **2017**, *10* (1). https://doi.org/10.1186/s13068-017-0926-6.
(307) Suriyachai, N.; Weerasai, K.; Upajak, S.; Khongchamnan, P.; Wanmolee, W.; Laosiripojana, N.; Champreda, V.; Suwannahong, K.; Imman, S. Efficiency of Catalytic Liquid Hot Water Pretreatment for Conversion of Corn Stover to Bioethanol. *ACS Omega* **2020**, *5* (46), 29872–29881. https://doi.org/10.1021/acsomega.0c04054.
(308) Gladysheva, E. K. Liquid Hot Water and Steam Explosion Pretreatment Methods for Cellulosic Raw Materials: A Review. *Polymers* **2025**, *17* (13), 1783. https://doi.org/10.3390/polym17131783.
(309) Overend, R. P.; Chornet, E. Fractionation of Lignocellulosics by Steam-Aqueous Pretreatments. *Philos. Trans. R. Soc. Lond. Ser. Math. Phys. Sci.* **1987**, *321* (1561), 523–536. https://doi.org/10.1098/rsta.1987.0029.
(310) Kim, Y.; Kreke, T.; Mosier, N. S.; Ladisch, M. R. Severity Factor Coefficients for Subcritical Liquid Hot Water Pretreatment of Hardwood Chips. *Biotechnol. Bioeng.* **2014**, *111* (2), 254–263. https://doi.org/10.1002/bit.25009.
(311) Liu, L.; Liu, W.; Hou, Q.; Chen, J.; Xu, N. Understanding of pH Value and Its Effect on Autohydrolysis Pretreatment Prior to Poplar Chemi-Thermomechanical Pulping. *Bioresour. Technol.* **2015**, *196*, 662–667. https://doi.org/10.1016/j.biortech.2015.08.034.
(312) El Seoud, O. A.; Kostag, M.; Jedvert, K.; Malek, N. I. Cellulose in Ionic Liquids and Alkaline Solutions: Advances in the Mechanisms of Biopolymer Dissolution and Regeneration. *Polymers* **2019**, *11* (12), 1917. https://doi.org/10.3390/polym11121917.
(313) Parviainen, A.; King, A. W. T.; Mutikainen, I.; Hummel, M.; Selg, C.; Hauru, L. K. J.; Sixta, H.; Kilpeläinen, I. Predicting Cellulose Solvating Capabilities of Acid–Base Conjugate Ionic Liquids. *ChemSusChem* **2013**, *6* (11), 2161–2169. https://doi.org/10.1002/cssc.201300143.
(314) Ma, J.; Zhu, M.; Yang, X.; Wang, Y.; Wang, B. Different Cation-Anion Interaction Mechanisms of Diamino Protic Ionic Liquids: A Density Functional Theory Study. *Chem. Phys. Lett.* **2021**, *774*. https://doi.org/10.1016/j.cplett.2021.138615.
(315) Ren, F.; Wang, J.; Luan, H.; Yu, J.; Copeland, L.; Wang, S.; Wang, S. Dissolution Behavior of Maize Starch in Aqueous Ionic Liquids: Effect of Anionic Structure and Water/Ionic Liquid Ratio. *ACS Omega* **2019**, *4* (12), 14981–14986. https://doi.org/10.1021/acsomega.9b01768.

(316) Blaga, A. C.; Tucaliuc, A.; Kloetzer, L. Applications of Ionic Liquids in Carboxylic Acids Separation. *Membranes* **2022**, *12* (8), 771. https://doi.org/10.3390/membranes12080771.
(317) Lawal, T. D.; Rieland, J. M.; Love, B. J. Water Regulates Ionic Liquid Solvation and Can Fine-Tune the Rheological Behavior of Dissolved Cellulose. *Results Eng.* **2025**, *28*, 107550. https://doi.org/10.1016/j.rineng.2025.107550.
(318) Hubbell, C. A.; Ragauskas, A. J. Effect of Acid-Chlorite Delignification on Cellulose Degree of Polymerization. *Bioresour. Technol.* **2010**, *101* (19), 7410–7415. https://doi.org/10.1016/j.biortech.2010.04.029.
(319) Liu, L.; Liu, W.; Hou, Q.; Chen, J.; Xu, N. Understanding of pH Value and Its Effect on Autohydrolysis Pretreatment Prior to Poplar Chemi-Thermomechanical Pulping. *Bioresour. Technol.* **2015**, *196*, 662–667. https://doi.org/10.1016/j.biortech.2015.08.034.
(320) Sluiter, J. B.; Ruiz, R. O.; Scarlata, C. J.; Sluiter, A. D.; Templeton, D. W. Compositional Analysis of Lignocellulosic Feedstocks. 1. Review and Description of Methods. *J. Agric. Food Chem.* **2010**, *58* (16), 9043–9053. https://doi.org/10.1021/jf1008023.
(321) Podgorbunskikh, E.; Kuskov, T.; Rychkov, D.; Lomovskii, O.; Bychkov, A. Mechanical Amorphization of Chitosan with Different Molecular Weights. *Polymers* **2022**, *14* (20). https://doi.org/10.3390/polym14204438.
(322) Granata, A.; Argyropoulos, D. S. 2-Chloro-4,4,5,5-Tetramethyl-1,3,2-Dioxaphospholane, a Reagent for the Accurate Determination of the Uncondensed and Condensed Phenolic Moieties in Lignins. *J. Agric. Food Chem.* **1995**, *43* (6), 1538–1544. https://doi.org/10.1021/jf00054a023.
(323) Nikafshar, S.; Nejad, M. Evaluating Efficacy of Different UV-Stabilizers/Absorbers in Reducing UV-Degradation of Lignin. *Holzforschung* **2022**, *76* (3), 235–244. https://doi.org/10.1515/hf-2021-0147.
(324) Reddy, K. O.; Zhang, J.; Zhang, J.; Rajulu, A. V. Preparation and Properties of Self-Reinforced Cellulose Composite Films from Agave Microfibrils Using an Ionic Liquid. *Carbohydr. Polym.* **2014**, *114*, 537–545. https://doi.org/10.1016/j.carbpol.2014.08.054.
(325) Deng, Z.; Xia, A.; Liao, Q.; Zhu, X.; Huang, Y.; Fu, Q. Laccase Pretreatment of Wheat Straw: Effects of the Physicochemical Characteristics and the Kinetics of Enzymatic Hydrolysis. *Biotechnol. Biofuels* **2019**, *12* (1), 159. https://doi.org/10.1186/s13068-019-1499-3.
(326) Hu, M.; Cai, Z.; Zhang, J.; Yuan, L.; Fu, Q.; Ji, D. Ammonia Fiber Expansion (AFEX) Combined with White-Rot Fungi Pretreatment to Improve Enzymatic Hydrolysis of Lignocellulose. *Biomass Convers. Biorefinery* **2024**, *14* (9), 10085–10099. https://doi.org/10.1007/s13399-022-03075-y.
(327) Park, S.; Baker, J. O.; Himmel, M. E.; Parilla, P. A.; Johnson, D. K. Cellulose Crystallinity Index: Measurement Techniques and Their Impact on Interpreting Cellulase Performance. *Biotechnol. Biofuels* **2010**, *3* (1), 10. https://doi.org/10.1186/1754-6834-3-10.
(328) Matthews, J. F.; Beckham, G. T.; Bergenstråhle-Wohlert, M.; Brady, J. W.; Himmel, M. E.; Crowley, M. F. Comparison of Cellulose Iβ Simulations with Three Carbohydrate Force Fields. *J. Chem. Theory Comput.* **2012**, *8* (2), 735–748. https://doi.org/10.1021/ct2007692.
(329) Uto, T.; Yui, T. DFT Optimization of Isolated Molecular Chain Sheet Models Constituting Native Cellulose Crystal Structures. *ACS Omega* **2018**, *3* (7), 8050–8058. https://doi.org/10.1021/acsomega.8b00834.

(330) Wan, J.; Luo, C. Accumulation of Hydrogen Bonds and van Der Waals Interactions Determines Force Response between Two Parallel Cellulose Chains: Steered Molecular Dynamics Simulations. *J. Phys. Chem. B* **2024**, *128* (28), 6742–6750. https://doi.org/10.1021/acs.jpcb.4c01826.
(331) Silva, N.; Silva, N.; Mulinari, D. Influence of Sequential Acid-Alkali Treatment on Palm Biomass Waste Properties. *J. Nat. Fibers* **2022**, *19* (14), 7502–7516. https://doi.org/10.1080/15440478.2021.1951421.
(332) *An Alternative Path for the Preparation of Triacetylcellulose from Unrefined Biomass*. https://www.scirp.org/journal/paperinformation?paperid=53005 (accessed 2026-06-27).
(333) *Prospecting fungal ligninases using corncob lignocellulosic fractions | Cellulose | Springer Nature Link*. https://link.springer.com/article/10.1007/s10570-017-1427-2?utm_source=researchgate.net&utm_medium=article (accessed 2026-06-27).
(334) Bagh, F. S. G.; Ray, S. Lignin Extraction from Black Liquor Using Acetate Based Ionic Liquids: Extraction Kinetics and Product Characterization. *J. Ion. Liq.* **2022**, *2* (1), 100028. https://doi.org/10.1016/j.jil.2022.100028.
(335) Lignin Depolymerization from Softwood Biomass Using Integrated Protic Ionic Liquid–Enzyme Pretreatment. *RSC Sustain.* **2025**, *3* (10), 4466–4477. https://doi.org/10.1039/d5su00351b.
(336) Heggset, E. B.; Syverud, K.; Øyaas, K. Novel Pretreatment Pathways for Dissolution of Lignocellulosic Biomass Based on Ionic Liquid and Low Temperature Alkaline Treatment. *Biomass Bioenergy* **2016**, *93*, 194–200. https://doi.org/10.1016/j.biombioe.2016.07.023.
(337) Li, D.; Qi, L.; Gibril, M. E.; Xue, Y.; Yang, G.; Yang, M.; Gu, Y.; Chen, J. Switchable Solvent for Separation and Extraction of Lignin from Lignocellulose Biomass: An Investigation of Chemical Structure and Molecular Weight. *Polymers* **2024**, *16* (24), 3560. https://doi.org/10.3390/polym16243560.
(338) Y. Suleman, M.; L. Judah, H.; Bexis, P.; Fennell, P.; P. Hallett, J.; Brandt-Talbot, A. The Acetate Anion Promotes Hydrolysis of Poly(Ethylene Terephthalate) in Ionic Liquid–Water Mixtures. *Green Chem.* **2025**, *27* (37), 11475–11490. https://doi.org/10.1039/D5GC02409A.
(339) Nikafshar, S.; Wang, J.; Dunne, K.; Sangthonganotai, P.; Nejad, M. Choosing the Right Lignin to Fully Replace Bisphenol A in Epoxy Resin Formulation. *ChemSusChem* **2021**, *14* (4), 1184–1195. https://doi.org/10.1002/cssc.202002729.
(340) *Molecular changes in corn stover lignin resulting from pretreatment chemistry :: BioResources*. https://bioresources.cnr.ncsu.edu/ (accessed 2026-06-25).
(341) Wen, J.-L.; Yuan, T.-Q.; Sun, S.-L.; Xu, F.; Sun, R.-C. Understanding the Chemical Transformations of Lignin during Ionic Liquid Pretreatment. *Green Chem.* **2013**, *16* (1), 181–190. https://doi.org/10.1039/C3GC41752B.
(342) King, A. W. T.; Zoia, L.; Filpponen, I.; Olszewska, A.; Xie, H.; Kilpeläinen, I.; Argyropoulos, D. S. In Situ Determination of Lignin Phenolics and Wood Solubility in Imidazolium Chlorides Using 31P NMR. *J. Agric. Food Chem.* **2009**, *57* (18), 8236–8243. https://doi.org/10.1021/jf901095w.
(343) Moxley, G.; Gaspar, A. R.; Higgins, D.; Xu, H. Structural Changes of Corn Stover Lignin during Acid Pretreatment. *J. Ind. Microbiol. Biotechnol.* **2012**, *39* (9), 1289–1299. https://doi.org/10.1007/s10295-012-1131-z.
(344) Peng, C.; Chen, Q.; Guo, H.; Hu, G.; Li, C.; Wen, J.; Wang, H.; Zhang, T.; Zhao, Z. K.; Sun, R.; Xie, H. Effects of Extraction Methods on Structure and Valorization of Corn Stover Lignin by a Pd/C Catalyst. https://doi.org/10.1002/cctc.201601501.

(345) Melro, E.; Alves, L.; Antunes, F. E.; Medronho, B. A Brief Overview on Lignin Dissolution. *J. Mol. Liq.* **2018**, *265*, 578–584. https://doi.org/10.1016/j.molliq.2018.06.021.
(346) Sadeghifar, H.; Wells, T.; Le, R. K.; Sadeghifar, F.; Yuan, J. S.; Jonas Ragauskas, A. Fractionation of Organosolv Lignin Using Acetone:Water and Properties of the Obtained Fractions. *ACS Sustain. Chem. Eng.* **2017**, *5* (1), 580–587. https://doi.org/10.1021/acssuschemeng.6b01955.
(347) Li, W.; Hao, J.; Zhou, P.; Liu, Y.; Lu, C.; Zhang, Z. Solvent-Solubility-Parameter-Dependent Homogeneity and Sol–Gel Transitions of Concentrated Polyacrylonitrile Solutions. *J. Appl. Polym. Sci.* **2017**, *134* (41), 45405. https://doi.org/10.1002/app.45405.
(348) Arefmanesh, M.; Nikafshar, S.; Master, E. R.; Nejad, M. From Acetone Fractionation to Lignin-Based Phenolic and Polyurethane Resins. *Ind. Crops Prod.* **2022**, *178*, 114604. https://doi.org/10.1016/j.indcrop.2022.114604.
(349) Evstigneyev, E. I.; Shevchenko, S. M. Structure, Chemical Reactivity and Solubility of Lignin: A Fresh Look. *Wood Sci. Technol.* **2019**, *53* (1), 7–47. https://doi.org/10.1007/s00226-018-1059-1.
(350) Vermaas, J. V.; Crowley, M. F.; Beckham, G. T. Molecular Lignin Solubility and Structure in Organic Solvents. *ACS Sustain. Chem. Eng.* **2020**, *8* (48), 17839–17850. https://doi.org/10.1021/acssuschemeng.0c07156.
(351) Straw, R. *Enhancing Glass Bonds With Silanes and Polymer Coatings*. MO SCI. https://mo-sci.com/enhancing-glass-bonding-characteristics-with-silanes-and-polymer-coatings/ (accessed 2026-06-27).
(352) Hopewell, J.; Dvorak, R.; Kosior, E. Plastics Recycling: Challenges and Opportunities. *Philos. Trans. R. Soc. B Biol. Sci.* **2009**, *364* (1526), 2115–2126. https://doi.org/10.1098/rstb.2008.0311.
(353) Forouzeshfar, F.; Coleman, M. R.; Lawrence, J. G. Glycolysis of Poly (Ethylene Terephthalate) Using DBU-Based Ionic Liquid Catalysts. *Catal. Today* **2025**, *450*. https://doi.org/10.1016/j.cattod.2025.115187.
(354) Hasan, M. M.; Haque, R.; Jahirul, M. I.; Rasul, M. G. Pyrolysis of Plastic Waste for Sustainable Energy Recovery: Technological Advancements and Environmental Impacts. *Energy Convers. Manag.* **2025**, *326*, 119511. https://doi.org/10.1016/j.enconman.2025.119511.
(355) *Genetically modified bacteria break down plastics in saltwater | NSF - U.S. National Science Foundation*. https://www.nsf.gov/news/genetically-modified-bacteria-break-down-plastics-saltwater (accessed 2026-06-27).
(356) Jiao, H.; Al-Tohamy, R.; Xiong, M.; Schagerl, M.; Reinthaler, T.; Al-Zahrani, M.; Sun, J.; Ali, S. S. Microplastic Biodegradation and Environmental Safety: From Microbial Mechanisms to Engineered Systems and Circular Bio-Based Implementation. *Ecotoxicol. Environ. Saf.* **2026**, *313*, 120016. https://doi.org/10.1016/j.ecoenv.2026.120016.
(357) Mohanan, N.; Montazer, Z.; Sharma, P. K.; Levin, D. B. Microbial and Enzymatic Degradation of Synthetic Plastics. *Front. Microbiol.* **2020**, *11*, 580709. https://doi.org/10.3389/fmicb.2020.580709.
(358) Artha, O.; Sudarno; Pramono, H.; Sari, L. Identification of Extracellular Enzyme-Producing Bacteria (Proteolytic, Cellulolytic, and Amylolytic) in the Sediment of Extensive Ponds in Tanggulrejo, Gresik. *IOP Conf. Ser. Earth Environ. Sci.* **2019**, *236* (1), 012003. https://doi.org/10.1088/1755-1315/236/1/012003.

(359) Gonçalves, A. R. P.; Paredes, X.; Cristino, A. F.; Santos, F. J. V.; Queirós, C. S. G. P. Ionic Liquids—A Review of Their Toxicity to Living Organisms. *Int. J. Mol. Sci.* **2021**, *22* (11), 5612. https://doi.org/10.3390/ijms22115612.
(360) Wiyantoko, B. DETERMINATION OF GLUCOSE CONTENT IN CELLULOSE DERIVED FROM BANANA STEM (MUSA SPP.) USING UV-VIS SPECTROPHOTOMETRY AND HPLC METHODS.
(361) Yuan, Q.; Liu, S.; Ma, M.-G.; Ji, X.-X.; Choi, S.-E.; Si, C. The Kinetics Studies on Hydrolysis of Hemicellulose. *Front. Chem.* **2021**, *9*, 781291. https://doi.org/10.3389/fchem.2021.781291.
(362) Araujo, A. C. C.; Rojas Salas, M.; Silva, W. R.; Margellou, A. G.; Triantafyllidis, K. S.; Wisniewski, A. Jr.; Funke, A. Comprehensive Characterization of Lignin Bio-Oils from Alkali and Kraft Lignin with Integrated 1H NMR Spectral Modeling. *Energy Fuels* **2026**. https://doi.org/10.1021/acs.energyfuels.6c00906.
(363) Kim, S.; Chung, H. Convenient Cross-Linking Control of Lignin-Based Polymers Influencing Structure–Property Relationships. *ACS Sustain. Chem. Eng.* **2023**, *11* (5), 1709–1719. https://doi.org/10.1021/acssuschemeng.2c05651.